THE UNIVERSITY OF CALGARY

NUMERICAL TECHNIQUES FOR PROCESSING AIRBORNE GRADIOMETER DATA

by

ANTHONY A. VASSILIOU

A THESIS

SUBMITTED TO THE FACULTY OF GRADUATE STUDIES

IN PARTIAL FULFILLMENT OF THE REQUIREMENTS FOR THE DEGREE OF

DOCTOR OF PHILOSOPHY

DEPARTMENT OF CIVIL ENGINEERING

DIVISION OF SURVEYING ENGINEERING

CALGARY, ALBERTA

MAY, 1986

ISBN 0-315-32771-5

THE UNIVERSITY OF CALGARY

FACULTY OF GRADUATE STUDIES

The undersigned certify that they have read, and recommend to the Faculty of Graduate Studies for acceptance, a thesis entitled NUMERICAL TECHNIQUES FOR PROCESSING AIRBORNE GRADIOMETER DATA by Anthony A. Vassiliou, in partial fulfillment of the requirements for the degree of Doctor of Philosophy.

K.P. Schwarz.

Dr. K.P. Schwarz
Department of Civil Engineering
Division of Surveying Engineering

Dr. E.J. Krakiwsky
Department of Civil Engineering
Division of Surveying Engineering

M. Nakiboglu

Dr. S.M. Nakiboglu
Department of Civil Engineering
Division of Surveying Engineering

R B Streets

Dr. R.B. Streets
Department of Electrical Engineering

Gerard Lachapelle

Dr. G. Lachapelle
Nortech Surveys (Canada) Ltd.

May 9, 1986

ABSTRACT

The objective of this thesis is the development of a computationally efficient estimation technique for computing the first-order gradients of the anomalous gravity potential T at the earth's surface from airborne second-order gradients of T. With the first operational test of airborne gravity gradiometry just a few months away, computationally efficient techniques are necessary for processing the huge amounts of second-order gradient data collected during a gradiometry survey. The technique developed in this thesis is based on the multiple input-single output filtering equations taking as input the fully-correlated second-order gravity gradients and as output individual first-order gradients. The method is capable of combining all second-order gradients and taking into account the gradiometer noise. More generally, the method developed is capable of combining all possible terrestrial and airborne first and second-order gravity gradient data collected in a local area, provided that they are sampled on a regular grid. The multiple input-single output filtering equations are equivalent to the Wiener filtering equations which in turn can be derived as the spectrum of the least-squares collocation formulas for stationary and ergodic signals. One of the major contributions of this thesis is that it shows these relationships explicitly. The advance the new method brings to Geodesy is the possibility of implementing gradient combinations for very large data sets.

Due to the lack of actual second-order gradient data, simulated data were used to test the developed technique. Numerical results

indicate that first-order gradients can be computed from airborne second-order gradients with an accuracy of better than 1 mgal when assuming currently planned profile spacing and the accuracy of the existing system. Each first-order gradient T_i is most accurately computed from the combination of the second-order gradients T_{ix}, T_{iy} and T_{iz}. The numerical tests demonstrate that results are not adversely affected if noise, much higher than that of the presently existing gradiometer, is assumed. In addition the tests show that for the assumed grid spacing and flying altitude, downward continuation amounts to less than 15% of the total error budget in the estimation of the first-order gradients T_i. The estimation technique developed in this thesis is very efficient computationally because it employs the Fast Fourier Transform.

ACKNOWLEDGEMENTS

I would like to express my gratitude to my supervisor, Professor Klaus-Peter Schwarz for his continuous advice and encouragement during the development of this thesis. I also want to thank Professors S.M. Nakiboglu and R. B. Streets for clarifying ideas particularly in the first stage of this research. The help provided by Dr. C. Jekeli and Mr. Rene Forsberg in specific problems is also acknowledged. Thanks are also due to Mrs. Norma Wilson for her expert typing.

Last, but not least, I would like to express my appreciation and to thank my father Andrew and my late mother Christine, for without their continuous support I might not have reached this education level.

This research was partially supported by a research agreement between the Earth Physics Branch of the Department of Energy, Mines and Resources, Ottawa and the University of Calgary.

Αφιερωνεται στην μνημη της

μητερας μου Χριστινας

TABLE OF CONTENTS

Page

Page

LIST OF TABLES

LIST OF FIGURES

NOTATIONS

Frequency used notations and symbols are listed below

b	windowing percentage
d	depth of a layer below the earth's surface
f	specific force sensed by an accelerometer
G_N	Newton's gravitational constant
h	flying altitude
j	square root of -1
log	logarithm to base 10
m	wavenumber in x direction; point mass
M	number of points in x direction
n	wavenumber in y direction, gradiometer noise
N	number of points in y direction
q	circular frequency
R	gradiometer red noise constant; distance between each accelerometer and origin in the Bell gradiometer
$R_{g,h}$	cross correlation function of the functions g,h
Rgg	auto correlation function of the function g
$S_{g,h}$	cross spectral density of the functions g,h
Sgg	power spectral density of the function g
T	anomalous gravity potential
T_i	first-order anomalous gravity gradient (i=x,y,z)
T_{ik}	second-order anomalous gravity gradient (i; k=x,y,z)
$\underline{T}_{ik}$	vector containing the second-order gradients T_{ik}
T_1	record length in x direction
T_2	record length in y direction

u	spatial frequency in x direction
U	normal gravity potential
u_N	Nyquist spatial frequency
v	spatial frequency in y direction
V	gravitational potential
w	windowing function
W	gravity potential, gradiometer white noise constant
x	cartesian coordinate
y	cartesian coordinate
z	cartesian coordinate
α	azimuth (in cartesian coordinates)
$\gamma^2_{g,h}$	coherence function of the functions g,h
δg	gravity disturbance
Δx	grid spacing in x direction
Δy	grid spacing in y direction
∂	partial differentiation symbol
λ	geodetic longitude
ϕ	geodetic latitude
ω	angular velocity
$E\{.\}$	expected value
$F\{.\}$	direct Fourier transform
$F^{-1}\{.\}$	inverse Fourier transform
$\lvert . \rvert$	amplitude of a complex function
$*$	convolution symbol
$\overset{F}{\longleftrightarrow}$	Fourier transform pair symbol

superscript *	complex conjugate of a complex number
superscript t	transpose of a vector or a matrix
superscript ^	estimated value

DFT	discrete Fourier transform
E	Eötvos ($=10^{-9}sec^{-2}$)
eqn.	equation
FFT	fast Fourier transform
Fig	figure
GGSS	Gravity Gradiometer Survey System
GPS	Global Positioning System
Hz	Hertz ($=sec^{-1}$)
mgal	milligal ($=10^{-3}cmsec^{-2}$)
PSD	power spectral density
RMS	root mean square value
2-D	two-dimensional
1-D	one-dimensional

Chapter 1

INTRODUCTION

Research on the determination of the earth's gravity field using airborne measurements of gravity started in 1959, when the concept of airborne gravimetry was first tested (Thompson, 1959). At that time, the possibility of success seemed rather remote. Considerable work has been done in airborne gravimetry since then (Nettleton et al., 1960; Coons et al., 1962, Gumert and Cobb, 1970, Szabo and Anthony, 1971; La Coste et al., 1977), but only in the last five years some progress has been reported (Hammer, 1982; Hammer, 1983; Brozena, 1984). The major advantage of airborne gravity methods compared to terrestrial methods is the speed with which gravity measurements can be taken. The major problem with airborne gravimetry is that, theoretically, the gravitational and the inertial forces can not be separated (Meissl, 1970). This problem has not been solved yet.

These difficulties led to the development of airborne gravity gradiometry, where work on these problems started towards the end of the sixties and has continued since then (Trageser, 1970; Moritz, 1975; Paik, 1976; Forward and Ames, 1977, Metzger and Jircitano, 1981). The inertial and gravitational forces are separated by mounting three gravity gradiometer sensors on an inertially stabilized platform (Moritz, 1967; Moritz, 1971). A gravity gradiometer measures the six second-order gravity gradients. Elimination of the effect of the earth's normal gravity field from these six gravity gradients and integration of the proper combination of the resulting gradients yields the first-order gradients of the anomalous potential. The

measurement of second-order instead of first-order gravity gradients provides more short-wavelength (high frequency) information which is needed for a precise determination of the gravity field in a local area. In addition, the high frequencies of the anomalous gravity field provide useful information for geophysical prospecting (Jordan, 1978).

Hardware development for gravity gradiometers started in the early '70s and has continued till now. During the seventies four gravity gradiometers were under development, the floated gradiometer (Trageser, 1975), the Hughes gradiometer (Forward, 1971), the Bell gradiometer (Metzger and Jircitano, 1977) and the superconducting gradiometer (Paik, et al., 1978). Of those four, two are further developed, namely the Gravity Gradiometer Survey System (GGSS) developed by Bell Aerospace and the superconducting gradiometer developed by Paik at the University of Maryland. The superconducting gradiometer is planned to be used for satellite gradiometry. The GGSS gradiometer is the one which will be employed for airborne gradiometry. The first flight tests are expected to be conducted at the end of 1986 or early in 1987.

Feasibility and accuracy studies on the determination of the anomalous gravity field from airborne gradiometry have been conducted since the middle of the last decade (Moritz, 1975; Schwarz, 1976, Schwarz, 1977). Those studies led to some important conclusions. First, the gradiometry survey geometry is the major factor in the precise determination of the earth's gravity field. Second, the vertical second-order gradient is necessary for downward continuation and the mixed vertical-horizontal gradients are needed for interpolation between flight tracks. Third, airborne second-order

gradients collected at altitude of 10 km, with across track spacing of 0°.3 determine 5'x 5' block anomalies at the earth's surface with an accuracy of 2.3 mgals. Fourth, least-squares collocation is a theoretically ideal method for estimating the first-order from the second-order gradients. In practice though, due to the large amount of data, it must be properly applied so that only one batch of data over a subregion of the whole area is processed at a time (Schwarz, 1977).

The satisfactory laboratory performance of the GGSS gradiometer, the development of the GPS providing good worldwide navigation capability and a decision for a 600 m flying altitude stimulated again interest in airborne gradiometry during the early '80s (Jordan, 1982; Heller and Senus, 1983; Jekeli, 1983; Jekeli, 1984a; Jekeli, 1984b). Covariance studies by Jekeli (1983, 1984a) showed clearly that with a flying altitude of 600 m and along, across-track sampling intervals of 1 and 5 km, respectively, gravity disturbances can be determined with an accuracy below the 1 mgal level. Simulation analysis performed by Hutcheson and Grierson (1985), showed that for an area of 315x315 km an accuracy of 0.9 mgal can be achieved for all the elements of the first-order gradient vector within 40 km inside the borders of the area.

The main problem with the determination of the gravity field from airborne gradiometry is the huge amount of gradient data collected during a gradiometry survey. For a survey over a 300x300 km area with 1 and 5 km along and across-track spacings, respectively about 216 000 measurements have to be processed. This large amount of data makes it impossible to apply space domain least-squares collocation for the estimation of the first-order gradients from second-

order gradient measurements. At present, three methods have been proposed for this estimation. The first one is a modification of least-squares collocation in the space domain similar to that employed by Schwarz (1977). The whole area is subdivided into different sets of data points, called templates. The gradient measurements are averaged over one template and least-squares collocation is employed. Then, this template is shifted from region to region so that finally the whole area is covered. This method is called the template method (White and Goldstein, 1984) and has been successfully tested with simulated gradient data. The second method is a hybrid method which combines least-squares collocation in the space domain and Wiener filtering in the frequency domain. Least-squares collocation deals with the low frequency part of the gradient signal while Wiener filtering takes care of the high frequency part of the spectrum (Hutcheson and Grierson, 1985). The third method employs Wiener filtering in the frequency domain and uses tie astrogeodetic points to estimate the low-frequency part of the local anomalous gravity field (Jekeli, 1985).

The objective of this research is to present an alternative method to the problem of processing large amounts of airborne gravity gradient measurements which incorporates gradient combination and computational efficiency and furthermore takes the gradiometer noise into account. The method is based on the application of multiple input-single output filtering equations, using as inputs the linearly correlated second-order gravity gradients and as output the first-order gradients. In this way, each first-order gradient (e.g. T_z) is estimated from a combination of its gradients (e.g. T_{xz}, T_{yz},

T_{zz}) in the frequency domain. The frequency domain formulas for plane integration lead to some new integral formulas in the space domain, relating for example T and T_x, T_y, T_z. The method uses all the gradient measurements at once for the whole area. To make the method computationally efficient, the Fast Fourier Transform (FFT) is employed. It requires the data points to be on a regular two-dimensional grid and assumes flat earth approximation. Due to the lack of actual gradiometer data, simulated data were used.

The thesis has been subdivided into four main parts. In the first part, i.e. Chapters 2 and 3, background information on the gradiometer sensor hardware is given and the Fourier transform as well as the multiple input-single output filtering equations are reviewed. The second part, namely Chapter 4, deals with the application of the multiple input-single output filtering equations to the estimation of the first-order gradients from the second-order gradients. The simulation of the airborne gradient data is discussed in the third part, consisting of Chapter 5. In the last part of the thesis, contained in Chapters 6, 7, 8, the theoretical formulation is implemented, results are analyzed, the conclusions are drawn and open questions discussed.

Chapter 2

GRAVITY GRADIOMETER SYSTEMS

2.1 THE BASIC HARDWARE CONFIGURATION OF THE BELL GRADIOMETER

The Gravity Gradiometer Survey System (GGSS) is scheduled to be used for airborne gravity gradiometry at the end of 1986 or the beginning of 1987. The system concept will be described in this section. First the basic sensor hardware is presented and then the mechanization equations are analyzed. The GGSS consists of three Bell rotating accelerometer gradiometers. These gradiometers are mounted on an inertially stabilized platform. The system will be integrated with the Global Positioning System (GPS) updating the position obtained from the inertial system at regular intervals.

Each of the three gradiometers consists of four accelerometers positioned on a rotating platform. The rotation axis is perpendicular to the sensitive axes of the accelerometers. A typical gradiometer is shown in Fig. 2.1 where ω denotes the angular velocity and z the rotation axis.

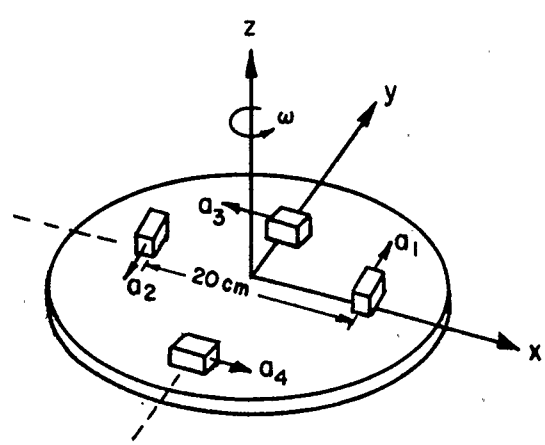

Fig. 2.1 Single Bell Gravity Gradiometer Sensor

The gradiometer measurement f is the combination of the specific forces sensed by all four accelerometers. In other words

$$f = f_1 + f_2 - f_3 - f_4 \tag{2.1}$$

where f_1, f_2, f_3, f_4 are the specific forces sensed by the accelerometers 1, 2, 3, 4. For ideal measurements the specific forces $f_i (i=1,2,3,4)$ can be written as

$$f_i = g_i - a_i \tag{2.2}$$

where g_i and a_i are the gravity component and the acceleration along the sensitive axis of the ith accelerometer respectively. The concept of gravity, gravity potential and gravity gradients are discussed in chapter 4 of this thesis and they are clearly introduced in Heiskanen and Moritz (1967). The gravity vector $\underline{g}_i$ at the location i can be described by the sum of the gravity vector at the origin $\underline{g}_0$ and the gravity gradient matrix $\underline{W}_{ij}$ multiplied by the position vector $\underline{r}_i$ of the point i

$$\underline{g}_i = \underline{g}_0 + \underline{W}_{ij}\, \underline{r}_i \tag{2.3}$$

where

$$\underline{W}_{ij} = \begin{bmatrix} W_{xx} & W_{xy} & W_{xz} \\ W_{xy} & W_{yy} & W_{yz} \\ W_{xz} & W_{yz} & W_{zz} \end{bmatrix} \tag{2.4}$$

$$\underline{r}_1 = -\underline{r}_2 = \begin{bmatrix} R\cos\omega t \\ R\sin\omega t \\ 0 \end{bmatrix} \tag{2.5}$$

$$\underline{r}_3 = -\underline{r}_4 = \begin{bmatrix} -R\sin\omega t \\ R\cos\omega t \\ 0 \end{bmatrix} \tag{2.6}$$

where R is the distance between the origin of the cartesian system of the platform and each accelerometer. In equations (2.3), (2.4), (2.5), (2.6) and all the following equations underlined small letters denote vectors and underlined capital letters denote matrices. The gravity component g_i is related to the gravity vector $\underline{g}_i$ by the following relation (White, 1980)

$$g_i = \underline{s}_i^t \, \underline{g}_i \tag{2.7}$$

where

$$\underline{s}_1 = -\underline{s}_2 = \begin{bmatrix} -\sin\omega t \\ \cos\omega t \\ 0 \end{bmatrix} \tag{2.8}$$

$$\underline{s}_3 = -\underline{s}_4 = \begin{bmatrix} -\cos\omega t \\ -\sin\omega t \\ 0 \end{bmatrix} \tag{2.9}$$

and the superscript t in equation (2.7) denotes the transpose of a vector. For a space-stable platform the accelerations are mutually opposite

$$\begin{aligned} a_1 &= -a_2 \\ a_3 &= -a_4 \, . \end{aligned} \tag{2.10}$$

Thus combining equations (2.1), (2.2), (2.3) and (2.10) the measurement f is expressed as

$$f = \underline{s}_1^t \, \underline{W}_{ij} \, \underline{r}_1 + \underline{s}_2^t \, \underline{W}_{ij} \, \underline{r}_2 - \underline{s}_3^t \, \underline{W}_{ij} \, \underline{r}_3 - \underline{s}_4^t \, \underline{W}_{ij} \, \underline{r}_4 \qquad (2.11)$$

and making use of equations (2.5), (2.6), (2.8), (2.9) and (2.10), equation (2.11) takes the form

$$f = 2 \, \underline{s}_1^t \, \underline{W}_{ij} \, \underline{r}_1 - 2 \, \underline{s}_3^t \, \underline{W}_{ij} \, \underline{r}_3 \quad \text{, or} \qquad (2.12)$$

$$f = R(W_{yy} - W_{xx})\sin 2\omega t + 2RW_{xy}\cos 2\omega t \; . \qquad (2.13)$$

Equation (2.13) shows clearly that the second-order gradients of the gravity potential are modulated at twice the frequency of the platform rotation. In case of angular velocity with components Ω_x, Ω_y in the x and y axes equation (2.13) is rewritten as

$$f = R(W_{yy} - W_{xx} + \Omega_x{}^2 - \Omega_y{}^2)\sin 2\omega t + 2R(W_{xy} - \Omega_x \, \Omega_y)\cos 2\omega t. \qquad (2.14)$$

The quantities $(\Omega_x^2 - \Omega_y^2)\sin 2\omega t$ and $(-\Omega_x \Omega_y)\cos 2\omega t$ are the so called centripetal gradients. Besides the gravity and the centripetal gradients, a gradiometer also senses self gradients and gradients caused by acceleration sensitivity (Hutcheson and Grierson, 1985). Self gradients are caused by masses close to the measuring instrument and are part of the total gravitational gradients. They are subdivided into two categories. One caused by masses in the outer area of the instrument and one in the close proximity of it. The self gradients are eliminated analytically by the self-gradient function. Most of the gradients caused by acceleration sensitivity

contain spectral components at frequency bands centered at multiples of the rotation rate ω and are eliminated by calibration. When the self-gradient, linear acceleration sensitivity and centripetal gradient corrections are made, the remaining signal is demodulated at twice the rotation frequency and it is filtered to generate the inline output f_I and the cross channel outputs f_c defined by

$$f_I = R(W_{yy} - W_{xx}) \tag{2.15}$$

$$f_c = 2RW_{xy} \ . \tag{2.16}$$

From equations (2.15), (2.16) the total gradiometer system output $\underline{l}$, after the elimination of the normal gravity field effect, is given after changing the signs of the in-line output, by

$$\underline{l} = \begin{bmatrix} \frac{T_{xx} - T_{yy}}{2} \\ T_{xy} \\ \frac{T_{zz} - T_{xx}}{2} \\ T_{xz} \\ \frac{T_{yy} - T_{zz}}{2} \\ T_{yz} \end{bmatrix} \tag{2.17}$$

where T denotes the anomalous gravity potential. The vector $\underline{l}$ is related linearly to the gradient vector $\underline{T}_{ij}$ containing the anomalous gradient tensor elements through the matrix $\underline{M}$

$$\underline{l} = \begin{bmatrix} 0.5 & -0.5 & 0.0 & 0.0 & 0.0 & 0.0 \\ 0.0 & 0.0 & 0.0 & 1.0 & 0.0 & 0.0 \\ -0.5 & 0.0 & 0.5 & 0.0 & 0.0 & 0.0 \\ 0.0 & 0.0 & 0.0 & 0.0 & 1.0 & 0.0 \\ 0.0 & 0.5 & -0.5 & 0.0 & 0.0 & 0.0 \\ 0.0 & 0.0 & 0.0 & 0.0 & 0.0 & 1.0 \end{bmatrix} \begin{bmatrix} T_{xx} \\ T_{yy} \\ T_{zz} \\ T_{xy} \\ T_{xz} \\ T_{yz} \end{bmatrix} \tag{2.18}$$

or $$\underline{l} = \underline{M}\,\underline{T}_{ij} \,. \tag{2.19}$$

The actual Bell GGSS system is oriented in an "umbrella" configuration (Jekeli, 1984a). Assuming that the gradiometer moves eastward the umbrella configuration is obtained by first rotating the local coordinate system x,y,z about the y axis by an angle equal to -arctan $\sqrt{2}$. The new coordinate system is then rotated about the new z axis by a -45° angle. In this way the local coordinate system and the new gradiometer coordinate system are related by

$$\begin{bmatrix} x_1 \\ x_2 \\ x_3 \end{bmatrix} = R_3(-45°)R_2(-\arctan\sqrt{2}) \begin{bmatrix} x \\ y \\ z \end{bmatrix} \tag{2.20}$$

where x_1, x_2, x_3 are the coordinates of a point in the gradiometer system. For example using equations (2.18) and (2.20) the final relation between the gradient measurement vector $\underline{l}$ and the gradient vector $\underline{T}_{ij}$ for eastward motion is obtained from

$$\underline{1} = \begin{bmatrix} 0 & 0 & 0 & -\frac{1}{\sqrt{3}} & 0 & -\frac{2}{\sqrt{6}} \\ \frac{1}{6} & -\frac{1}{2} & \frac{1}{3} & 0 & \frac{\sqrt{2}}{3} & 0 \\ \frac{1}{4} & -\frac{1}{4} & 0 & \frac{1}{2\sqrt{3}} & -\frac{\sqrt{2}}{2} & \frac{1}{\sqrt{6}} \\ -\frac{1}{3} & 0 & \frac{1}{3} & \frac{1}{\sqrt{3}} & -\frac{1}{3\sqrt{2}} & -\frac{1}{\sqrt{6}} \\ -\frac{1}{4} & \frac{1}{4} & 0 & \frac{1}{2\sqrt{3}} & \frac{\sqrt{2}}{2} & \frac{1}{\sqrt{6}} \\ -\frac{1}{3} & 0 & \frac{1}{3} & -\frac{1}{\sqrt{3}} & -\frac{1}{3\sqrt{2}} & \frac{1}{\sqrt{6}} \end{bmatrix} \underline{T}_{ij} \tag{2.21}$$

or $$\underline{1} = \underline{M}_1 \, \underline{T}_{ij} \, . \tag{2.22}$$

When the gradiometer is moving northward, equation (2.21) is modified as follows

$$\underline{1} = \begin{bmatrix} 0 & 0 & 0 & \frac{1}{\sqrt{3}} & \frac{2}{\sqrt{6}} & 0 \\ -\frac{1}{2} & \frac{1}{6} & \frac{1}{3} & 0 & 0 & \frac{\sqrt{2}}{3} \\ -\frac{1}{4} & \frac{1}{4} & 0 & -\frac{1}{2\sqrt{3}} & -\frac{1}{\sqrt{6}} & -\frac{\sqrt{2}}{2} \\ 0 & -\frac{1}{3} & \frac{1}{3} & -\frac{1}{\sqrt{3}} & \frac{1}{\sqrt{6}} & -\frac{1}{3\sqrt{2}} \\ \frac{1}{4} & -\frac{1}{4} & 0 & -\frac{1}{2\sqrt{3}} & -\frac{1}{\sqrt{6}} & \frac{\sqrt{2}}{2} \\ 0 & -\frac{1}{3} & \frac{1}{3} & \frac{1}{\sqrt{3}} & -\frac{1}{\sqrt{6}} & -\frac{1}{3\sqrt{2}} \end{bmatrix} \underline{T}_{ij} \tag{2.23}$$

or $$\underline{l} = \underline{M}_1 \, \underline{T}_{ij} \; . \tag{2.24}$$

The gradient vector $\underline{T}_{ij}$ cannot be recovered because the matrices $\underline{M}$ and $\underline{M}_1$ in equations (2.18), (2.21) and (2.23) are singular. For reasons of simplicity only the recovery of $\underline{T}_{ij}$ from equation (2.18) is analyzed. The vector $\underline{T}_{ij}$ has a triad of gradients, namely T_{xx}, T_{yy}, T_{zz} linearly related via Laplace's equation

$$T_{xx} + T_{yy} + T_{zz} = 0 \; . \tag{2.25}$$

Eliminating the element T_{zz} from the vector $\underline{T}_{ij}$, substituting (2.25) into (2.17), (2.18), the following relation holds

$$\underline{l}_R = \underline{M}_R \, \underline{T}_{ij_R} \tag{2.26}$$

or

$$\underline{l}_R = \begin{bmatrix} \dfrac{T_{xx} - T_{yy}}{2} \\ T_{xy} \\ -\dfrac{2T_{xx} + T_{yy}}{2} \\ T_{xz} \\ \dfrac{T_{xx} + 2T_{yy}}{2} \\ T_{yz} \end{bmatrix} = \begin{bmatrix} 0.5 & -0.5 & 0 & 0 & 0 \\ 0 & 0 & 1 & 0 & 0 \\ -1 & -0.5 & 0 & 0 & 0 \\ 0 & 0 & 0 & 1 & 0 \\ 0.5 & 1 & 0 & 0 & 0 \\ 0 & 0 & 0 & 0 & 1 \end{bmatrix} \begin{bmatrix} T_{xx} \\ T_{yy} \\ T_{xy} \\ T_{xz} \\ T_{yz} \end{bmatrix} . \tag{2.27}$$

The matrix $\underline{M}_R$ is still singular but it now has a full column rank. Thus a unique vector $\underline{T}_{ij_R}$ can be computed from the simple least-squares solution

$$\underline{T}_{ij_R} = (\underline{M}_R^T \underline{M}_R)^{-1} \underline{M}_R^T \underline{l}_R \ . \tag{2.28}$$

The full vector $\underline{T}_{ij}$ is then given by the equation

$$\underline{T}_{ij} = \begin{bmatrix} \underline{T}_{ij_R} \\ T_{zz} \end{bmatrix} = \begin{bmatrix} \underline{T}_{ij_R} \\ -(T_{xx}+T_{yy}) \end{bmatrix} . \tag{2.29}$$

2.2 THE BELL GRADIOMETER NOISE

The gradiometer system noise model is derived from spectral analysis of data from the Bell gradiometer. The data were analyzed using Fast Fourier Transform (FFT) techniques and least-squares autoregressive model fitting (White, 1980). Thus the noise models are presented in terms of power spectral densities defined by

$$S_{gg}(u) = \int_{-\infty}^{\infty} e^{-j2\pi ut} R_{gg}(t)\, dt \tag{2.30}$$

where S_{gg} is the power spectral density (PSD) of the function g(t), u is the frequency (in cycles/sec), R_{gg} is the autocorrelation function of g(t) and j is the square root of -1.

Results from the spectral analysis of the gradient data showed that the PSD of the noise is characterized by a low frequency "red" noise and a high frequency white noise. The "red" noise is decaying as u^{-2}, thus the noise PSD can be written as follows

$$S_{nn}(u) = \frac{R}{u^2} + W \tag{2.31}$$

where n denotes the gradiometer noise, R is the red noise constant and W is the white noise constant. The break frequency between the red

and the white noise is between 0.1 mHz and 2 mHz. The constants R,W have been determined for the gradiometer spin axis in vertical position and in horizontal position and are shown in the following table (White, 1980).

Table 2.1

Red and white noise constants (in E^2/Hz)

Red noise		White noise	
Spin axis vertical	Spin axis horizontal	Spin axis vertical	Spin axis horizontal
2.0×10^{-6}	16.0×10^{-6}	81.0	86.0

The gradiometer noise PSD is shown in Fig. 2.2

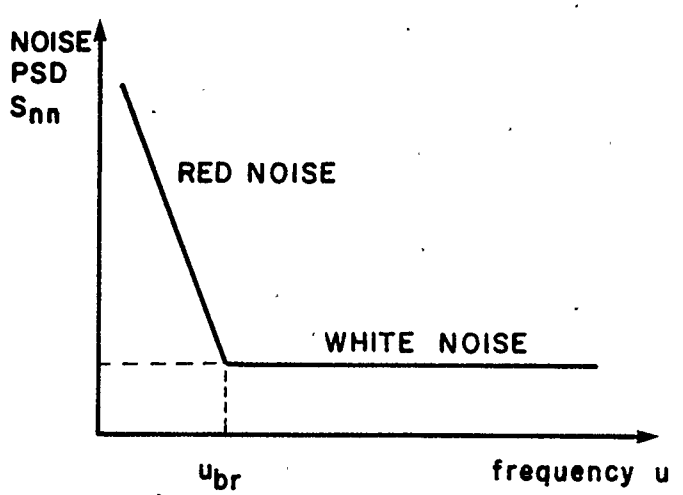

Fig. 2.2 Gradiometer noise PSD(u_{br} denotes break frequency)

Since 1980, the gradiometer noise model has been improved so that the rms noise is 1 Eötvos using a 10 second moving window averager.

2.3 THE SUPERCONDUCTING GRAVITY GRADIOMETER

The recent developments in cryogenic technology and superconductivity have led to the design of gravity gradiometers with much higher sensitivity than room temperature gradiometers as e.g. the Bell gradiometer. The much improved sensitivity in a cryogenic gravity gradiometer is demonstrated mathematically by the equation of the minimum detectable gravity gradient signal W_{ij} (Paik, 1979)

$$W_{ij}^2 \geq \frac{8\omega_o}{Ml^2} \Delta f \{\frac{K_B T_o}{Q} + \frac{K_B T_N}{\beta} [\frac{\omega_o}{\omega_s}]\} \tag{2.32}$$

where M, ω_o, Q, T_o, l, ω_s, β, T_N, Δf are the mass, resonance frequency, quality factor, operational temperature, baseline of the proof masses, signal frequency, transducer coupling coefficient, amplifier noise temperature and detection bandwidth. The resonance frequency ω_o is considered as much higher than the signal frequency. To reduce the level of the minimum detectable gravity gradient signal the two terms inside the parenthesis of eqn. (2.32) have to be minimized. This is achieved by having high quality factors Q as well as very low amplifier noise temperatures T_N. For the operational temperature T_o of liquid helium (4.2° K), quality factors of certain metals can be as high as 10^8. At the same temperature T_o some amplifiers have very low noise temperatures T_N. Under liquid helium temperature the overall reduction in noise is three to four orders of

magnitude smaller than that of a device operating under room temperature (Paik, 1981). Operating a gravity gradiometer in low temperatures provides an environment almost free of thermal gradients. On the other hand superconductivity provides a very good magnetic shielding.

A superconducting gravity gradiometer can either be built in the form of an in-line component gradiometer, or in the form of a cross component gradiometer. Both of these types of gradiometers are non-rotating instruments. A single axis in-line component gradiometer senses the gravity gradient T_{ii} along the sensitive axis i and the common mode forces g_i. A cross-component gradiometer with its super conducting circuit and its sensitive axis j perpendicular to the sensitive axis i, provides the gravity gradient W_{ij} and the common mode angular acceleration a_k. A single in-line superconducting gradiometer is shown in Fig. 2.3.

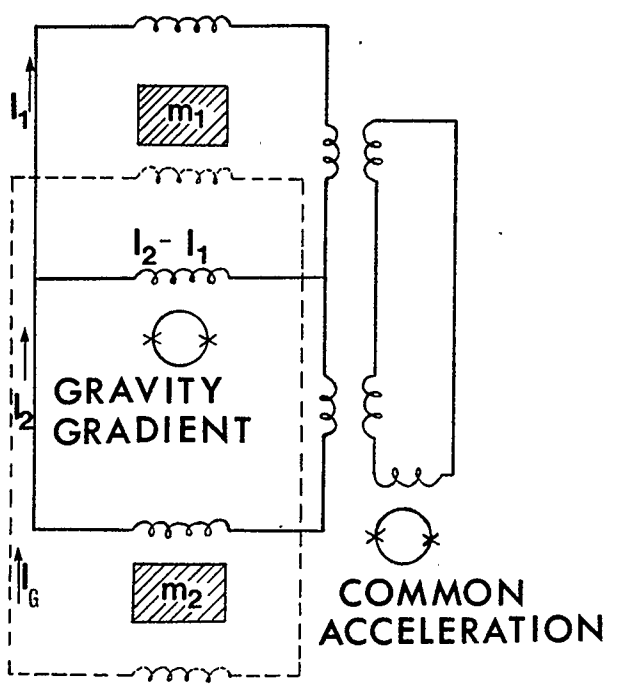

Fig. 2.3 Diagram of an in-line gravity gradiometer.

The superconducting in-line gradiometer consists of two superconducting proof masses allowed to move along a common axis. Each proof mass is surrounded by a pair of superconducting coils connected to form a loop on which a current I_1 or I_2 is stored, respectively. Due to the superconductivity of this loop, magnetic flux is coupled with the displacement of the proof masses. The magnetic signals thus generated are proportional to the gravity gradient T_{ii} and to the common mode acceleration g_i, and are detected by two SQUID (Superconducting Quantum Interference Device) amplifiers, shown in Fig. 2.3 by circles with crosses. Assuming that the sensitive axes of the two proof masses are properly aligned, the common mode accelerations can be balanced by controlling the ratio I_1/I_2 of the two currents stored in the two sensing loops. The same operation principle holds for a cross-component gradiometer, in which the common mode angular accelerations are balanced by properly controlling the ratio of the currents stored in each pair of superconducting loops. The common mode balance of both linear and angular accelerations coupled with the high stability of persistent currents in a superconducting loop provides a low-drift gradiometer with stable scale factors. The linear and angular accelerations of the gradiometer platform are monitored by a superconducting accelerometer (Paik, 1976). The high sensitivity of the superconducting accelero- meters to translational and rotational motions of the platform in the order of $4\times10^{-12}ms^{-2}Hz^{-\frac{1}{2}}$ and $3\times10^{-11}rads^{-2}Hz^{-\frac{1}{2}}$, respectively, opens the way for using an integrated superconducting gradiometer-accelerometer system as an inertial navigation system as well.

At present, a superconducting gradiometer measuring three in-line components of the gradient tensor, has been developed at the University of Maryland by Paik. This gradiometer has been chosen by NASA to be used for satellite gradiometry in the early 90's. The design of the superconducting gradiometer is for a noise of less than $0.07 EHz^{-\frac{1}{2}}$. The noise level currently achievable is definitely much higher than this design noise level. For lower frequencies, between 0.01 Hz and 0.03 Hz, the noise level is about 10-50 $EHz^{-\frac{1}{2}}$. For the rest of the spectrum the noise is at the level of 0.7 to 0.3 $E.Hz^{-\frac{1}{2}}$ (Paik, 1985). It is expected that in a few years however the goal for the noise level will be reached.

Chapter 3

THE FOURIER TRANSFORM, INPUT-OUTPUT FILTERING EQUATIONS

3.1 THE FOURIER TRANSFORM

3.1.1 The Continuous and the Discrete Fourier Transforms

In this section and throughout the following sections two-dimensional problems are analyzed, therefore only two-dimensional Fourier transforms will be discussed. Since many textbooks exist in which Fourier transforms are treated in detail (Brigham, 1974; Bracewell, 1978; Bloomfield, 1975), only a review of the Fourier transform will be given in this section.

The continuous two-dimensional Fourier transform is defined (Bracewell, 1978) as

$$G(u,v) = \mathbf{F}\{g(x,y)\} = \int_{-\infty}^{\infty} \int_{-\infty}^{\infty} g(x,y)\, e^{-j2\pi(ux+vy)}\, dxdy \qquad (3.1)$$

where $G(u,v)$ is the Fourier transform of $g(x,y)$, $\mathbf{F}$ denotes Fourier transform, u and v are the spatial frequencies in cycles per distance (or time) unit and j is the imaginary unit. The continuous inverse two-dimensional Fourier transform is given by

$$g(x,y) = \mathbf{F}^{-1}\{G(u,v)\} = \int_{-\infty}^{\infty} \int_{-\infty}^{\infty} G(u,v)\, e^{j2\pi(ux+vy)}\, dudv \qquad (3.2)$$

where $\mathbf{F}^{-1}$ is the inverse Fourier transform symbol. The autocorrelation function $R_{gg}(x,y)$ of a function $g(x,y)$ is defined by

$$R_{gg}(x,y) = \lim_{\substack{T_1\to\infty \\ T_2\to\infty}} \frac{1}{T_1T_2} \int_{-\frac{T_1}{2}}^{\frac{T_1}{2}} \int_{-\frac{T_2}{2}}^{\frac{T_2}{2}} g(x_0,y_0)g(x+x_0,y+y_0)dx_0dy_0 \tag{3.3}$$

where T_1, T_2 are the record lengths in the x and y directions respectively. For a stationary signal g(x,y) the autocovariance function $C_{gg}(x,y)$ is the same as the autocorrelation function $R_{gg}(x,y)$ except for the fact that the mean is subtracted from the data

$$C_{gg}(x,y) = R_{gg}(x,y) - \mu_g^{\,2} \tag{3.4}$$

where μ_g is the mean of the stationary signal g(x,y). The two-dimensional continuous power spectral density function $S_{gg}(x,y)$ is defined as the Fourier transform of the autocorrelation function

$$S_{gg}(x,y) = \int_{-\infty}^{\infty} \int_{-\infty}^{\infty} R_{gg}(x,y)\, e^{-j2\pi(ux+vy)}\, dxdy\ . \tag{3.5}$$

Cross-correlation, cross-covariance and cross-power spectral density functions are defined in an analogous way as correlation, covariance and power spectral density functions.

The functions given in real-world applications are discrete function values at a finite number of points. If the data are sampled at equidistant points, then the Discrete Fourier Transform (DFT) is used. The DFT of a function g(x,y) sampled at MN points on a regular {x,y} grid is given by

$$G(m\Delta u,n\Delta v) = \Delta x\Delta y \sum_{k=0}^{M-1} \sum_{l=0}^{N-1} g(k\Delta x,l\Delta y)e^{-j2\pi(mk\Delta u\Delta x+nl\Delta v\Delta y)} \tag{3.6}$$

where Δx, Δy are the space intervals in the x, y directions of the grid, $k\Delta x$, $l\Delta y$ are the wavelengths in the x, y directions, Δu, Δv are the frequency intervals in the x,y directions, defined by $\Delta u = 1/T_1$, $\Delta v = 1/T_2$ T_1, T_2 are the record lengths in the x,y directions defined as $T_1 = M\Delta x$, $T_2 = N\Delta y$. Substituting the expressions for Δu, Δv, T_1, T_2 in equation (3.6), the discrete Fourier transform of the function g(x,y) is given by

$$G(m\Delta u,n\Delta v) = \frac{T_1}{M} \frac{T_2}{N} \sum_{k=0}^{M-1} \sum_{l=0}^{N-1} g(k\Delta x,l\Delta y)e^{-j2\pi(\frac{mk}{M} + \frac{nl}{N})} \tag{3.7}$$

and similarly the inverse discrete Fourier transform is defined as

$$g(k\Delta x,l\Delta y) = \frac{1}{T_1} \frac{1}{T_2} \sum_{m=0}^{M-1} \sum_{n=0}^{N-1} G(m\Delta u,n\Delta v)e^{j2\pi(\frac{mk}{M} + \frac{nl}{N})} . \tag{3.8}$$

Using only k,l and m,n instead of wavelengths $k\Delta x$, $l\Delta y$ and frequencies $m\Delta u$, $n\Delta v$ respectively, equations (3.7), (3.8) take the form

$$G(m,n) = F\{g(k,l)\} = \frac{T_1}{M} \frac{T_2}{N} \sum_{k=0}^{M-1} \sum_{l=0}^{N-1} g(k,l)e^{-j2\pi(\frac{mk}{M} + \frac{nl}{N})} \tag{3.9}$$

$$g(k,l) = F^{-1}\{G(m,n)\} = \frac{1}{T_1}\frac{1}{T_2}\sum_{m=0}^{M-1}\sum_{n=0}^{N-1} G(m,n)e^{j2\pi(\frac{mk}{M}+\frac{nl}{N})} . \quad (3.10)$$

An unbiased estimate of the discrete power spectral density for ν sample records is obtained from the formula

$$\hat{S}_{gg}(m,n) = \frac{1}{\nu T_1 T_2}\sum_{\tau=1}^{\nu} G_\tau^*(m,n)G_\tau(m,n) \quad (3.11)$$

where G is the discrete spectrum of the function g(x,y) and G* is the complex conjugate of G. The discrete autocorrelation and autocovariance functions $R_{gg}(k,l)$ and $C_{gg}(k,l)$ are defined as the inverse discrete Fourier transforms of the discrete power spectral density function

$$R_{gg}(k,l) = C_{gg}(k,l) + \mu_g^2 = F^{-1}\{S_{gg}(m,n)\} . \quad (3.12)$$

3.1.2 The Properties of the Discrete Fourier Transform

The properties of the Fourier transform are derived in a number of text books (Papoulis, 1968; Bracewell, 1978). Here only the properties necessary for this research are listed.

i) Space shifting $g(k-k_0,l-l_0) \xleftrightarrow{F} G(m,n)\, e^{-j2\pi(\frac{mk_0}{M}+\frac{nl_0}{N})}$ (3.13)

ii) Time scaling $g(ak,bl) \xleftrightarrow{F} \frac{1}{|ab|} G(\frac{m}{a},\frac{n}{b})$ (3.14)

iii) Space domain convolution $g_1(k,l)*g_2(k,l) \xleftrightarrow{F} G_1(m,n)G_2(m,n)$ (3.15)

iv) Partial differentiation $\frac{\partial g(k,l)}{\partial k} \overset{F}{\longleftrightarrow} j2\pi m G(m,n)$ (3.16)

$$\frac{\partial g(k,l)}{\partial l} \overset{F}{\longleftrightarrow} j2\pi n G(m,n) \tag{3.17}$$

$$\frac{\partial^2 g(k,l)}{\partial k^2} + \frac{\partial^2 g(k,l)}{\partial l^2} \overset{F}{\longleftrightarrow} -4\pi^2(m^2+n^2)G(m,n) \tag{3.18}$$

v) Multiplication by wavelength $kg(k,l) \overset{F}{\longleftrightarrow} j\,\frac{\partial G(m,n)}{\partial m}$ (3.19)

$$lg(k,l) \overset{F}{\longleftrightarrow} j\,\frac{\partial G(m,n)}{\partial n} \tag{3.20}$$

$$klg(k,l) \overset{F}{\longleftrightarrow} -\frac{\partial^2 G(m,n)}{\partial m \partial n} \tag{3.21}$$

vi) dc value $G(0,0) = \frac{T_1}{M}\frac{T_2}{M}\sum_{k=0}^{M-1}\sum_{l=0}^{N-1} g(k,l) = T_1 T_2 \mu_g$ (3.22)

For an isotropic function g(k,l) we also have

$$g(k,l) = g(\sqrt{k^2 + l^2})\ . \tag{3.23}$$

In this case the two-dimensional Fourier transform equals the Hankel transform

$$G(m,n) = \bar{G}(\sqrt{m^2 + n^2}) \tag{3.24}$$

where the Hankel transform of an isotropic function g(r) is defined by

$$g(r) \overset{h}{\longleftrightarrow} \bar{G}(\omega) = \int_0^\infty r\, g(r)\, J_0(\omega r)\, dr \tag{3.25}$$

where the symbol h denotes Hankel transform, and the function $J_0(x)$ is the unmodified zero-order Bessel function.

3.1.3 Spectral Leakage and Aliasing Effects

The discrete Fourier transform is periodic in both domains, the space and the frequency domain. This implies that the finite data sets on which the DFT is applied should be strictly speaking periodic. In practice though, it is rather rare to deal with data sets periodic over their record length. Most of the time the data sets are not periodic, and furthermore they are discontinuous at the edges of the record length. When these non-periodic discontinuous sets of data are transformed in the frequency domain, through the DFT, the components with frequencies other than those spanning the discrete sampled spectrum contribute to those "basis" frequencies. This is the problem of spectral leakage (Brigham, 1974). To reduce the spectral leakage effects, smooth windows eliminating discontinuities at the edges of the record length are used to multiply the data. These windows have zero values at the edges. By multiplying a set of data by a window, a spectral component of any frequency is projected only on those basis frequencies which are very close to this component frequency. Two windows are used in this research, the Kaiser-Bessel window and the cosine taper rectangular window. The one-dimensional Kaiser-Bessel window has a flat part for the (1-b) portion of its record length and a (b/2) part expressed in terms of the zero-order modified Bessel function at each edge of the record length. It can be expressed by

$$w(l) = \begin{cases} \dfrac{I_0(\pi\alpha[1-(\frac{2l}{M})^2]^{\frac{1}{2}})}{I_0(\pi\alpha)} & , \quad \text{for} \quad 0 \leq l \leq b\,\frac{M}{2} \\ 1.0 & , \quad \text{for} \quad \frac{b}{2}M \leq l \leq [1-\frac{b}{2}]M \\ \dfrac{I_0(\pi\alpha[1-(\frac{2(M-l)}{M})^2]^{\frac{1}{2}})}{I_0(\pi\alpha)} & , \quad \text{for} \quad [1-\frac{b}{2}]M \leq l \leq M-1 \end{cases} \tag{3.26}$$

where $I_0(x)$ is the zero-order modified Bessel function of the first kind, and the argument α is equal to 3.0. The one-dimensional cosine taper window has a flat part for the (1-b) part of the record length and a (b/2) cosine lobe part at each edge of the record length. It is expressed by

$$w(l) = \begin{cases} 0.5(1.0 - \cos[\frac{2}{b}\frac{\pi l}{M}]) & , \quad \text{for } 0 \leq l \leq \frac{b}{2}M \\ 1.0 & , \quad \text{for } \frac{b}{2}M \leq l \leq [1-\frac{b}{2}]M \\ 0.5(1.0 - \cos[\frac{2}{b}\frac{\pi(M-l)}{M}]) & , \quad \text{for } [1-\frac{b}{2}]M \leq l \leq M-1 \,. \end{cases}$$

For two dimensional problems the gridded data are first windowed row by row and then column by column using a 1-D window or vice versa. When a window is applied to a data set, there is clearly a loss of power. This lost power in the data set can be accounted for by applying a correction factor

$$CF = \frac{1}{MN} \sum_{k=0}^{M-1} \sum_{l=0}^{N-1} w^2(k,l) \tag{3.27}$$

where M, N is the number of points in the two dimensions and w(k,l) is the window. More details on specific windows and their spectral characteristics can be found in Harris (1978).

As was mentioned in section 3.1.1, the data sets encountered in actual applications consist of a number of discrete regularly spaced points. These points can be considered as the sample values of a continuous function. The sampling theorem states under which conditions the original function can be reconstructed from its sampled values. A continuous function g(x) can be uniquely reconstructed from a set of known sample values $g(x_i)$, if the Fourier transform of g(x), G(u), is zero for all frequencies higher than u_N. The frequency u_N is called the Nyquist frequency. The quantity Δx

$$\Delta x = \frac{1}{2u_N} \tag{3.28}$$

is called the Nyquist sampling rate and it is the maximum sampling rate allowable to represent the original function. In case of a larger sampling rate, the spectrum of this function is distorted. This distortion of the spectrum is called aliasing. Details on aliasing, its effects and how to minimize aliasing are given in Bendat and Piersol (1971) and Brigham (1974).

3.1.4 The Fast Fourier Transform (FFT)

The Fast Fourier Transform is an ingenious way to compute the Discrete Fourier Transform (DFT) of a data set. It computes the DFT

of a data set using complex operations proportional to MlogM. The normal DFT requires complex operations proportional to M^2. The Fast Fourier Transform was originally developed by Cooley and Tukey (1965). Since then it has made the spectral analysis much more efficient. Furthermore it has contributed to the solution of a broad range of problems which previously were considered almost intractable. In geodesy for example the use of FFT has facilitated the computation of global geoidal undulations and gravity anomalies (Colombo, 1981), the use of gravity data for geophysical inversion problems (Forsberg, 1984a), the computation gravity anomaly covariance functions (Vassiliou and Schwarz, 1985), etc. Standard routines exist for computing the FFT of a given data set. The International Mathematical and Statistical Library (IMSL) and the geophysics software package MAGEV contain such routines. For the purpose of this research, the FFT subroutines from IMSL were used.

3.1.5 Interpolation Using the Fast Fourier Transform

A signal sampled at equidistant points can be interpolated using the Fourier transform. For simplicity, this section deals with one-dimensional signals only. Suppose that the given signal $h(k\Delta x)$, where Δx is the sampling interval, has to be interpolated in such a way that the new sampling interval is L times smaller than the initial one

$$\Delta x' = \frac{\Delta x}{L} \tag{3.29}$$

where L is a positive integer and $\Delta x'$ is the new sampling interval. The meaning of this interpolation is that L-1 sample values are

estimated between a pair of sample values of the original signal. To get the interpolation procedure going, L-1 zeros are filled in between each pair of samples of the signal h(k), thus resulting in the new signal g(l) expressed as

$$g(l) = \begin{cases} h(l/L) & \text{for} \quad l = 0, \pm L, \pm 2L, \ldots \\ 0 & \text{elsewhere} . \end{cases} \tag{3.30}$$

The new signal g(l) has the following spectrum, see eqn. (3.14)

$$G(m) = H(mL) \tag{3.31}$$

where G,H are the Fourier transforms of the input signals g,h respectively, and m is the wavenumber in the frequency domain. The previous equation entails that the spectrum G has a period equal L times the period of the spectrum H. Therefore this spectrum has besides the band frequencies in the interval (- 1/L, 1/L), which are of interest, the same frequency band centered at the frequencies $\pm \frac{2}{L}$, $\pm \frac{4}{L}$ etc. Those frequencies are not wanted, and therefore, have to be filtered out by a low-pass filter which ideally would be expressed as

$$E_1(m) = \begin{cases} C & \text{for frequencies} \quad -\frac{1}{L} \leq v \leq \frac{1}{L} \\ 0 & \text{elsewhere} \end{cases} \tag{3.32}$$

where E_1 is the frequency response of the filter $e_1(l)$ and C is a constant which remains to be determined. The signal $g_1(l)$ resulting from the filtering of the signal $h(l)$ with the filter $e_1(l)$, has a Fourier transform G_1

$$G_1(m) = \begin{cases} CH(mL) & \text{for frequencies} \quad -1/L \leq v \leq 1/L \\ 0 & \text{elsewhere} . \end{cases} \tag{3.33}$$

The constant C can be determined by matching the zero samples of the signals $h(l)$ and $g_1(l)$, $h(0)$ and $g_1(0)$ respectively. The sample $g_1(0)$ is expressed

$$g_1(0) = \int_{-1}^{1} G_1(v)dv = \int_{-L}^{L} E_1(v)H(vL)dv \quad , \text{ or}$$

$$g_1(0) = C \int_{-\frac{1}{L}}^{\frac{1}{L}} H(vL)dv = C \int_{-1}^{1} H(v)dv/L \quad , \text{ or} \tag{3.34}$$

$$g_1(0) = \frac{C}{L} h(0) .$$

Hence, in order to match the amplitudes of the interpolated and original signals $g_1(l)$ and $h(l)$ respectively, the constant C has to be equal to L. More details about interpolation and decimation of a signal using digital filters can be found in Schafer and Rabiner (1973), and a tutorial review in Crochiere and Rabiner (1981).

3.2 INPUT-OUTPUT FILTERING EQUATIONS

The problem of estimating the first-order from the second-order gradients of the anomalous potential can be considered as a filtering problem. In this filtering process each first-order gradient is the output of one or at most five second-order gradients. Therefore the present estimation problem can be thought of as a multiple (single) input-single output filtering problem. This filtering is discussed in the next two sections. First the single input-single output filtering problem is discussed and then the multiple input-single output filtering is presented. All these filtering problems are formulated in the frequency domain. An alternative method in the space domain which can handle this estimation problem is least-squares collocation (Krarup, 1969; Moritz, 1980). However as it has already been mentioned in chapter 1, the application of least-squares collocation to very large data sets is practically impossible. Also application of frequency-domain collocation for very large data sets is not advisable. A better way of solving the estimation problem posed in this thesis is by employing a multidimensional Wiener filter. The relations among multiple input-single output, multidimensional Wiener filter and least-squares collocation in the space domain are presented in section 3.3.

3.2.1 Single Input - Single Output Filtering Equations

Suppose that a continuous stationary signal described by a function $f(x,y)$ is filtered by the filter function $h(x,y)$, thus producing an output signal described by the function $g(x,y)$. This can be mathematically described by the equation

$$g(x,y) = \int_{-\infty}^{\infty}\int_{-\infty}^{\infty} h(x_0,y_0)\, f(x-x_0,y-y_0)\, dx_0 dy_0 \tag{3.35}$$

where (x_0,y_0) are the points at which the signal $h(x,y)$ takes non zero values. From equation (3.35), the autocorrelation function of the signal $g(x,y)$ as well as the cross-correlation function of the signals $f(x,y)$, $g(x,y)$ are derived

$$R_{gg}(x,y)= \int_{-\infty}^{\infty}\int_{-\infty}^{\infty} h(x_1,y_1)h(x_2,y_2)R_{ff}(x+x_1-x_2,y+y_1-y_2)dx_1dx_2dy_1dy_2 \tag{3.36}$$

$$R_{f,g}(x,y)= \int_{-\infty}^{\infty}\int_{-\infty}^{\infty} h(x_1,y_1)R_{ff}(x-x_1,y-y_1)dx_1dy_1 \ . \tag{3.37}$$

Taking the Fourier transforms of both sides of equations (3.36) and (3.37) leads to

$$S_{gg}(u,v) = |H(u,v)|^2\, S_{ff}(u,v) \tag{3.38}$$

$$S_{f,g}(u,v) = H(u,v)\, S_{ff}(u,v) \tag{3.39}$$

where $H(u,v)$ is the Fourier transform of the filter function $h(x,y)$ and is called frequency response function or transfer function. Equations (3.38), (3.39) are the well-known input/output filtering equations, for an ideal linear system (Bendat and Piersol, 1980). The filtering equation (3.35) can be readily transformed in the frequency domain using property (3.15) of the Fourier transform

$$G(u,v) = H(u,v)\, F(u,v) \tag{3.40}$$

where $G(u,v)$, $F(u,v)$ are the Fourier transforms of the functions $f(x,y)$, $g(x,y)$. The coherence function between the functions $f(x,y)$, $g(x,y)$ is defined as

$$\gamma^2_{f,g}(u,v) = \frac{|S_{f,g}(u,v)|^2}{S_{ff}(u,v)S_{gg}(u,v)} \quad . \tag{3.41}$$

The coherence function takes values in the range (0,1). A coherence function equal to unity means that the input-output signals are linearly related. In case of a coherence function not equal to unity, there is either a non-linear relation between input and output, or there exists another input or noise. In this last case assuming uncorrelated input signal $f(x,y)$ and noise $n(x,y)$, equations (3.38) and (3.39) are modified as follows

$$S_{gg}(u,v) = |H(u,v)|^2\{S_{ff}(u,v) + S_{nn}(u,v)\} \tag{3.42}$$

$$S_{f,g}(u,v) = H(u,v)\{S_{ff}(u,v) + S_{nn}(u,v)\} \tag{3.43}$$

where $S_{nn}(u,v)$ is the power spectral density of the noise. Equations (3.38), (3.39) (3.42) and (3.43) are used in this research for system identification, which means that given the PSD's of the input and output signals, the frequency response function can be readily computed. Then the use of the inverse Fourier transform provides directly the impulse response function in the space domain.

3.2.2 Multiple Input-Single Output Filtering Equations

A number of q stationary signals $f_i(x,y)$ $(i=1,2,\ldots,q)$ are filtered through q linear systems with frequency response functions $H_i(u,v)$, so that they produce a single output $g(x,y)$. For the sake of simplicity it is assumed that q=2, in other words two inputs $f_i(x,y)$, $(i=1,2)$, produce a single output $g(x,y)$. This is illustrated in Fig. 3.1.

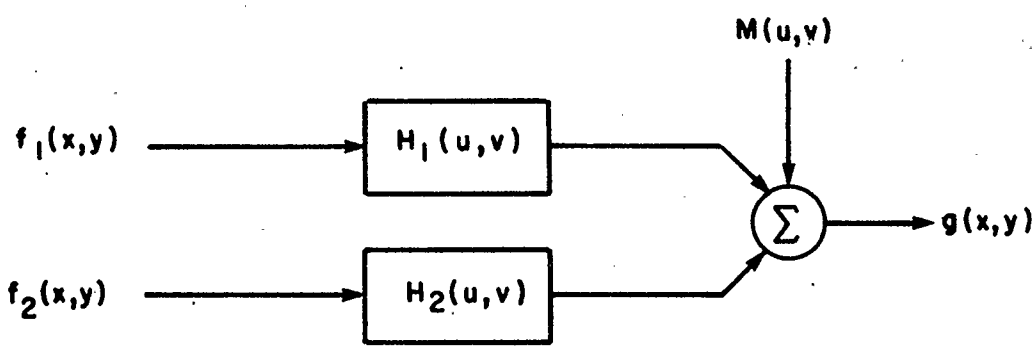

Fig. 3.1 Two input-single output system

In Fig. 3.1 above, the spectrum of the output signal equals the sum of the spectra of the filtered input signals (ideal linear system). Any deviations from the ideal linear system are modelled by the system errors $m(x,y)$ the spectrum of which $M(u,v)$ is shown in this figure.

In most cases $M(u,v)$ represents the spectrum of small high frequency effects from other possible inputs. For simplicity it is noted in Fig. 3.1 as additive effect to the sum of the filtered inputs f_1, f_2 . The perturbed two input-single output system is described by the equation

$$G(u,v) = H_1(u,v)F_1(u,v) + H_2(u,v)F_2(u,v) + M(u,v) \quad (3.44)$$

where $F_1(u,v)$, $F_2(u,v)$, $G(u,v)$ are the spectra of the signals $f_1(x,y)$, $f_2(x,y)$ and $g(x,y)$ respectively. From equation (3.44) it is easy to derive the power spectral density of the output $g(x,y)$, as well as the cross-spectral densities of $g(x,y)$ with each of the inputs

$$S_{gg}(u,v) = \sum_{i=1}^{2} \sum_{j=1}^{2} H_i^*(u,v)H_j(u,v)S_{f_i,f_j}(u,v) + S_{mm}(u,v) \quad (3.45)$$

$$S_{f_i,g}(u,v) = \sum_{j=1}^{2} H_j(u,v)S_{f_i,f_j}(u,v) + S_{f_i,m}(u,v) \quad i=1,2 . \quad (3.46)$$

The optimum double input-single output system is the one which minimizes the PSD of the system errors $m(x,y)$ for all possible choices of the transfer functions H_i (Bendat and Piersol, 1980). From equation (3.45) the PSD of $m(x,y)$ equals

$$S_{mm}(u,v) = S_{gg}(u,v) - \sum_{i=1}^{2} \sum_{j=1}^{2} H_i^*(u,v)H_j(u,v)S_{f_i,f_j}(u,v) . \quad (3.47)$$

According to the previously stated criterion of optimality, the following conditions should be fulfilled

$$\frac{\partial S_{mm}(u,v)}{\partial H_i^*(u,v)} = 0 \qquad i=1,2 \ . \tag{3.48}$$

Using equation (3.47), equation (3.48) can be rewritten

$$S_{f_i,g}(u,v) - \sum_{j=1}^{2} H_j(u,v) S_{f_i,f_j}(u,v) = 0 \ , \quad \text{or}$$

$$S_{f_i,g}(u,v) = \sum_{j=1}^{2} H_j(u,v) S_{f_i,f_j}(u,v) \qquad i=1,2 \ . \tag{3.49}$$

Equation (3.49) is similar to equation (3.46), except for the fact that the cross-spectral density between each input and the system error m(x,y) is zero. This in turn implies that the optimum system requires that each input be uncorrelated with the system error function. The optimum frequency response functions for the double input-single output system are obtained from the solution of the two linear equations (3.49) which can be written analytically

$$S_{f_1,g}(u,v) = H_1(u,v) S_{f_1,f_1}(u,v) + H_2(u,v) S_{f_1,f_2}(u,v) \tag{3.50a}$$

$$S_{f_2,g}(u,v) = H_1(u,v) S_{f_2,f_1}(u,v) + H_2(u,v) S_{f_2,f_2}(u,v) \ . \tag{3.50b}$$

The solution to the system of linear equations (3.50a), (3.50b) is given (Bendat and Piersol, 1980) by

$$H_1(u,v) = \frac{S_{f_2,f_2}(u,v) S_{f_1,g}(u,v) - S_{f_1,f_2}(u,v) S_{f_2,g}(u,v)}{S_{f_1,f_1}(u,v) S_{f_2,f_2}(u,v) - |S_{f_1,f_2}(u,v)|^2} \tag{3.51a}$$

$$H_2(u,v) = \frac{S_{f_1,f_1}(u,v)S_{f_2,g}(u,v) - S_{f_2,f_1}(u,v)S_{f_1,g}(u,v)}{S_{f_1,f_1}(u,v)S_{f_2,f_2}(u,v) - |S_{f_1,f_2}(u,v)|^2} \cdot \quad (3.51b)$$

A very interesting case occurs when the input signals $f_1(x,y)$, $f_2(x,y)$ are linearly related. In this case the formulas (3.51a), (3.51b) can not be applied simply because, due to the linear relation, the coherence function becomes unity. This means that the denominator of both equations (3.51a) and (3.51b) is zero. In this case the optimum transfer functions $H_i(u,v)$ (i=1,2) can be derived in an easy way analytically by observing that due to the linearity of the input signals the following relations hold

$$H_2(u,v)S_{f_1,f_2}(u,v) = H_1(u,v)S_{f_2,f_2}(u,v) \quad (3.52a)$$

$$H_1(u,v)S_{f_2,f_1}(u,v) = H_2(u,v)S_{f_1,f_1}(u,v) \ . \quad (3.52b)$$

Substitution of equations (3.52a) and (3.52b) into equations (3.50a), (3.50b) yields the solution for the transfer functions $H_1(u,v)$, $H_2(u,v)$ for the case of linearly dependent inputs

$$H_1(u,v) = \frac{S_{f_1,g}(u,v)}{S_{f_1,f_1}(u,v) + S_{f_2,f_2}(u,v)} \quad (3.53a)$$

$$H_2(u,v) = \frac{S_{f_2,g}(u,v)}{S_{f_1,f_1}(u,v) + S_{f_2,f_2}(u,v)} . \quad (3.53b)$$

Assuming that the same measurement noise $\eta(x,y)$ affects both input signals $f_1(x,y)$, $f_2(x,y)$, equations (3.53a), (3.53b) take the form

$$H_1(u,v) = \frac{S_{f_1,g}(u,v)}{S_{f_1,f_1}(u,v) + S_{f_2,f_2}(u,v) + S_{nn}(u,v)} \tag{3.54a}$$

$$H_2(u,v) = \frac{S_{f_2,g}(u,v)}{S_{f_1,f_1}(u,v) + S_{f_2,f_2}(u,v) + S_{nn}(u,v)} \tag{3.54b}$$

where $S_{nn}(u,v)$ is the PSD of the noise. Equations (3.51a), (3.51b), (3.53a), (3.53b), (3.54a), (3.54b) can be easily extended to the multidimensional case when more than two input signals exist. More details on multiple/single output problems can be found in Bendat and Piersol (1980). The multiple input-single output filtering equations were used extensively in this research. The second-order gradients of the anomalous gravity potential are used as input signals, individual single first-order gradient as output. Due to the linear relations among the second-order gradients, equations (3.53a), (3.53b), (3.54a), (3.54b) are particularly useful as will be shown in chapters 4 and 7.

3.3 WIENER FILTERS, LEAST-SQUARES COLLOCATION AND MULTIPLE INPUT-SINGLE OUTPUT FILTERS

Recently, Jekeli (1985) derived a relation between the second-order gradients and the first-order gradients based on multidimensional Wiener filtering. The derivation of this relation emanates from least-squares collocation and multiple input-single output filtering. The following discussion goes along similar lines to the derivation of the Wiener filter equations discussed in Jekeli (1984a, 1985).

Suppose a vector of p_1 continuous stationary measurements of field-related quantities $\underline{u}_1$ collected at each point (x,y) of the infinite plane is given. Those measurements are corrupted by stationary noise $\underline{n}(x,y)$ uncorrelated to $\underline{u}_1$

$$\underline{l}(x,y) = \underline{u}_1(x,y) + \underline{n}(x,y) \ . \tag{3.55}$$

Assume that another vector of field-related quantities $\underline{u}_2(x,y)$ with p_2 elements jointly stationary with $\underline{u}_1(x,y)$ has to be estimated. The Wiener filter estimates $\underline{u}_2$ from $\underline{u}_1$ in the sense that provides the linear minimum variance estimator $\hat{\underline{u}}_2$. A linear estimator of $\underline{u}_2$ in terms of $\underline{u}_1$ is an integral estimator of the form

$$\hat{\underline{u}}_2(x_0,y_0) = \int_{-\infty}^{\infty}\int_{-\infty}^{\infty} \underline{K}[(x_0,y_0),(x,y)]\ \underline{u}_1(x,y)dx_1dy_1 \tag{3.56}$$

where $\underline{K}[(x_0,y_0),(x,y)]$ is a $p_1 x p_2$ matrix of (x_0,y_0) and (x,y) which remains to be determined. Due to the joint stationarity of $\underline{u}_1(x,y)$, $\underline{u}_2(x,y)$ the matrix $\underline{K}$ possesses the following property

$$\underline{K}[(x_0+x_1,y_0+y_1),\ (x+x_1,y+y_1)] = \underline{K}[(x_0,y_0),\ (x,y)] \ . \tag{3.57}$$

Combining equations (3.56) and (3.57) leads to

$$\hat{\underline{u}}_2(x_0,y_0) = \int_{-\infty}^{\infty}\int_{-\infty}^{\infty} \underline{K}(x_0-x,y_0-y)\ \underline{u}_1(x,y)dx_1dy_1 \ . \tag{3.58}$$

A minimum variance estimate is obtained by determining the matrix $\underline{K}$ in such a way that the variance of the ith residual in the estimate $\hat{\underline{u}}_2(x_0,y_0)$ is minimum. This can be mathematically expressed by

$$\mathrm{var}\{u_{2_i}(x_0,y_0)-\hat{u}_{2_i}(x_0,y_0)\} = \mathrm{var}\{\delta u_{2_i}(x_0,y_0)\} = \text{minimum.} \quad (3.59)$$

If the random quantities $u_i(x,y)$ $(i=1,2,3,\ldots,p_1)$ generate a Hilbert space H_1, then obviously the elements of the estimator $\underline{\hat{u}}_2(x_0,y_0)$ belong to that space as well. From the well known projection theorem of Hilbert spaces, it follows that the residual of the ith element of the estimator $\underline{\hat{u}}_2(x_0,y_0)$ must be orthogonal to each element of the Hilbert space H_1, and thus to each element of the measurement vector $\underline{1}$

$$E\{[u_{2_i}(x_0,y_0)-\hat{u}_{2_i}(x_0,y_0)]1_k(x,y)\} = 0 \quad (3.60)$$

where E denotes the expectation operator. The element $\hat{u}_{2_i}(x_0,y_0)$ is expressed by formula (3.58)

$$\hat{u}_{2_i}(x_0,y_0) = \sum_{j=1}^{p_1} \int_{-\infty}^{\infty} \int_{-\infty}^{\infty} \underline{K}_{ij}(x_0-x_1,y_0-y_1)u_{1_j}(x_1,y_1)dx_1dy_1 \quad (3.61)$$

Substitution of (3.61) into (3.60) yields

$$\underline{R}_{u_2,1} = \int_{-\infty}^{\infty} \cdot \int_{-\infty}^{\infty} \underline{K}(\underline{r}-\underline{r}_1)\, \underline{R}_{1,1}(\underline{r}_1)\, ds_1ds \quad (3.62)$$

where $\underline{R}_{u_2,1}$ is the cross-correlation matrix of $\underline{u}_2,\underline{1}$ and $\underline{R}_{11}$ is the autocorrelation matrix of $\underline{1}$ and

$$\underline{r} = (x_0-x,\ y_0-y) \quad (3.63a)$$

$$\underline{r}_1 = (x_1-x,\ y_1-y)\ . \tag{3.63b}$$

Taking the Fourier transforms of both sides of equation (3.62) leads to the equation

$$\underline{S}_{u_2,l}(u,v) = \underline{K}_1(u,v)\ \underline{S}_{ll}(u,v) \tag{3.64a}$$

where $\underline{S}_{u_2,l}$ is the cross power spectral density of $\underline{u}_2,\underline{l}$, $\underline{K}_1(u,v)$ is the spectrum of the matrix $\underline{K}(x,y)$ and $\underline{S}_{ll}$ is the power spectral density of $\underline{l}$. Eqn. (3.64a) yields the spectrum $\underline{K}_1(u,v)$

$$\underline{K}_1(u,v) = \underline{S}_{u_2,l}(u,v)\ \underline{S}_{ll}^{-1}(u,v)\ . \tag{3.64b}$$

Equation (3.64b) states that given the power spectral densities $\underline{S}_{ll}$, $\underline{S}_{u_2,l}$ the filter matrix $\underline{K}(x,y)$ can be easily computed from its spectrum. Equation (3.64b) can also be derived by transforming in the frequency domain the least-squares collocation formula in the two-dimensional case

$$\underline{C}_{u_2,l}(x-x_1,y-y_1) = \underline{A}(x-x_k,y-y_k)\ \underline{C}_{ll}(x_k-x_1,y_k-y_1) \tag{3.65a}$$

or

$$\underline{A}(x-x_k,y-y_k) = \underline{C}_{u_2,l}(x-x_1,y-y_1)\ \underline{C}_{ll}^{-1}(x_k-x_1,y_k-y_1) \tag{3.65b}$$

where $\underline{C}_{u_2,l}$ is the cross-covariance matrix between $\underline{u}_2$, $\underline{l}$, $\underline{C}_{ll}$ is the autocovariance matrix of the vector $\underline{l}$, and $\underline{A}$ is the best linear

estimator according to least-squares collocation estimation. The signals $\underline{u}_1$, $\underline{u}_2$ are assumed to be stationary.

From equations (3.64b) and (3.65b) the relationship between Wiener filtering and least-squares collocation becomes clear. From the practical point of view, equation (3.64b) offers the advantage that for the estimation of the spectrum $\underline{K}_1(u,v)$, the matrix $\underline{S}_{11}(u,v)$ with a dimension equal to the number of observations per point has to be inverted. In contrast, in least squares collocation the matrix $\underline{C}_{1,1}$ with a size equal to the total number of observations needs to be inverted. For example assume that two measurements are made per point and that a 2-D grid is established with 65 points in each dimension. Then for the estimation of $\underline{K}_1(u,v)$ from (3.64b) only a 2x2 matrix needs to be inverted for each pair of frequencies u,v, while in the least squares collocation formula (3.65b), a 16 900 x 16 900 symmetric positive definite matrix needs to be inverted. Matrices that large, are very difficult to invert even on supercomputers. Typically a 15 000 x 15 000 symmetric positive definite matrix needs approximately 6 CPU hours to be inverted on a two - pipeline supercomputer CDC Cyber 205 (Hodus, 1985). Least-squares collocation can be employed in both the space domain, as is usually the case, as well as in the frequency domain (Eren, 1980). Least-squares collocation in the frequency domain converges to Wiener filtering for infinite number of noisy observations. However for non noisy observations of fully correlated inputs, the Wiener filtering equations cannot be used because the matrix $\underline{S}_{11}$ in eqn. (3.64b) is singular. In this case the multiple input- single output filtering equations should be employed.

It is important to notice that the Wiener filtering and the

multiple input-single output filtering equations are the same. This can be seen by inspecting formulas (3.50a), (3.50b) and (3.64b). The coefficients of the system of linear equations (3.50a), (3.50b) are the same as the elements of the matrix $\underline{S}_{11}$ in equation (3.64b). Furthermore it can be proved that even in the case of linear relations existing among all elements of the vector $\underline{l}$, the resulting Wiener filtering equations are exactly the same as those from the multiple input-single output equations (3.54a), (3.54b) (Jekeli, 1985). In this special case a matrix of size 1x1 needs to be inverted for each pair (u,v). This is definitely a very significant computational advantage of the multiple input-single output and Wiener filtering equations compared to the least-squares collocation formulas. The computational efficiency with which the gradient data processing is performed in this research, is mainly attributed to this computational advantage.

For geodetic applications a statistical analysis of the residuals of the observations is always needed. Depending on the estimation method different expressions of the residuals are evaluated. For instance, in least-squares collocation the covariance matrix of the residuals is computed. In Wiener filtering due to the frequency domain formulation of the problem, the PSD of the residuals is computed. The derivation of the PSD of the residuals is given in the following. The expectation of the residuals $\delta\underline{u}_2$ is given by

$$E\{\delta\underline{u}_2(x_0,y_0)\delta\underline{u}_2^{\,t}(x_0-x,y_0-y)\} = E\{[u_2(x_0,y_0)-\hat{u}_2(x_0,y_0)][u_2(x_0-x,y_0-y) - \hat{u}_2(x_0-x,y_0-y)]^t\} \quad , \text{ or}$$

$$E\{\delta\underline{u}_2(x_0,y_0)\delta\underline{u}_2^{\,t}(x_0-x,y_0-y)\} = E\{[\underline{u}_2(x_0,y_0)-\hat{\underline{u}}_2(x_0,y_0)]\underline{u}_2^{\,t}(x_0-x,y_0-y)\}$$

$$- E\{[\underline{u}_2(x_0,y_0) - \hat{\underline{u}}_2(x_0,y_0)][\hat{\underline{u}}_2(x_0-x,y_0-y)]^t\} \ . \qquad (3.66)$$

The second term on the right hand side of (3.66) is zero because the residual $\delta u_2(x_0,y_0)$ is orthogonal to each element of the Hilbert space H_1 and thus to each linear combination of its elements. Hence equation (3.76) takes the form

$$E\{\delta\underline{u}_2(x_0,y_0)\delta\underline{u}_2{}^t(x_0-x,y_0-y)\} = E\{\underline{u}_2(x_0,y_0)\underline{u}_2{}^t(x_0-x,y_0-y)\}$$

$$- E\{\hat{\underline{u}}_2(x_0,y_0)\underline{u}_2{}^t(x_0-x,y_0-y)\} \ . \qquad (3.67)$$

The first term on the right hand side of equation (3.67) is the autocorrelation matrix of $\underline{u}_2$

$$E\{\underline{u}_2(x_0,y_0)\underline{u}_2{}^t(x_0-x,y_0-y)\} = \underline{R}_{u_2,u_2}(x,y) \ . \qquad (3.68)$$

In addition the second term on the right hand side of equation (3.67) can be explicitly expressed in terms of the cross-correlation matrix between $\underline{u}_2,\underline{1}$

$$E\{\hat{\underline{u}}_2(x_0,y_0)\underline{u}_2^t(x_0-x,y_0-y)\} = \int_{-\infty}^{\infty}\int_{-\infty}^{\infty} \underline{K}(x_1,y_1)\underline{R}_{1,u_2}(x-x_1,y-y_1)dx_1dy_1 \ . \qquad (3.69)$$

Substitution of equations (3.68) and (3.69) into (3.67) leads to the equation

$$E\{\delta\underline{u}_2(x_0,y_0)\delta\underline{u}_2^t(x_0-x,y_0-y)\}=\underline{R}_{u_2,u_2}(x,y)$$

$$- \int_{-\infty}^{\infty}\int_{-\infty}^{\infty} \underline{K}(x_1,y_1)\underline{R}_{1,u_2}(x-x_1,y-y_1)dx_1,dy_1. \qquad (3.70)$$

Transforming equation (3.70) in the frequency domain yields

$$\underline{S}_{\delta u_2,\delta u_2}(u,v) = \underline{S}_{u_2,u_2}(u,v) - \underline{K}_1(u,v)\ \underline{S}_{1,u_2}(u,v)\ . \tag{3.71}$$

Finally, combining equations (3.64b) and (3.71) the final expression for the PSD of the residuals is obtained from

$$\underline{S}_{\delta u_2,\delta u_2}(u,v) = \underline{S}_{u_2,u_2}(u,v) - \underline{S}_{u_2,1}(u,v)\ \underline{S}^{-1}_{1,1}(u,v)\ \underline{S}_{1,u_2}(u,v)\ . \tag{3.72}$$

The above PSD for the residuals can be directly obtained from the transformation of the residual covariance matrix in the frequency domain

$$\underline{C}_{\delta u_2,\delta u_2}(x_0,y_0) = \underline{C}_{u_2,u_2}(x_0,y_0) - \underline{A}(x_0-x_k,y_0-y_k)\ \underline{C}_{1,u_2}(x_k,y_k)\ . \tag{3.73}$$

Again equations (3.72), (3.73) demonstrate clearly the relationship between least-squares collocation and Wiener filtering in the two-dimensional case. Furthermore they show the computational superiority of Wiener filtering compared to least-squares collocation. Assuming statistical independence between the measurement noise and the estimated vector $\underline{u}_2$, equation (3.72) takes the form

$$\underline{S}_{\delta u_2,\delta u_2}(u,v) = \underline{S}_{u_2,u_2}(u,v) - \underline{S}_{u_2,u_1}(u,v)\{\underline{S}_{u_1,u_1}(u,v)$$

$$+\ \underline{S}_{n,n}(u,v)\}^{-1}\ \underline{S}_{u_1,u_2}(u,v)\ . \tag{3.74}$$

Thus for the computation of the PSD of the residuals δu_2, the measurement noise is explicitly taken into account via its PSD. This equation will be used in the next chapter for the estimation of the PSD of the residuals of the estimation of the first-order gradients.

Chapter 4

ESTIMATION OF FIRST-ORDER GRADIENTS OF T FROM SECOND-ORDER GRADIENTS

As an introduction to this chapter the concept of the anomalous gravity potential is presented and least-squares collocation as an estimation technique for the determination of the anomalous gravity potential is briefly discussed. Next the transfer functions between the anomalous potential and all of its first and second-order gradients are derived. Then in the main part of this chapter the multiple input-single output filtering equations are applied to the estimation of the first-order gradients of T from second-order gradients. First the estimation of the vertical first-order gradient T_z is presented and then the estimation of the horizontal gradients T_x, T_y is discussed.

4.1 THE ANOMALOUS GRAVITY POTENTIAL

Any point at the surface of the earth is subjected to a force, which is the combined effect of the gravitational force and the centrifugal force of the earth's rotation. The total force is called gravity and the corresponding potential is called gravity potential and is denoted by W. The gravity potential is composed of the gravitational and the centrifugal potential V and Φ respectively.

The surface of the earth is usually approximated by an ellipsoid of revolution which is an equipotential surface of a normal gravity field of the earth as defined in Heiskanen and Moritz (1967). The normal gravity potential is denoted by U and the normal gravity by γ. At each point with rectangular coordinates x,y,z, the anomalous

gravity potential T is given as the difference between the actual gravity potential W and the normal potential U, both of them evaluated at the earth's surface

$$T(x,y,z) = W(x,y,z) - U(x,y,z) \tag{4.1}$$

The first-order anomalous gravity gradients are defined as

$$T_x = \frac{\partial T}{\partial x} \tag{4.2}$$

$$T_y = \frac{\partial T}{\partial y} \tag{4.3}$$

$$T_z = \frac{\partial T}{\partial z} \quad . \tag{4.4}$$

In addition the elements of the second-order anomalous gravity gradient tensor are defined by

$$T_{xx} = \frac{\partial^2 T}{\partial x^2} \tag{4.5}$$

$$T_{yy} = \frac{\partial^2 T}{\partial y^2} \tag{4.6}$$

$$T_{zz} = \frac{\partial^2 T}{\partial z^2} \tag{4.7}$$

$$T_{xy} = T_{yx} = \frac{\partial^2 T}{\partial x \partial y} \tag{4.8}$$

$$T_{xz} = T_{zx} = \frac{\partial^2 T}{\partial x \partial z} \tag{4.9}$$

$$T_{yz} = T_{zy} = \frac{\partial^2 T}{\partial y \partial z} \quad . \tag{4.10}$$

The diagonal elements of the second-order gravity gradient tensor satisfy Laplace's equation outside the surface of the earth

$$T_{xx} + T_{yy} + T_{zz} = 0 \ . \tag{4.11}$$

Usually measurements of the anomalous gravity potential are not available and thus it has to be determined from measurements of its first and second-order gradients. Least-squares collocation is one method which estimates the anomalous potential from such measurements, by fitting a smooth approximation to the given measurements of the linear functionals of T. More explicitly the problem can be formulated as follows. Given are m measurements l of linear functionals of T, corrupted by noise n

$$l_i = L_i \ T + n_i \qquad i=1,2,\ldots,m \tag{4.12}$$

where the operator L_i describes the linear function operating on the potential T. In this research the measured linear functionals are the second-order anomalous gravity gradients defined above. Least-squares collocation provides the smoothest estimate of the anomalous potential based on the available measurements. The estimate of T at point P is given by

$$\hat{T}(P) = \underline{C}_{sl}\, \underline{C}_{ll}^{-1}\, \underline{l} \tag{4.13}$$

or

$$\hat{T}(P)=[C_{p1} \quad C_{p2} \cdots C_{PM}] \begin{bmatrix} C_{11} & C_{12} & \cdot & \cdot & \cdot & C_{1m} \\ C_{21} & C_{22} & \cdot & \cdot & \cdot & C_{2m} \\ \cdot & & & & & \cdot \\ \cdot & & & & & \cdot \\ \cdot & & & & & \cdot \\ C_{m1} & & & & & C_{mm} \end{bmatrix}^{-1} \begin{bmatrix} l_1 \\ l2 \\ \cdot \\ \cdot \\ \cdot \\ l_m \end{bmatrix} \tag{4.14}$$

where $\hat{T}(P)$ is the estimated anomalous potential at P, C_{pi} (i=1,2,..,m) are the cross covariances between T(P) and the measurements l_i forming the vector (matrix) $\underline{C}_{sl}$, and C_{ij} are the elements of the covariance matrix $\underline{C}_{ll}$ equal to the covariances of the measurements l_i, l_j(j=1,2,...,m). In chapter 3, the multiple input-single output filtering equations as well as the Wiener filtering equations were analyzed. The necessary condition for the application of those filtering equations is that all the participating signals are stationary and ergodic. For a 2-D case, the Wiener filter (or multiple input-single output filter) was shown in section 3.3 to be the spectrum of the least-squares collocator assuming that the stationarity and ergodicity conditions hold.

Least-squares collocation provides the least-squares minimum-error estimate of the anomalous potential and possesses three main invariance properties. First, it reproduces the measurements, provided that they are errorless. Second, least-squares collocation is invariant with respect to any linear transformation of the estimated signal. Third, it is also invariant to any linear

transformation of the measurements. The statistical approach to collocation is widely used although there are some difficulties with the ergodicity assumption. Besides the probabilistic point of view with which least-squares collocation has been discussed in this section, it can be analyzed using Hilbert space theory (Krarup, 1969; Tscherning, 1985). The statistical formulation is used here because it is always assumed in applications to gradiometry.

Least-squares collocation can be used to estimate T or any of its linear functional from measurements of other linear functionals of T. It thus can theoretically be applied to the estimation of the first-order gradients T_x, T_y, T_z from second-order gradients T_{xx}, T_{xy}, T_{xz}, T_{yz}, T_{yy}, T_{zz}. In practice the application of space domain collocation to this particular problem is not advisable however due to the large amounts of data l_i, which makes the inversion of the matrix $\underline{C}_{ll}$ a major numerical problem.

4.2 TRANSFER FUNCTIONS BETWEEN THE ANOMALOUS POTENTIAL AND ITS GRADIENTS

Airborne gravity gradiometry surveys will be conducted over areas approximately 300 x 300 km. Without loss of accuracy the area, where the survey is to take place, can be approximated by a plane. This is the so-called flat earth approximation which indeed simplifies the relations between T and its gradients.

Let the plane have x, y, z as east, north and vertical (upward) coordinate axes. Then the anomalous potential, and any of its functionals, at altitude h is expressed by the equation (Heiskanen and Moritz, 1967)

$$T(x,y,h) = \frac{h}{2\pi} \int_{-\infty}^{\infty}\int_{-\infty}^{\infty} \frac{T(x_1,y_1,0)}{[(x-x_1)^2+(y-y_1)^2+h^2]^{3/2}}\, dx_1 dy_1 \qquad (4.15)$$

The above integral is clearly a convolution integral between the anomalous potential at the surface of the earth and a geometrical kernel. The convolution is transformed into a multiplication of spectra in the frequency domain

$$F\{T(x,y,h)\} = \frac{h}{2\pi}\, F\{T(x,y,0)\}\, F\{\frac{1}{(x^2+y^2+h^2)^{3/2}}\} \qquad (4.16)$$

The spectrum of the geometrical kernel appearing on the right hand side of equation (4.16) is known (Bracewell, 1978)

$$F\{\frac{1}{(x^2+y^2+h^2)^{3/2}}\} = \frac{2h}{\pi}\, e^{-2\pi h(u^2+v^2)^{1/2}} \quad . \qquad (4.17)$$

Combining equations (4.16) and (4.17), the final equation relating the spectra of the anomalous potential at altitude zero and at altitude h is derived

$$F\{T(x,y,h)\} = F\{T(x,y,0)\}e^{-2\pi hq} \qquad (4.18)$$

where $q = (u^2 + v^2)^{1/2}$. (4.19)

Equation (4.18) demonstrates the smoothing effect which the upward continuation has on the anomalous potential. It should be noted that the same equation as (4.18) holds for any gradient of T (e.g. T_x, T_y, T_z, T_{xz}, T_{yy}, etc.). The inverse operation of the upward continuation is the downward continuation expressed by equation

$$F\{T(x,y,0)\} = F\{T(x,y,h)\}e^{2\pi hq} \ . \tag{4.20}$$

The above equation illustrates clearly the problems related to downward continuation. On the one hand, the function T is smoother at altitude h than at altitude zero. On the other hand the high frequencies are amplified in the downward continuation which in turn implies that the effect of the measurement errors is getting larger. More details about downward continuation and generally improperly posed problems can be found in Schwarz (1979).

The spectra of the first-order gradients can be derived from the spectrum of the anomalous potential. Those gradients are given as partial horizontal and vertical derivatives of the anomalous potential T as can be seen from equations (4.2), (4.3), (4.4). Applying properties (3.16), (3.17) of the Fourier transform to equations (4.16) (4.18) and considering also upward continuation leads to

$$F\{T_x(x,y,h)\} = j2\pi u e^{-2\pi hq} F\{T(x,y,0)\} \tag{4.21}$$

$$F\{T_y(x,y,h)\} = j2\pi v e^{-2\pi hq} F\{T(x,y,0)\} \ . \tag{4.22}$$

Straightforward differentiation of (4.18) with respect to h yields the spectrum of the vertical first order gradient

$$F\{T_z(x,y,h)\} = 2\pi q e^{-2\pi hq} F\{T(x,y,0)\} \ . \tag{4.23}$$

The spectra of the second-order anomalous gradients are derived from the spectrum of the anomalous potential in the same way. The first and second-order gradients of T as well as their frequency response

functions with respect to T are listed in the following table 4.1. The transfer functions from T to any gradient at altitude h are obtained by multiplying the transfer functions in table 4.1 by the upward continuation operator $e^{-2\pi hq}$.

Table 4.1. The Gradients of the Anomalous Potential and their Corresponding Transfer Functions with Respect to T.

Gravity Gradient	Relation to Anomalous Potential T	Transfer Function from T
T_x	$\frac{\partial}{\partial x} T(x,y,0)$	$j2\pi u$
T_y	$\frac{\partial}{\partial y} T(x,y,0)$	$j2\pi v$
T_z	$\frac{\partial}{\partial z} T(x,y,0)$	$-2\pi q$
T_{xx}	$\frac{\partial^2}{\partial x^2} T(x,y,0)$	$-4\pi^2 u^2$
T_{yy}	$\frac{\partial^2}{\partial y^2} T(x,y,0)$	$-4\pi^2 v^2$
T_{zz}	$\frac{\partial^2}{\partial z^2} T(x,y,0)$	$4\pi^2 q^2$
T_{xy}	$\frac{\partial^2}{\partial x \partial y} T(x,y,0)$	$-4\pi^2 uv$
T_{xz}	$\frac{\partial^2}{\partial x \partial z} T(x,y,0)$	$-j4\pi^2 uq$
T_{yz}	$\frac{\partial^2}{\partial y \partial z} T(x,y,0)$	$-j4\pi^2 vq$

4.3 ESTIMATION OF THE VERTICAL FIRST-ORDER GRADIENT T_z

4.3.1 Estimation of T_z from T_{zz}

From Table 4.1, the spectrum of the airborne gradients T_{zz} is given as

$$F\{T_{zz}\} = 4\pi^2 q^2 e^{-2\pi hq} F\{T\} . \tag{4.24}$$

Since the spectrum of T_z at zero altitude is given by

$$F\{T_z\} = -2\pi q \, F\{T\}, \tag{4.25}$$

it follows that

$$F\{T_{zz}\} = -2\pi q e^{-2\pi hq} F\{T_z\} \quad , \text{ or}$$

$$F\{T_z(x,y,0)\} = -\frac{1}{2\pi} \frac{e^{2\pi hq}}{q} F\{T_{zz}(x,y,z=h)\} . \tag{4.26}$$

Using the above equation, the spectrum of the gradient T_z is expressed explicitly in terms of the spectrum of the airborne gradients T_{zz}. The downward continuation operation appears through the exponential operator $e^{2\pi hq}$. However as it will be shown later on in chapter 7, the downward continuation from a flying altitude of 600 m does not present any serious numerical problem. The same formula as (4.26) has been derived in Vassiliou (1985b) combining plane integration and downward continuation in the frequency domain. If the gradients T_z are estimated at flying altitude, then equation (4.26) is modified to

$$F\{T_z(x,y,h)\} = -\frac{1}{2\pi q} F\{T_{zz}(x,y,h)\} . \tag{4.27}$$

Equation (4.27) can be transformed into the space domain, taking the form of the Stokes integral formula for flat earth approximation (Heiskanen and Moritz, 1967)

$$T_z(x,y,h) = -\frac{1}{2\pi}\int_{-\infty}^{\infty}\int_{-\infty}^{\infty} \frac{T_{zz}(x_1,y_1,h)}{[(x-x_1)^2+(y-y_1)^2]^{1/2}}\, dx_1 dy_1. \qquad (4.28)$$

Unfortunately there is no analytical inverse Fourier transform for equation (4.26), which incorporates plane integration and downward continuation. Therefore the values of the gradient T_z are computed from (4.26) numerically through the FFT. An extended form of equation (4.27) where the gradient measurement noise is taken into account, using eqn. (3.43) results in

$$H_1(u,v) = \frac{S_{T_{zz},T_z}(u,v)}{S_{T_{zz},T_{zz}}(u,v)+S_{n,n}(u,v)} \quad , \text{ or}$$

$$H_1(u,v) = -\frac{8\pi^3 q^3 e^{-2\pi hq} S_{T,T}(u,v)}{16\pi^4 q^4 e^{-4\pi hq} S_{T,T}(u,v)+S_{n,n}(u,v)} \qquad (4.29)$$

where $H_1(u,v)$ is the frequency response function from $T_{zz}(x,y,h)$ to $T_z(x,y,0)$, $S_{T,T}$ is the PSD of the anomalous potential T and $S_{n,n}$ is the PSD of the noise n. By setting the noise level equal to zero, equation (4.29) becomes identical to (4.26).

4.3.2 Estimation of T_z from a linear combination of T_{xz} and T_{yz}

The multiple input-single output filtering equations (3.53a), (3.53b), (3.54a), (3.54b), where the inputs are linearly related, are used in this section. Assuming for the sake of simplicity that the measurements are noise-free, the frequency-response functions $H_1(u,v)$, $H_2(u,v)$ relating T_{xz}, T_{yz} with T_z are derived from (3.53a), (3.53b)

$$H_1(u,v) = \frac{S_{T_{xz},T_z}(u,v)}{S_{T_{xz},T_{xz}}(u,v)+S_{T_{yz},T_{yz}}(u,v)} =$$

$$= \frac{j4\pi^2 uq(-2\pi q)e^{-2\pi hq}S_{T,T}(u,v)}{(16\pi^4u^2q^2+16\pi^4v^2q^2)e^{-4\pi hq}S_{T,T}(u,v)} \quad \text{, or}$$

$$H_1(u,v) = -\frac{jue^{2\pi hq}}{2\pi q^2} \quad . \tag{4.30}$$

Similarly, the transfer function $H_2(u,v)$ is derived as

$$H_2(u,v) = -\frac{jve^{2\pi hq}}{2\pi q^2} \quad . \tag{4.31}$$

Thus the spectrum of the gradient T_z at the surface of the earth is given in terms of the spectra of the airborne second-order gradients T_{xz} and T_{yz}

$$F\{T_z(x,y,0)\} = -\frac{jue^{2\pi hq}}{2\pi q^2} F\{T_{xz}(x,y,h)\} - \frac{jve^{2\pi hq}}{2\pi q^2} F\{T_{yz}(x,y,h)\}. \tag{4.32}$$

The above equation combines downward continuation and plane integration in the frequency domain, and it can not be transformed analytically into the space domain. This transformation can be made numerically via FFT. Considering for a moment only plane integration, equation (4.32) takes the form

$$F\{T_z(x,y,h)\} = -\frac{ju}{2\pi q^2} F\{T_{xz}(x,y,h)\} - \frac{jv}{2\pi q^2} F\{T_{yz}(x,y,h)\}. \qquad (4.33)$$

This equation can be analytically transformed into the space domain where it takes the form

$$T_z(x,y) = -\frac{1}{2\pi} \int_{-\infty}^{\infty} \int_{-\infty}^{\infty} T_{xz}(x_1,y_1) \frac{(x-x_1)}{[(x-x_1)^2+(y-y_1)^2]} dx_1 dy_1$$

$$-\frac{1}{2\pi} \int_{-\infty}^{\infty} \int_{-\infty}^{\infty} T_{yz}(x_1,y_1) \frac{(y-y_1)}{[(x-x_1)^2+(y-y_1)^2]} dx_1 dy_1, \text{ or}$$

$$T_z(x,y) = -\frac{1}{2\pi} \int_{-\infty}^{\infty} \int_{-\infty}^{\infty} \frac{T_{xz}(x_1,y_1)\sin\alpha}{[(x-x_1)^2+(y-y_1)^2]^{1/2}} dx_1 dy_1$$

$$-\frac{1}{2\pi} \int_{-\infty}^{\infty} \int_{-\infty}^{\infty} \frac{T_{yz}(x_1,y_1)\cos\alpha}{[(x-x_1)^2+(y-y_1)^2]^{1/2}} dx_1 dy_1 \qquad (4.34)$$

where α is the azimuth of the straight line passing through the points (x,y) and (x_1,y_1). The above relation is new relating the first order gradient T_z to its horizontal gradients T_{xz} and T_{yz}. It can be shown

in exactly the same way that a similar equation holds for the anomalous potential T and its two horizontal gradients T_x and T_y

$$T(x,y)= -\frac{1}{2\pi}\int_{-\infty}^{\infty}\int_{-\infty}^{\infty}\frac{T_x(x_1,y_1)\sin\alpha}{[(x-x_1)^2+(y-y_1)^2]^{1/2}}\,dx_1dy_1$$

$$-\frac{1}{2\pi}\int_{-\infty}^{\infty}\int_{-\infty}^{\infty}\frac{T_y(x_1,y_1)\cos\alpha}{[(x-x_1)^2+(y-y_1)^2]^{1/2}}\,dx_1dy_1\ . \qquad (4.35)$$

The above equation states that the anomalous potential T can be determined from both north and east deflections of the vertical gridded on a two dimensional regular grid.

Taking explicitly the gradiometer noise into account, equation (4.32) takes the form

$$\mathbf{F}\{T_z(x,y,0)\}=H_1(u,v)\ \mathbf{F}\{T_{xz}(x,y,h)\}+H_2(u,v)\ \mathbf{F}\{T_{yz}(x,y,h)\}. \qquad (4.36)$$

where the frequency response functions $H_1(u,v)$ and $H_2(u,v)$ are given by the equations

$$H_1(u,v) = -\frac{j8\pi^3uq^2e^{-2\pi hq}S_{T,T}(u,v)}{16\pi^4q^4e^{-4\pi hq}S_{T,T}(u,v)+S_{n,n}(u,v)} \qquad (4.37)$$

$$H_2(u,v) = -\frac{j8\pi^3vq^2e^{-2\pi hq}S_{T,T}(u,v)}{16\pi^4q^4e^{-4\pi hq}S_{T,T}(u,v)+S_{n,n}(u,v)}\ . \qquad (4.38)$$

The PSD of the residuals of T_z are computed from equation (3.74) taking into account the linear relation between the gradients T_{xz} and T_{yz}

$$S_{\delta T_z,\delta T_z}(u,v)=S_{T_z,T_z}(u,v)-\{S_{T_{xz},T_z}(u,v)\quad S_{T_{yz},T_z}(u,v)\}\{S_{T_{xz},T_{xz}}(u,v)+$$

$$S_{T_{yz},T_{yz}}(u,v)\ +\ S_{n,n}(u,v)\}^{-1}\ \{\frac{S_{T_z,T_{xz}}(u,v)}{S_{T_z,T_{yz}}(u,v)}\}\quad ,\ \text{or}$$

$$S_{\delta T_z,\delta T_z}(u,v)=4\pi^2q^2S_{T,T}(u,v)$$

$$-\ \{64\pi^6q^6e^{-4\pi hq}|S_{T,T}(u,v)|^2\}\{16\pi^4q^4e^{-4\pi hq}S_{T,T}(u,v)+S_{n,n}(u,v)\}^{-1}\ .$$

(4.39)

A similar expression for the PSD of the residuals of T_z can be derived for the plane integration only. The estimated spectrum of T_z (eqn. (4.36)) as well as the estimated PSD of the residuals (eqn. (4.39)) are transformed into the space domain via FFT.

4.3.3 Estimation of T_z from Combination of T_{xz}, T_{yz}, T_{zz}

Assuming noise-free measurements the frequency response functions of the gradients T_{xz}, T_{yz} and T_{zz} with respect to T_z, H_1, H_2 and H_3 respectively are given from the multiple input-single output filtering equations as follows

$$H_1(u,v)=\frac{S_{T_{xz},T_z}(u,v)}{S_{T_{xz},T_{xz}}(u,v)+S_{T_{yz},T_{yz}}(u,v)+S_{T_{zz},T_{zz}}(u,v)}=-\frac{jue^{2\pi hq}}{4\pi q^2}$$

(4.40)

$$H_2(u,v)=\frac{S_{T_z,T_{yz}}(u,v)}{S_{T_{xz},T_{xz}}(u,v)+S_{T_{yz},T_{yz}}(u,v)+S_{T_{zz},T_{zz}}(u,v)}=-\frac{jve^{2\pi hq}}{4\pi q^2}$$

(4.41)

$$H_3(u,v)=\frac{S_{T_{zz},T_z}(u,v)}{S_{T_{xz},T_{xz}}(u,v)+S_{T_{yz},T_{yz}}(u,v)+S_{T_{zz},T_{zz}}(u,v)}=-\frac{e^{2\pi hq}}{4\pi q}\ . \tag{4.42}$$

The estimated spectrum of the gradient T_z is given by the equation

$$\mathbf{F}\{T_z(x,y)\}=H_1(u,v)\mathbf{F}\{T_{xz}(x,y,h)\}+H_2(u,v)\mathbf{F}\{T_{yz}(x,y,h)\}$$

$$+\ H_3(u,v)\mathbf{F}\{T_{zz}(x,y,h)\}\ . \tag{4.43}$$

Assuming that the noise-free gradient measurements are made at the surface of the earth, equation (4.43) becomes

$$\mathbf{F}\{T_z(x,y)\}=-\frac{ju}{4\pi q^2}\mathbf{F}\{T_{xz}(x,y)\}-\frac{jv}{4\pi q^2}\mathbf{F}\{T_{yz}(x,y)\}-\frac{1}{4\pi q}\mathbf{F}\{T_{zz}(x,y)\}, \tag{4.44}$$

and transforming this equation into the space domain yields the following integration formula

$$T_z(x,y)=-\frac{1}{4\pi}\int_{-\infty}^{\infty}\int_{-\infty}^{\infty}\frac{T_{xz}(x_1,y_1)\sin\alpha}{[(x-x_1)^2+(y-y_1)^2]^{1/2}}\,dx_1dy_1$$

$$-\frac{1}{4\pi}\int_{-\infty}^{\infty}\int_{-\infty}^{\infty}\frac{T_{yz}(x_1,y_1)\cos\alpha}{[(x-x_1)^2+(y-y_1)^2]^{1/2}}\,dx_1dy_1$$

$$-\frac{1}{4\pi}\int_{-\infty}^{\infty}\int_{-\infty}^{\infty}\frac{T_{zz}(x_1,y_1)}{[x-x_1)^2+(y-y_1)^2]^{1/2}}\,dx_1dy_1. \tag{4.45}$$

This integral equation is very important because it shows the explicit relationship among the first-order gradient T_z and of its second-order

gradients T_{xz}, T_{yz} and T_{zz}. This integral equation is preferable to equations (4.28) and (4.35) because it uses all the gradients of T_z at once, which in turn means that it uses all the spectral information contained in the medium and high frequency part of T_z. In addition, a similar equation can be written for the anomalous potential T

$$T(x,y) = -\frac{1}{4\pi}\int_{-\infty}^{\infty}\int_{-\infty}^{\infty}\frac{T_x(x_1,y_1)\sin\alpha}{[(x-x_1)^2+(y-y_1)^2]^{1/2}}\,dx_1dy_1$$

$$-\frac{1}{4\pi}\int_{-\infty}^{\infty}\int_{-\infty}^{\infty}\frac{T_y(x_1,y_1)\cos\alpha}{[(x-x_1)^2+(y-y_1)^2]^{1/2}}\,dx_1dy_1$$

$$-\frac{1}{4\pi}\int_{-\infty}^{\infty}\int_{-\infty}^{\infty}\frac{T_z(x_1,y_1)}{[(x-x_1)^2+(y-y_1)^2]^{1/2}}\,dx_1dy_1\ . \qquad (4.46)$$

The meaning of this equation is that given a regular two-dimensional grid on which the gravity disturbances and the deflections of the vertical are sampled, the anomalous potential can be explicitly computed in terms of those sampled gradients. This equation, however, is of rather theoretical interest because there are no areas worldwide where a two-dimensional grid of north and south deflections of the vertical is available. In contrast equation (4.45) is of immediate use for the estimation of T_z simply because all its gradients (i.e., T_{xz}, T_{yz}, T_{zz}) are available from the gradiometer system.

When the gradiometer noise is taken into account, then the transfer functions described by equations (4.40), (4.41) and (4.42)

are modified to the following equations

$$H_1(u,v) = -\frac{j8\pi^3 uq^2 e^{-2\pi hq} S_{T,T}(u,v)}{32\pi^4 q^4 e^{-4\pi hq} S_{T,T}(u,v)+S_{n,n}(u,v)} \tag{4.47}$$

$$H_2(u,v) = -\frac{j8\pi^3 vq^2 e^{-2\pi hq} S_{T,T}(u,v)}{32\pi^4 q^4 e^{-4\pi hq} S_{T,T}(u,v)+S_{n,n}(u,v)} \tag{4.48}$$

$$H_3(u,v) = -\frac{8\pi^3 q^3 e^{-2\pi hq} S_{T,T}(u,v)}{32\pi^4 q^4 e^{-4\pi hq} S_{T,T}(u,v)+S_{n,n}(u,v)}\ , \tag{4.49}$$

and again the spectrum of T_z is estimated from equation (4.43) for which no analytical inverse Fourier transform exists. The accuracy of the estimation of T_z can be estimated from the PSD of the residuals of T_z.

$$S_{\delta T_z,\delta T_z}(u,v)=S_{T_z,T_z}(u,v)-\{S_{T_{xz},T_z}(u,v) \mid S_{T_{yz},T_z}(u,v) \mid S_{T_{zz},T_z}(u,v)\}.$$

$$\{S_{T_{xz},T_{xz}}(u,v)+S_{T_{yz},T_{yz}}(u,v)+S_{T_{zz},T_{zz}}(u,v)+S_{n,n}(u,v)\}^{-1}$$

$$\begin{Bmatrix} S_{T_z,T_{xz}}(u,v) \\ \hline S_{T_z,T_{yz}}(u,v) \\ \hline S_{T_z,T_{zz}}(u,v) \end{Bmatrix}\ , \text{ or}$$

$$S_{\delta T_z,\delta T_z}(u,v)=4\pi^2q^2S_{T,T}(u,v)-\{128\pi^6q^6e^{-4\pi hq}|S_{T,T}(u,v)|^2\}$$

$$\{32\pi^4q^4e^{-4\pi hq}S_{T,T}(u,v)+S_{n,n}(u,v)\}^{-1} \ . \qquad (4.50)$$

Reviewing sections 4.2.1, 4.2.2 and 4.2.3 it can be said that the spectral relations relating T_z at the surface of the earth to either the T_{zz} or T_{xz}, T_{yz} or T_{xz}, T_{yz}, T_{zz} at flying altitude are now well established by using the multiple (single) input-single output filtering equations. Theoretically, the combination of five independent second-order gradients will give the optimal estimate of a first-order gradient. As it will be shown in chapter 7 a smaller number of gradients will often give a result which is practically equivalent to the optimal solution.

4.4 ESTIMATION OF THE HORIZONTAL GRADIENTS T_x AND T_y

The gradient T_x at the surface of the earth can be estimated from T_{xz}; T_{xx},T_{xy}; T_{xx},T_{xy},T_{xz} at flying altitude. The procedure for the derivation of the equations is exactly the same as in sections 4.3.1, 4.3.2 and 4.3.3. Assuming noise-free gradient measurements, the spectrum of T_x is given from the spectra of the airborne T_{xz}; T_{xx},T_{xy}; T_{xx},T_{xy},T_{xz} by the following equations

$$F\{T_x(x,y)\} = = \frac{1}{2\pi} \ \frac{e^{2\pi hq}}{q} \ F\{T_{xz}(x,y,h)\} \qquad (4.51)$$

$$F\{T_x(x,y)\}= - \frac{jue^{2\pi hq}}{2\pi q^2} \ F\{T_{xx}(x,y,h)\} - \frac{jve^{2\pi hq}}{2\pi q^2} \ F\{T_{xy}(x,y,h)\} \qquad (4.52)$$

$$F\{T_x(x,y)\} = -\frac{jue^{2\pi hq}}{4\pi q^2} F\{T_{xx}(x,y,h)\} - \frac{jve^{2\pi hq}}{4\pi q^2} F\{T_{xy}(x,y,h)\} -$$

$$- \frac{e^{2\pi hq}}{4\pi q} F\{T_{xz}(x,y,h)\} . \tag{4.53}$$

The spectrum of T_x as given in the above equations cannot be transformed analytically into the space domain. The transformation is performed numerically through the use of FFT. The plane integration formulas for the earth's surface analogous to (4.40), (4.41), (4.42) can be obtained by setting the flying altitude equal to zero

$$F\{T_x(x,y)\} = -\frac{1}{2\pi q} F\{T_{xz}(x,y)\} \tag{4.54}$$

$$F\{T_x(x,y)\} = -\frac{ju}{2\pi q^2} F\{T_{xx}(x,y)\} - \frac{jv}{2\pi q^2} F\{T_{xy}(x,y)\} \tag{4.55}$$

$$F\{T_x(x,y)\} = -\frac{ju}{4\pi q^2} F\{T_{xx}(x,y)\} - \frac{jv}{4\pi q^2} F\{T_{xy}(x,y)\} - \frac{1}{4\pi q} F\{T_{xz}(x,y)\}. \tag{4.56}$$

An analogous formula to (4.54) has been derived in a very elegant way for the spherical earth approximation by Herring (1978). All three formulas above can be transformed analytically in the space domain .

$$T_x(x,y) = -\frac{1}{2\pi} \int_{-\infty}^{\infty} \int_{-\infty}^{\infty} \frac{T_{xz}(x_1,y_1)}{[(x-x_1)^2+(y-y_1)^2]^{1/2}} dx_1 dy_1 \tag{4.57}$$

$$T_x(x,y) = -\frac{1}{2\pi}\int_{-\infty}^{\infty}\int_{-\infty}^{\infty}\frac{T_{xx}(x_1,y_1)\sin\alpha}{[(x-x_1)^2+(y-y_1)^2]^{1/2}}\,dx_1dy_1$$

$$-\frac{1}{2\pi}\int_{-\infty}^{\infty}\int_{-\infty}^{\infty}\frac{T_{xy}(x_1,y_1)\cos\alpha}{[(x-x_1)^2+(y-y_1)^2]^{1/2}}\,dx_1dy_1, \tag{4.58}$$

$$T_x(x,y) = -\frac{1}{4\pi}\int_{-\infty}^{\infty}\int_{-\infty}^{\infty}\frac{T_{xx}(x_1,y_1)\sin\alpha}{[(x-x_1)^2+(y-y_1)^2]^{1/2}}\,dx_1dy_1$$

$$-\frac{1}{4\pi}\int_{-\infty}^{\infty}\int_{-\infty}^{\infty}\frac{T_{xy}(x_1,y_1)\cos\alpha}{[(x-x_1)^2+(y-y_1)^2]^{1/2}}\,dx_1dy_1 \tag{4.59}$$

$$-\frac{1}{4\pi}\int_{-\infty}^{\infty}\int_{-\infty}^{\infty}\frac{T_{xz}(x_1,y_1)}{[(x-x_1)^2+(y-y_1)^2]^{1/2}}\,dx_1dy_1.$$

Taking now the gradiometer noise into account, equations (4.51), (4.52), (4.53) take the form

$$F\{T_x(x,y)\} = -\frac{j8\pi^3u^2qe^{-2\pi hq}S_{T,T}(u,v)}{16\pi^4u^2q^2e^{-4\pi hq}S_{T,T}(u,v)+S_{n,n}(u,v)}\,F\{T_{xz}(x,y,h)\} \tag{4.60}$$

$$F\{T_x(x,y)\} = -\frac{j8\pi^3u^3e^{-2\pi hq}S_{T,T}(u,v)}{16\pi^4u^2q^2e^{-4\pi hq}S_{T,T}(u,v)+S_{n,n}(u,v)}\,F\{T_{xx}(x,y,h)\}$$

$$-\frac{j.8\pi^3u^2ve^{-2\pi hq}S_{T,T}(u,v)}{16\pi^4u^2q^2e^{-4\pi hq}S_{T,T}(u,v)+S_{n,n}(u,v)}\,F\{T_{xy}(x,y,h)\} \tag{4.61}$$

$$F\{T_x(x,y)\} = -\frac{j8\pi^3u^3e^{-2\pi hq}S_{T,T}(u,v)}{32\pi^4u^2q^2e^{-4\pi hq}S_{T,T}(u,v)+S_{n,n}(u,v)}\,F\{T_{xx}(x,y,h)\}$$

$$-\frac{j.8\pi^3u^2ve^{-2\pi hq}S_{T,T}(u,v)}{32\pi^4u^2q^2e^{-4\pi hq}S_{T,T}(u,v)+S_{n,n}(u,v)}\,F\{T_{xy}(x,y,h)\} \qquad (4.62)$$

$$-\frac{8\pi^3u^2qe^{-2\pi hq}S_{T,T}(u,v)}{32\pi^4u^2q^2e^{-4\pi hq}S_{T,T}(u,v)+S_{n,n}(u,v)}\,F\{T_{xz}(x,y,h)\}\ .$$

The power spectral densities of the residuals of T_x estimated from the three previous equations are

$$S_{\delta T_x,\delta T_x}(u,v)=4\pi^2u^2S_{T,T}(u,v)-\{64\pi^6u^4q^2e^{-4\pi hq}|S_{T,T}(u,v)|^2\}$$

$$\{16\pi^4u^2q^2e^{-4\pi hq}S_{T,T}(u,v)+S_{n,n}(u,v)\}^{-1} \qquad (4.63)$$

$$S_{\delta T_x,\delta T_x}(u,v)=4\pi^2u^2S_{T,T}(u,v)-\{64\pi^6u^4q^2e^{-4\pi hq}|S_{T,T}(u,v)|^2\}$$

$$\{16\pi^4u^2q^2e^{-4\pi hq}S_{T,T}(u,v)+S_{n,n}(u,v)\}^{-1} \qquad (4.64)$$

$$S_{\delta T_x,\delta T_x}(u,v)=4\pi^2u^2S_{T,T}(u,v)-\{128\pi^6u^4q^2e^{-4\pi hq}|S_{T,T}(u,v)|^2\}$$

$$\{32\pi^4u^2q^2e^{-4\pi hq}S_{T,T}(u,v)+S_{n,n}(u,v)\}^{-1}. \qquad (4.65)$$

The power spectral densities expressed by (4.63), (4.64), (4.65) show

that, theoretically the signal to noise ratio gets higher when more second-order gradients are used. The highest signal to noise ratio is obtained for the combination of T_{xx}, T_{xy}, T_{xz}.

In addition to the estimation of T_x from airborne T_{xz}, T_{xx}, T_{xy}, T_{yy}, T_{xy}, T_{xz}, the gradient T_x can be estimated from the gradient T_{zz}. The transfer function from T_{zz} to T_x, assuming zero gradiometer noise is derived from the single input-single output filtering equations

$$H_1(u,v) = \frac{S_{T_{zz},T_x}(u,v)}{S_{T_{zz},T_{zz}}(u,v)} = \frac{jue^{2\pi hq}}{2\pi q^2} \quad . \tag{4.66}$$

Thus the spectrum of T_x is expressed in terms of the airborne T_{zz}

$$\mathbf{F}\{T_x(x,y)\} = \frac{jue^{2\pi hq}}{2\pi q^2} \quad \mathbf{F}\{T_{zz}(x,y,h)\} \ . \tag{4.67}$$

This is an extended form of the equation derived in Vassiliou (1985b) relating T_x to T_{zz}. The plane integration formula corresponding to (4.67) is

$$\mathbf{F}\{T_x(x,y)\} = \frac{ju}{2\pi q^2} \ \mathbf{F}\{T_{zz}(x,y)\} \tag{4.68}$$

and can be transformed analytically into the space domain

$$T_x(x,y) = \frac{1}{2\pi} \int_{-\infty}^{\infty} \int_{-\infty}^{\infty} \frac{T_{zz}(x_1,y_1)\sin\alpha}{[(x-x_1)^2+(y-y_1)^2]^{1/2}} \, dx_1 dy_1 \ . \tag{4.69}$$

Considering now the more complicated case when the gradiometer noise

is taken into account, equations (4.67), (4.68) take the form

$$F\{T_x(x,y)\} = \frac{j8\pi^3 uq^2 e^{-2\pi hq} S_{T,T}(u,v)}{16\pi^4 q^4 e^{-4\pi hq} S_{T,T}(u,v)+S_{n,n}(u,v)} \tag{4.70}$$

$$F\{T_x(x,y)\} = \frac{j8\pi^3 uq^2 S_{T,T}(u,v)}{16\pi^4 q^4 S_{T,T}(u,v)+S_{n,n}(u,v)} \ . \tag{4.71}$$

The PSD of the residuals of T_x estimated from the airborne T_{zz} measurements

$$S_{\delta T_x,\delta T_x}(u,v)=4\pi^2 u^2 S_{T,T}(u,v)-\{64\pi^6 u^2 q^4 e^{-4\pi hq}|S_{T,T}(u,v)|^2\}$$

$$\{16\pi^4 q^4 e^{-4\pi hq}\ S_{T,T}(u,v)+S_{n,n}(u,v)\}^{-1} \ . \tag{4.72}$$

A general comment which can be made about all equations relating directly the spectra of the first-order gradients to the spectra of the airborne second-order gradients is that these equations cannot be used to estimate the mean of the first-order gradients. The mean has to be estimated from other sources.

The horizontal gradient T_y can be estimated from airborne gradients T_{yz}; T_{xy}, T_{yy}; T_{xy}, T_{yy}, T_{yz} with formulas similar to those developed in this section for the estimation of T_x. Thus limiting the estimation of T_y to the case of noise-free gradients, the spectrum of T_y is given in terms of the spectra of the above mentioned gradients by the following equations

$$F\{T_y(x,y)\}= -\frac{1}{2\pi}\ \frac{e^{2\pi hq}}{q}\ F\{T_{yz}(x,y,h)\} \tag{4.73}$$

$$F\{T_y(x,y)\} = -\frac{jue^{2\pi hq}}{2\pi q^2} F\{T_{xy}(x,y,h)\} - \frac{jve^{2\pi hq}}{2\pi q^2} F\{T_{yy}(x,y,h)\} \tag{4.74}$$

$$F\{T_y(x,y)\} = -\frac{jue^{2\pi hq}}{4\pi q^2} F\{T_{xy}(x,y,h)\} - \frac{jve^{2\pi hq}}{4\pi q^2} F\{T_{yy}(x,y,h)\} - \frac{e^{2\pi hq}}{4\pi q} F\{T_{yz}(x,y,h)\} \tag{4.75}$$

$$F\{T_y(x,y)\} = \frac{jve^{2\pi hq}}{2\pi q^2} F\{T_{zz}(x,y,h)\} . \tag{4.76}$$

It must be mentioned that the same frequency domain equations relating the first order and the second order gravity gradients can be developed by the use of the Wiener filter equation (3.64) taking into account the linear relations between the second-order gradients.

Chapter 5

SIMULATION OF AIRBORNE GRADIOMETER DATA

5.1 MODELLING THE LOCAL ANOMALOUS GRAVITY FIELD

Because flat earth approximation is used throughout this research it is plausible to employ planar mass anomaly models, with their planes parallel to the surface of the earth, for the modelling of a local anomalous gravity field. In addition it would be advantageous if these mass fields are sampled on regular two-dimensional grids. There is a number of approaches which can be used for the modelling of a local gravity field. Some of the well known models are multi-layer point mass models, vertical dipoles and vertical mass line models. Details on these models can be found in Forsberg (1984b) and Vassiliou (1985a). In this research a two-layer point-mass model was used.

A local coordinate system with origin at the center of the local area, x, y and z axes pointing east, north and upward is used in the following. A point mass buried at depth d below the earth's surface generates an isotropic anomalous potential. The gravity disturbance $\delta g(x,y)$ at the surface of the earth is given by

$$\delta g(x,y) = G_N \, m(x_p,y_p) \frac{d}{[(x_p-x)^2+(y_p-y)^2+d^2]^{3/2}} \tag{5.1}$$

where G_N is the Newton's gravitational constant and $m(x_p,y_p)$ is the point mass located at the point (x_p,y_p) at depth d below the surface of the earth. The Fourier transform and the PSD of the gravity disturbance caused by a point mass are expressed as

$$F\{\delta g(x,y)\} = 2\pi G_N m e^{-2\pi q d} \tag{5.2}$$

$$S_{\delta g,\delta g}(u,v) = 4\pi^2 G_N^2 m^2 e^{-4\pi q d} \ . \tag{5.3}$$

A stationary white noise distribution of point masses on a plane parallel to the earth's surface generates a gravity field described by the following spectrum and PSD

$$F\{\delta g(x,y)\} = 2\pi G_N F\{m(x,y)\} e^{-2\pi q d} \tag{5.4}$$

$$S_{\delta g,\delta g}(u,v) = 4\pi^2 G_N^2 S_{m,m}(u,v) e^{-4\pi q d} \tag{5.5}$$

where by m(x,y) in equation (5.4) is denoted the white noise mass distribution of the anomalous masses on the plane at depth d below the surface of the earth, and $S_{m,m}$ is the PSD of this mass distribution. Considering a two-layer stationary white-noise point mass model, with the two layers being statistically independent, the power spectral density of the gravity disturbance is given by

$$S_{\delta g,\delta g}(u,v) = 4\pi^2 G_N^2 S_{m_1,m_1}(u,v) e^{-4\pi q d_1} + 4\pi^2 G_N^2 S_{m_2,m_2}(u,v) e^{-4\pi q d_2} \tag{5.6}$$

where the subscripts 1,2 correspond to the layers 1 and 2, respectively. The two layers are considered as statistically independent because they model high frequency uncompendated mass anomaly features. However for regional modelling of the anomalous gravity field, there is compensation and the resulting deeper layers (probably at depths 20 km and 40 km) are negatively correlated. The synthetic PSD shown in eqn. (5.6) is the basis for the determination of the depths d_1, d_2 and is plotted logarithmically in Fig. 5.1.

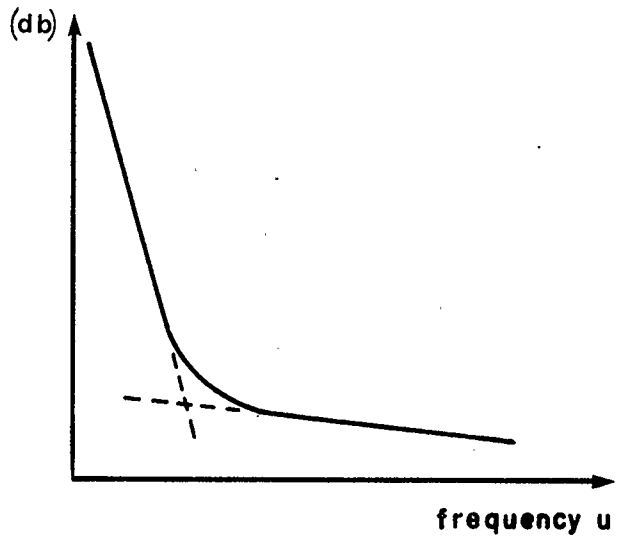

Figure 5.1 Gravity disturbance PSD generated by a two layer point mass model.

The PSD plotted logarithmically in Fig. 5.1, is mainly composed of two straight line segments each of which is a measure of the depth of the corresponding layer. Hence, provided a 2-D grid at the surface of the earth on which gravity disturbances are sampled, the slope of each of these straight line segments composing the isotropic PSD, provides the depth of each layer. In this way two of the parameters of the two layer point mass model are determined. The remaining parameters for modelling a local gravity field are the grid spacings of the two layers and the distribution of the gridded point masses on the two layers. The next step in modelling a local gravity field by a two layer point mass model, is the determination of the anomalous masses on the two layers. As is always the case in the gravity inversion problem, there are many mass distributions which can be used to model

a certain gravity field. To overcome this ambiguity the following approach was adopted in this thesis. First, the low frequencies of the given anomalous gravity field are modelled by point masses on the deep layer only. Then the spectral content of those frequencies modelled by the deep layer point masses, is subtracted from the original gravity disturbance signal and the residual gravity disturbances are modelled by shallow layer point masses.

Assuming one-to-one correspondence between the gravity disturbance sample points and the anomalous masses on one layer at depth d below the surface of the earth, the gravity disturbance at a grid point can be expressed as a convolution of the anomalous masses and the proper geometrical kernel

$$\delta g(x_k,y_l) = G_N \sum_{i=1}^{M} \sum_{j=1}^{N} d \frac{m(x_i,y_j)}{[(x_k-x_i)^2+(y_l-y_j)^2+d^2]^{3/2}} \tag{5.7}$$

where x_k,y_l are the coordinates of the evaluation point, x_i, y_j are the coordinates of the mass point $m(x_i,y_j)$ and M, N is the number of points in the x,y directions respectively. This convolution equation can be readily transformed in the frequency domain (in a discrete form) as

$$F\{\delta g(k,l)\} = 2\pi G_N \, F\{m(i,j)\} \, e^{-2\pi qd} \, . \tag{5.8}$$

Equation (5.8) can be readily inverted to model the gridded gravity disturbances by a set of gridded anomalous masses

$$F\{m(i,j)\} = \frac{1}{2\pi G_N} \, F\{\delta g(k,l)\} \, e^{2\pi qd} \, . \tag{5.9}$$

The spectrum of the anomalous masses is directly computed from the spectrum of the gravity disturbances. There is a major problem though related to this equation, the downward continuation instability, appearing through the exponential operator $e^{2\pi qd}$. The deeper the layer is buried, the more troublesome the downward continuation becomes. There is a number of methods to get around the downward continuation problem mentioned in Nashed (1976). One of those methods is to smooth the data with a low pass filter so that the errors at the high frequencies are not amplified.

5.2 IMPLEMENTATION OF THE MODELLING OF GIVEN GRAVITY DISTURBANCES BY A TWO-LAYER POINT MASS MODEL

The modelling of the gravity disturbances by the two-layer point mass model is done in three major steps. First the grid spacings of the two layers are assigned. Second the anomalous point masses on the deep layer are determined and third the anomalous point masses on the shallow layer are computed. First, the grid spacings of the two layers, of which the depths have been already determined (in section 5.1), are chosen. The grid spacings of the deep layer are set equal to the double grid spacings of the original gravity disturbance grid, while the grid spacings of the shallow layer are the same as the ones of the gravity grid. Then the spectra of the geometrical kernels appearing in equation (5.7) are computed for both layers using either FFT or the continuous form of the spectra as shown in equation (5.8). The second step of the method then starts by sampling the gravity disturbances on a grid with double the grid spacings of the given grid and windowing the resulting data by a 2-D cosine taper window. The

spectrum of the windowed gravity disturbances is computed afterwards by a 2-D FFT. Then, since the kernel spectrum is known for the deep layer, the spectrum of the anomalous masses can be readily computed from equation (5.9). The downward continuation instability is taken care of by filtering the data with a 2-D low-pass filter having a cut-off frequency at 0.35 cycles/grid spacing in each direction. The anomalous masses can then be computed by transforming the spectrum of the mass anomalies in the space domain. The disturbances generated by the deep layer point masses are interpolated using 2-D FFT, as it is shown in section 3.1.5, so that the interpolated disturbances correspond to the original gravity grid.

The third modelling step starts with the subtraction of the interpolated from the given gravity disturbances. The residual disturbances are then windowed and their spectrum is computed using the 2-D FFT. From those residual gravity disturbances and the geometrical kernel of the shallow layer, the spectrum of the anomalous masses located on the shallow layer is estimated using equation (5.9). The downward continuation instabilities are avoided by using a 2-D low-pass filter with cut-off frequency of 0.45 cycles/grid spacing in each direction. Then the spectrum of the anomalous masses is transformed via FFT into the space domain to yield the anomalous masses on the shallow layer. Using these anomalous masses and the kernel of the shallow layer, the gravity disturbances corresponding to the shallow layer can be computed. The sum of the gravity disturbances corresponding to the deep and to the shallow layer is within 0.1 to 0.2 mgals of the original gravity disturbances.

The mass anomalies computed from the modelling of the gravity

disturbances (gravity anomalies) by the two layer point mass model are used to compute any functional of the anomalous potential, for example first-order gradients are computed from the combined effect of the anomalous masses of the two layers. The expressions for the first-order and second-order gradients at the earth's surface and their spectra generated by the anomalous masses of a single layer are given by

$$T_x(x,y) = -G_N \sum_{k=1}^{M} \sum_{l=1}^{N} m(x_k,y_l) \frac{(x-x_k)}{[(x-x_k)^2+(y-y_l)^2+d^2]^{3/2}} \tag{5.10}$$

$$F\{T_x(x,y)\} = G_N\, F\{m(x,y)\} \frac{ju}{q} e^{-2\pi qd} \tag{5.11}$$

$$T_y(x,y) = -G_N \sum_{k=1}^{M} \sum_{l=1}^{N} m(x_k,y_l) \frac{(y-y_l)}{[(x-x_k)^2+(y-y_l)^2+d^2]^{3/2}} \tag{5.12}$$

$$F\{T_y(x,y)\} = G_N\, F\{m(x,y)\} \frac{jv}{q} e^{-2\pi qd} \tag{5.13}$$

$$T_{xx}(x,y) = G_N \sum_{k=1}^{M} \sum_{l=1}^{N} m(x_k,y_l) \frac{[2(x-x_k)^2-(y-y_l)^2-d^2]}{[(x-x_k)^2+(y-y_l)^2+d^2]^{5/2}} \tag{5.14}$$

$$F\{T_{xx}(x,y)\} = -G_N\, F\{m(x,y)\} \frac{2\pi u^2}{q} e^{-2\pi qd} \tag{5.15}$$

$$T_{yy}(x,y) = G_N \sum_{k=1}^{M} \sum_{l=1}^{N} m(x_k,y_l) \frac{[2(y-y_l)^2-(x-x_k)^2-d^2]}{[(x-x_k)^2+(y-y_l)^2+d^2]^{5/2}} \tag{5.16}$$

$$F\{T_{yy}(x,y)\} = -G_N\, F\{m(x,y)\}\ \frac{2\pi v^2}{q}\, e^{-2\pi q d} \tag{5.17}$$

$$T_{zz}(x,y) = G_N \sum_{k=1}^{M} \sum_{l=1}^{N} m(x_k,y_l)\, \frac{[2d^2-(x-x_k)^2-(y-y_l)^2]}{[(x-x_k)^2+(y-y_l)^2+d^2]^{5/2}} \tag{5.18}$$

$$F\{T_{zz}(x,y)\} = G_N\, F\{m(x,y)\}\ 2\pi q e^{-2\pi q d} \tag{5.19}$$

$$T_{xy}(x,y) = G_N \sum_{k=1}^{M} \sum_{l=1}^{N} m(x_k,y_l)\, \frac{3(x-x_k)(y-y_l)}{[(x-x_k)^2+(y-y_l)^2+d^2]^{5/2}} \tag{5.20}$$

$$F\{T_{xy}(x,y)\} = -G_N\, F\{m(x,y)\} \frac{2\pi uv}{q}\, e^{-2\pi q d} \tag{5.21}$$

$$T_{xz}(x,y) = G_N \sum_{k=1}^{M} \sum_{l=1}^{N} m(x_k,y_l) \frac{3d(x-x_k)}{[(x-x_k)^2+(y-y_l)^2+d^2]^{5/2}} \tag{5.22}$$

$$F\{T_{xz}(x,y)\} = -G_N\, F\{m(x,y)\} j2\pi u e^{-2\pi q d} \tag{5.23}$$

$$T_{yz}(x,y) = G_N \sum_{k=1}^{M} \sum_{l=1}^{N} m(x_k,y_l) \frac{3d(y-y_k)}{[(x-x_k)^2+(y-y_l)^2+d^2]^{5/2}} \tag{5.24}$$

$$F\{T_{yz}(x,y)\} = -G_N\, F\{m(x,y)\} j2\pi v e^{-2\pi q d} \tag{5.25}$$

The airborne first-order and second-order gradients can be computed by upward continuation of the earth's surface gradients. This can be easily realized in the frequency domain by substituting $e^{-2\pi qd}$ by $e^{-2\pi q(d+h)}$ in equations (5.8), (5.11), (5.13), (5.15), (5.17), (5.19), (5.21), (5.23), (5.25) where h is the flying altitude. Similarly in the corresponding space domain relations the height difference d should be replaced by (d+h).

The gradient data at either the surface of the earth, or flying altitude are computed first in the frequency domain, taking advantage of the convolution property (3.15) of the Fourier transform. The spectra of the point mass anomalies on the two layers are known from the modelling of the gravity disturbance data. The spectra of the geometrical kernels corresponding to the gravity gradients can be computed from either the FFT of the space domain geometrical kernels, or from the corresponding continuous spectra appearing in equations (5.11), (5.13), etc.

5.3 THE SIMULATED GRADIENT DATA

Airborne gradient data were simulated in Northern Saskatchewan, Canada, where free-air gravity anomalies are given on a 5'x10' grid. The extent of the area is

$$56°02'30'' \leqq \phi \leqq 60°13'00''$$

$$250°05'00' \leqq \lambda \leqq 258°35'00''.$$

There are 52 points in each direction, 2704 points totally. Flat earth approximation was employed with the following transformation

$$dy = Rd\phi$$

$$dx = R\cos\phi d\lambda$$

with mean earth radius R=6371 km. In the above transformation the grid spacings in North-South and East-West directions are

$$\Delta y = 9.266 \text{ km}$$

$$\Delta x = 9.775 \text{ km.}$$

The spherical harmonic expansion of the Rapp 1978 geopotential model (Rapp, 1978) truncated at degree 36 was subtracted from the free-air gravity anomalies to eliminate the long-wavelengths to which airborne gravity gradiometry is not sensitive. The contour map of the gravity anomalies is shown in Fig. 5.2. The units along the x,y axes are in km and the gravity anomalies are in mgals.

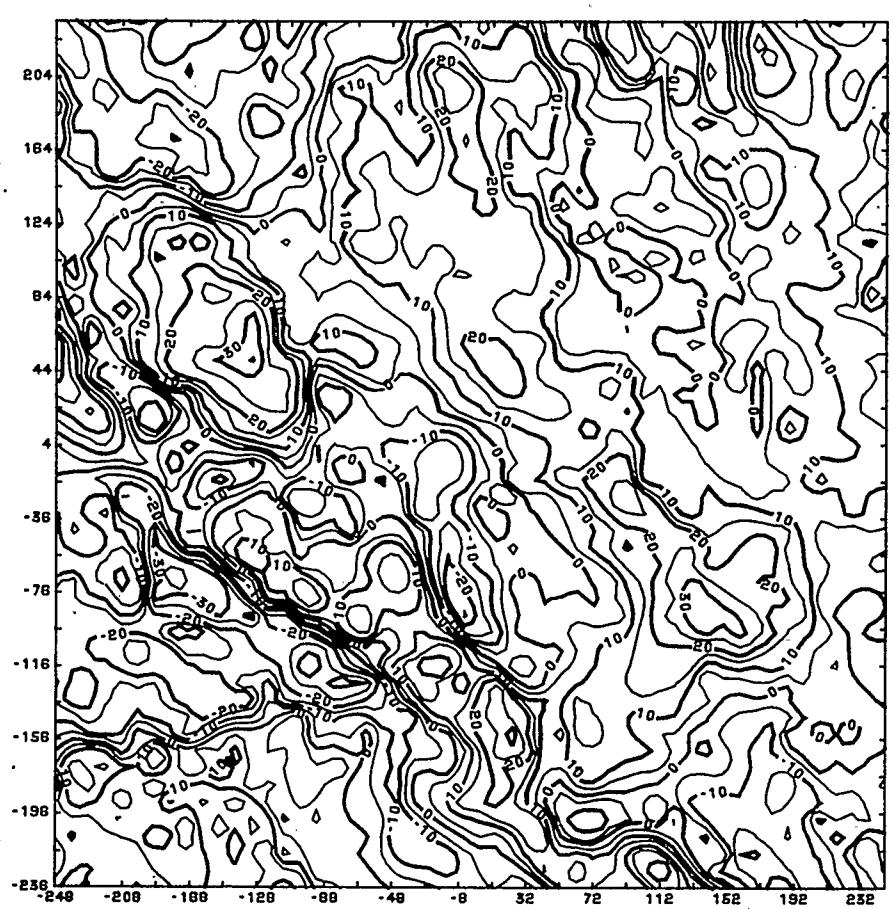

Fig. 5.2 Contour map of the reduced 5'x10' gravity anomalies

Then the isotropic PSD of the data was computed and from its logarithmic plot the depths of the two layers are determined in Fig. 5.3.

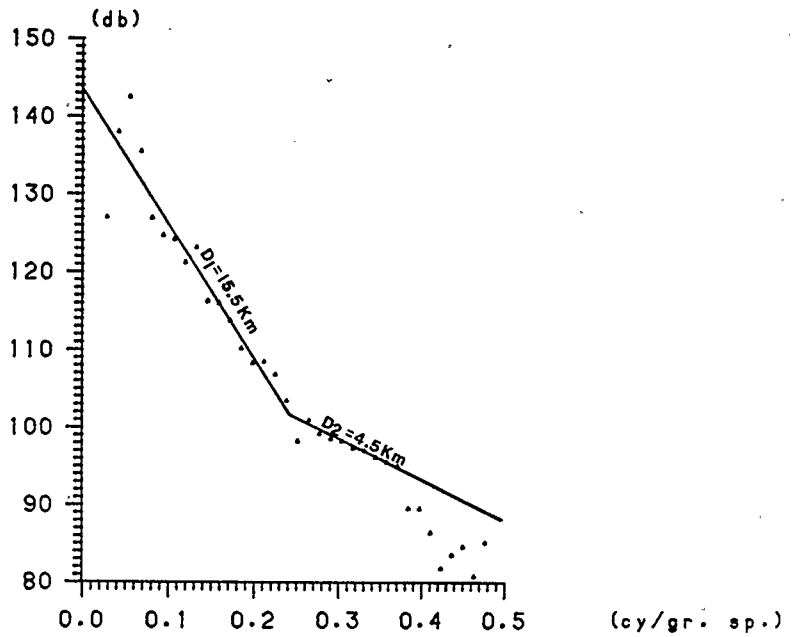

Fig. 5.3 Isotropic power spectral density of the gravity anomalies

The point masses of the two layers and the first and second-order gradients at the surface of the earth and at flying altitude of 600 m were computed as described in section 5.2. The results of the point mass computations are given in Vassiliou (1985a). The computed gradient data are given on the 9.266 km (north) x 9.755 km (east) grid. These grid spacings are too large to ensure resolution of the gravity signal down to the 1 mgal level. Spectral analysis of Canadian gravity anomaly data has shown that for flat areas a minimum grid spacing of 3 km is necessary to resolve the gravity signal to the 1 mgal level (Vassiliou and Schwarz, 1985).

Therefore the data were densified to a 2.315 km (north) x 2.444 km (east) grid. The new grid has 204 points in each direction and 41616 points totally. The grid spacings are quarters of the former grid spacings, so the FFT interpolation method described in section 3.1.5 can be employed to sample the gradient data on the new denser grid. However, the interpolated gravity signal sampled has the same smoothness as the original one. To add more high frequency content in the gradient data, a white noise distribution of anomalous point masses was sampled at a 2-D grid on a layer buried 1 km below the surface of the earth. This white noise point mass grid has the same spacings as the new denser gradient grid (2.315 x 2.444 km). The simulated white noise masses have zero mean and standard error of 2.5 x 10^6 grams. The simulation was performed using the subrouting OU of the simulation software package ACSL installed on the CDC Cyber 175 computer at the University of Calgary. The anomalous masses thus generated are used to compute the first and second-order gradient at the surface of the earth and at flying altitude of 600 m. Those gradients are added to the smoother gradients already sampled on the new grid, and thus the final simulated gradient data are created. The contour maps as well as the block diagrams of the first-order gradients T_x, T_y, T_z simulated at the surface of the earth are shown in Figs. 5.4, 5.5, 5.6, 5.7, 5.8 and 5.9 respectively. The units of the x, y axes in the contour maps are in km and the first-order gradient data are in mgals.

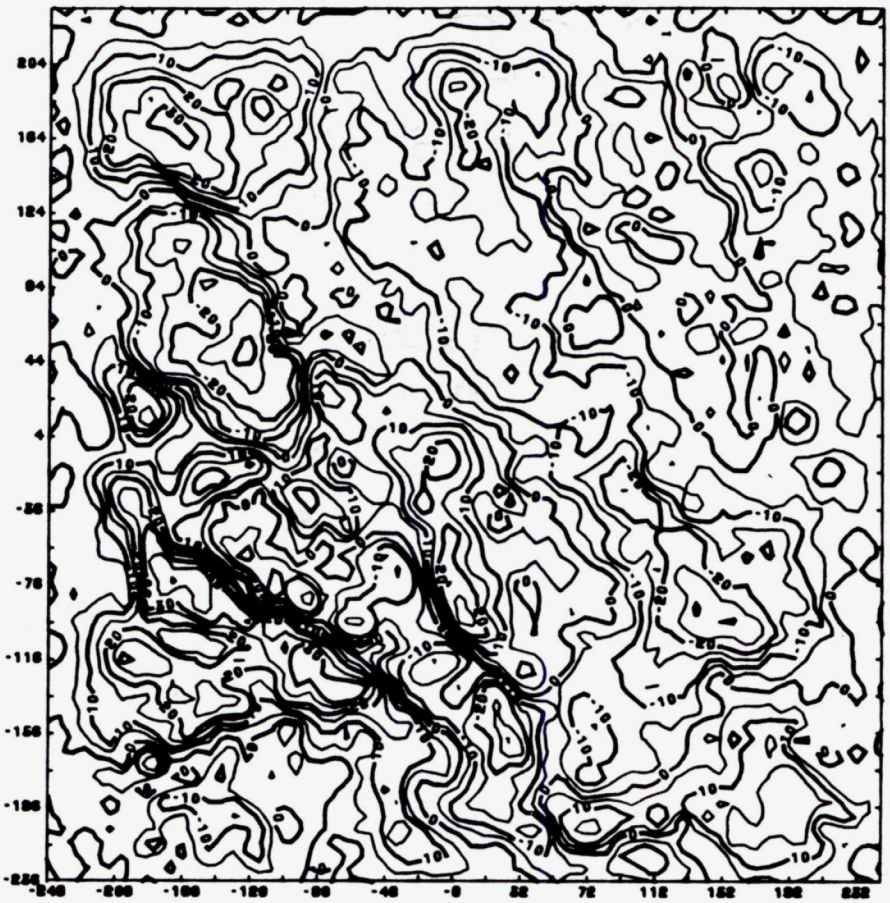

Fig. 5.4 Contour map of the simulated T_z gradients (h=0.0)

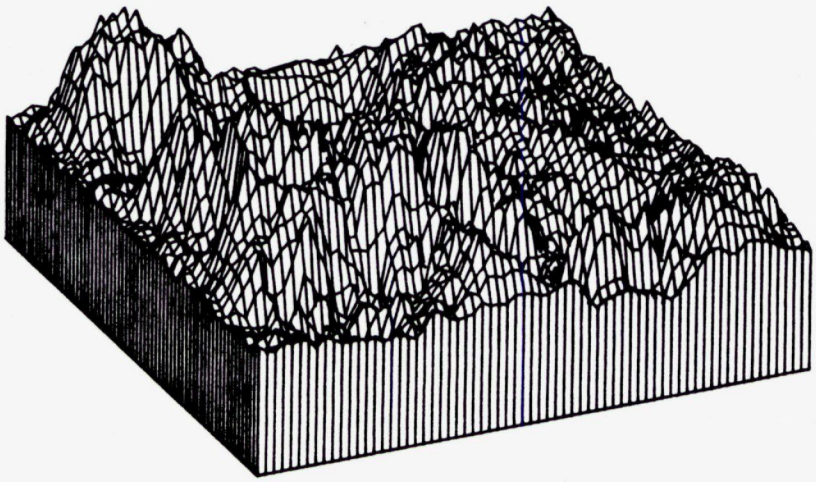

Fig. 5.5 Block diagram of the simulated T_z gradients (h=0.0)

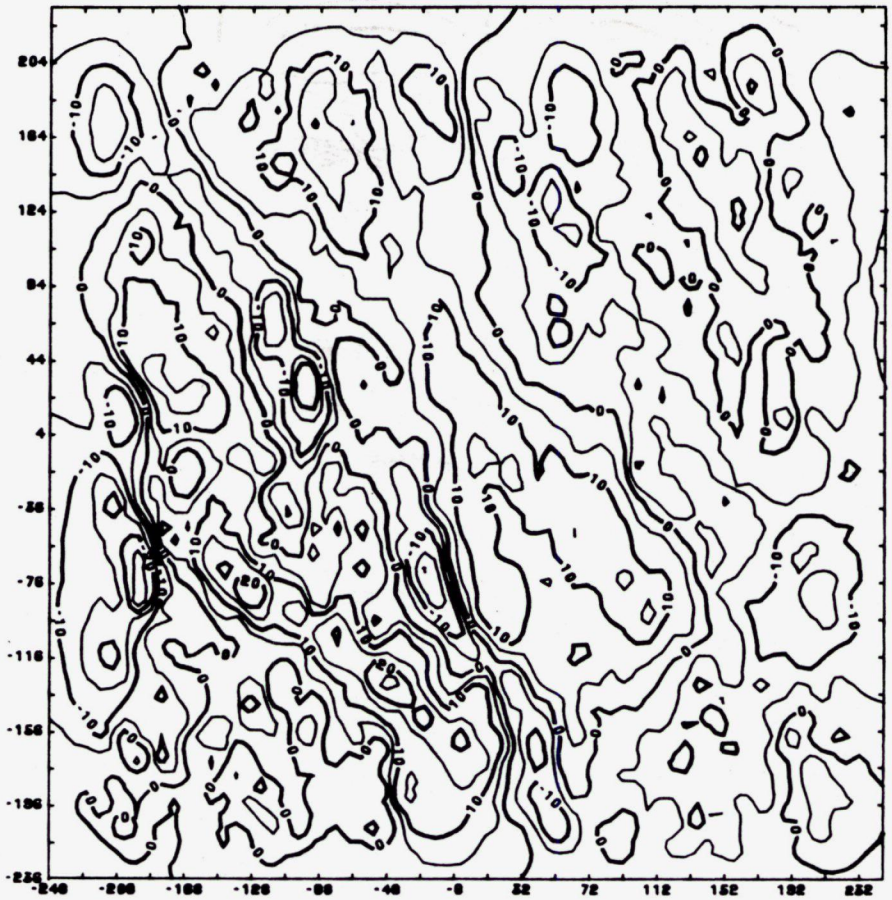

Fig. 5.6 Contour map of the simulated T_x gradients (h=0.0)

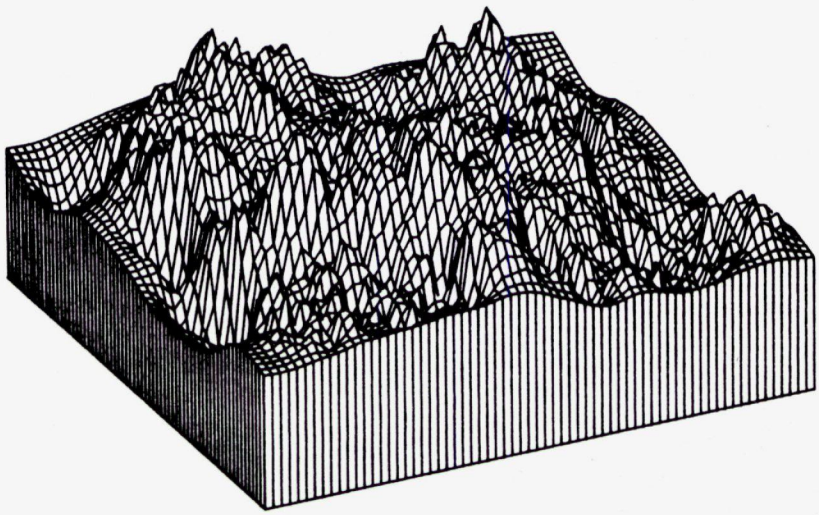

Fig. 5.7 Block diagram of the simulated T_x gradients (h=0.0)

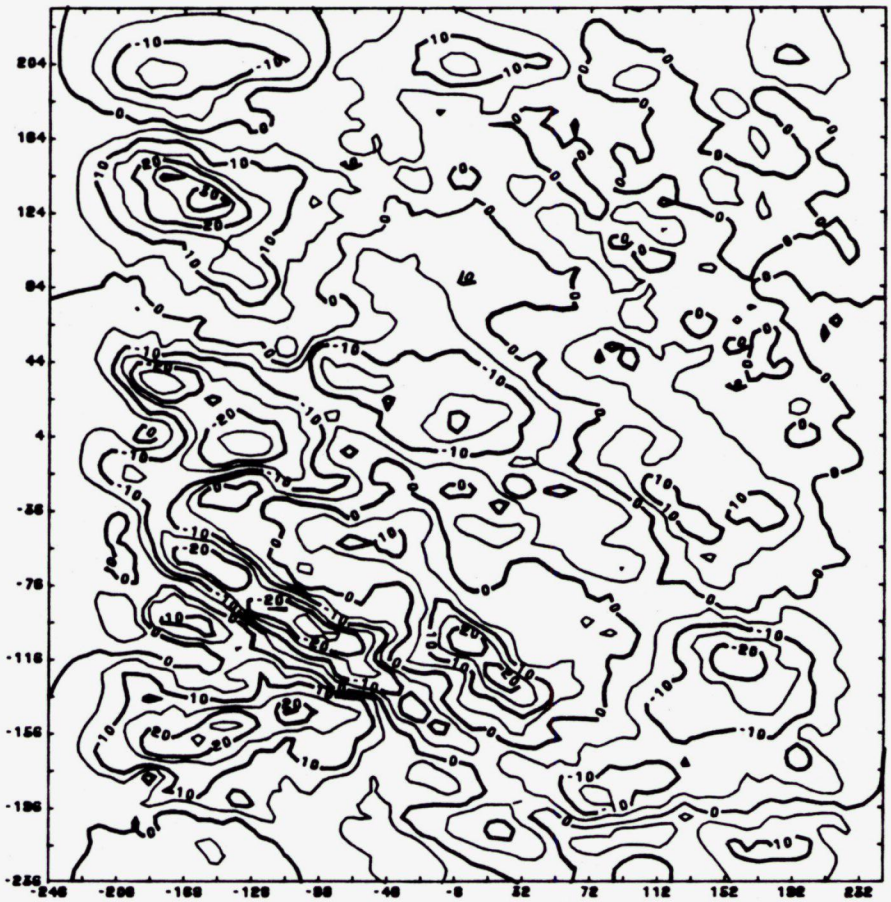

Fig. 5.8 Contour map of the simulated T_y gradients (h=0.0)

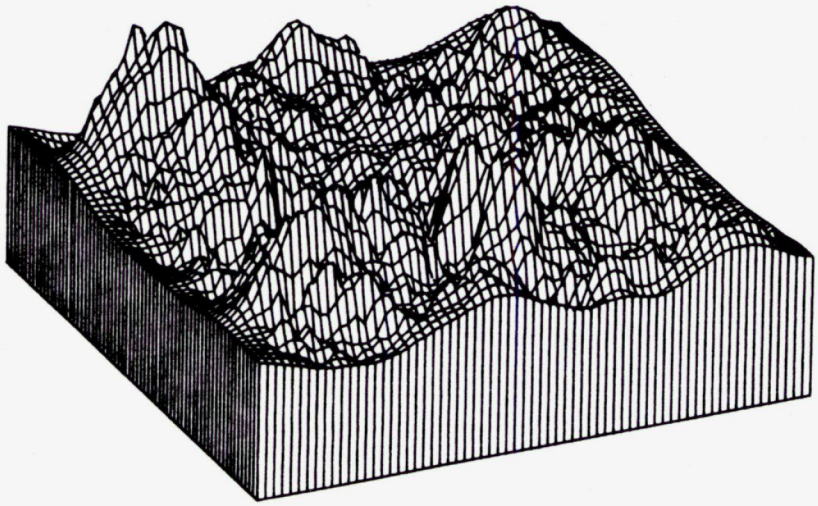

Fig. 5.9 Block diagram of the simulated T_y gradients (h=0.0)

Gradiometer noise was added to the second-order gradient data at flying altitude. The simulated gradiometer noise is based on the Bell gradiometer noise model already discussed in section 2.2. The simulation of the noise is explained in detail in the next section.

5.4 SIMULATION OF THE GRADIOMETER NOISE

The gradiometer noise, based on the Bell gradiometer noise (White, 1980), was simulated using a time-domain Markov model. The model produces a spectrum consisting of low frequency red noise and high frequency white noise, similar to the one discussed in section 2.2. The simulation starts with the generation of white noise, employing subrouting OU of the simulation software package ACSL The white noise has mean zero and 1 Eötvos standard error. Then the white noise is integrated numerically from time zero to the evaluation time t_1 and is multiplied by $2\pi \sqrt{R}$, where R is the red noise constant. The numerical integration was performed by the trapezoidal rule, or the midpoint rule. The result of this integration-multiplication is the red noise part of the total noise at time t_1. The zero mean, 1 Eötvos standard error white noise at time t_1, is multiplied by $\sqrt{W}$, where W is the white noise constant, to yield the white noise part at this time. The red and white parts of the noise are then summed to yield the total noise at time t_1. This whole procedure is shown in Fig. 5.10.

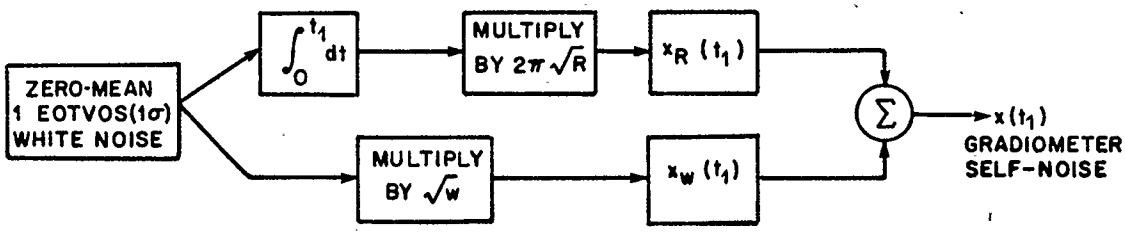

Fig. 5.10 Simulation of gradiometer noise by a time domain Markov model.

Chapter 6

SOFTWARE

Twenty five FORTRAN programs were written for this research. The first ten of those programs deal with the gravity data modelling and the simulation of the airborne gradient data and they are discussed in section 6.1. The output of the last six of these programs are used as inputs for the airborne gradiometry programs. The other fifteen programs compute the first-order gravity gradients from the airborne second-order gravity gradients using the estimation procedures presented already in section 4. Those last fifteen computer programs are described in section 6.2 in more detail than the first ten simulation programs.

The programs written for this thesis were optimized with respect to memory space. However the memory requirements for some of them were so high that some programs had to be split into two parts. For instance the program computing T_z from the gradients T_{zz}; T_{xz}, T_{yz}; T_{xz}, T_{yz}, T_{zz} taking into account the noise or neglecting it, had to be split into two programs, one taking the noise into account and the second one neglecting it.

6.1 DESCRIPTION OF THE PROGRAMS FOR GRAVITY SIMULATION

The first two programs, GENER1 and GENER11 compute the gravity disturbance geometrical kernels for the three layers used for the modelling of the gravity data. The next program SHFA reads in the gravity disturbance geometrical kernels for the very shallow layer (1 km depth) and the white noise point masses located at the grid points

of this layer. It computes the spectra of the anomalous masses and of the geometrical kernels, it multiplies the two spectra and then inverts the resulting spectrum via the inverse 2-D FFT to get the gravity disturbances at the surface of the earth.

The fourth program GRAVITYMOD reads in the reduced 5'x10' gravity anomalies, shown in Fig. 5.2, the gravity disturbances corresponding to the very shallow layer, and the geometrical kernels corresponding to the two deeper layers. The gravity disturbances are windowed by a 2-D cosine taper window. Then they are modelled by the two layer point mass model exactly as analyzed in section 5.2, and thus the anomalous point masses on the two deeper layers are computed. Finally the gravity disturbances resulting from the anomalous point masses of all three layers are summed yielding the final gridded gravity disturbances at the surface of the earth.

The next two programs GRAVMODEL1 and GRAVMODEL11 compute the first-order anomalous gravity gradients at the surface of the earth and at flying altitude of 600 m respectively. The first program GRAVMODEL1, reads in the anomalous point masses of the three layers and computes the spectra of the gradients T_x, T_y, T_z at the earth's surface using formulas (5.11), (5.13) and (5.8) respectively. Then by using the inverse 2-D FFT, the values of T_x, T_y, T_z at the earth's surface grid points are computed. The second program GRAVMODEL11, reads in the same data and performs the same computations as the program GRAVMODEL1. There is only one major difference, the exponential operator $e^{-2\pi qd}$ in equations (5.8), (5.11) and (5.13) is replaced by $e^{-2\pi q(d+h)}$, where h is the flying altitude of 600 m.

The seventh and eighth programs GRAVMODEL2 and GRAVMODEL22 compute the second order anomalous gravity gradients T_{xx}, T_{yy}, T_{zz} both at the surface of the earth and at flying altitude of 600 m. The procedure is almost the same as with the programs GRAVMODEL1 and GRAVMODEL11, but instead of the equations (5.8), (5.11) and (5.13), the equations (5.15), (5.17) and (5.19) are used. In addition the gradients T_{xx}, T_{yy}, T_{zz} are corrupted by gradiometer noise, which is computed as described in section 5.4. The last two of the simulation programs GRAVMODEL3 and GRAVMODEL33 compute the second-order anomalous gravity gradients T_{xy}, T_{xz} and T_{yz} at the surface of the earth and at flying altitude of 600 m.

6.2 DESCRIPTION OF THE PROGRAMS FOR AIRBORNE GRADIOMETRY

The first program, DOWNWTZD, computes the first-order gradient T_z at the surface of the earth, exactly below the grid measurement points, from airborne gradients T_{zz}; T_{xz}, T_{yz}; T_{xz}, T_{yz}, T_{zz} performing both plane integration and downward continuation. First, the program reads the general data, the true gradients T_z at the earth's surface and the airborne gradients T_{xz}, T_{yz}, T_{zz}. It sets the mean of T_z equal to zero, windows the second-order gradient data and computes the spectra of those data using the 2-D FFT. Then the program proceeds to compute the transfer functions corresponding to the estimation of T_z from T_{zz}; T_{xz}, T_{yz}; T_{xz}, T_{yz}, T_{zz} according to equations (4.15), (4.21) and (4.29), (4.30), (4.31) and (4.32) respectively. The gradiometer noise is not taken into account in the computations of those transfer functions. Next, the spectra of T_{zz}; T_{xz}, T_{yz}; T_{xz}, T_{yz}, T_{zz} are multiplied by the appropriate transfer

functions and the resulting spectra are transformed in the space domain by using the inverse 2-D FFT to yield the three estimates of T_z at the surface of the earth. Finally the differences between the true T_z and the three estimated T_z are computed and printed for a block about 45 km inside the borders of the area. In addition the root mean square value of those differences is computed and printed. The flow-chart of this program is given in Fig. 6.1.

The next program, DOWNWTXD, computes the horizontal first-order gravity gradient T_x at the surface of the earth from airborne gradient measurements T_{zz}; T_{xz}; T_{xx}, T_{xy}; T_{xx}, T_{xy}, T_{xz}. The program neglects the gradiometer noise and has the same structure as the program DOWNWTZD. The program DOWNWTYD computes the gradient T_y at the earth's surface from airborne gradient measurements T_{zz}; T_{xz}; T_{xx}, T_{xy}; T_{xx}, T_{xy}, T_{xz}. The program neglects the gradiometer noise and has the same structure as the programs DOWNWTZD and DOWNWTXD.

The next three programs DOWNWTZDN, DOWNWTXDN, DOWNWTYDN compute the first-order gradients T_x, T_y, T_z from airborne second-order gradient data, taking the gradiometer noise into account. More specifically the program DOWNWTZDN computes T_z at the surface of the earth from airborne gradients T_{zz}; T_{xz}, T_{yz}; T_{zz}, T_{xz}, T_{yz}. The programs DOWNWTXDN and DOWNWTYDN compute the gradients T_x, T_y respectively. The structure of these three programs is the same as of the program DOWNWTZD.

The following three programs FINTZD, FINTXD and FINTYD compute the first-order gradients T_z, T_x and T_y respectively at flying altitude from airborne second-order gradient data. These three programs perform plane integration only and neglect the gradiometer

noise. They use almost the same formulas as the programs DOWNWTZD, DOWNWTXD and DOWNWTYD respectively, the only difference being that the downward continuation operator $e^{2\pi hq}$ becomes unity. The next three programs FINTZDN, FINTXDN and FINTYDN compute the first-order gradients T_z, T_x, T_y at flying altitude from second-order gradient data, taking the gradiometer noise into account.

The final three programs INTERTZ, INTERTX and INTERTY compute the gradients T_z, T_x, T_y at the surface of the earth, but on a denser grid, which has grid spacings equal to one half of the spacings of the measurement grid. Thus T_x, T_y, T_z are estimated besides the points directly below the points of the original grid, along orthogonal bidirectional profiles (running north-south and east-west) of the densified grid. The program INTERTZ begins by first reading the true gradients T_z and the estimated gradients T_{z_1}, T_{z_2}, T_{z_3} computed from the program DOWNWTZD all of them sampled on the 2.31 x 2.44 km grid. Next the gradients T_z and the estimated gradients T_{z_1}, T_{z_2}, T_{z_3} are interpolated at the grid points of the new grid, using the FFT interpolation procedure analyzed in section 3.1.5. Then the differences between the interpolated true gradients T_z and the interpolated estimated gradients T_{z_1}, T_{z_2}, T_{z_3} are computed and at the same time all interpolated gradients about 45 km inside the borders of the area are printed. Finally the rms values of these differences are computed and printed.

Six subroutines were written to support the above programs:

1. CAISBESWIND applies a 2-D Kaiser-Bessel window with argument α=3.0 to a set of 2-D gridded values.

2. BESSMOD computes the zero order modified Bessel function of the first kind.

3. COSWINDOW applies a 2-D cosine taper rectangular window to a set of 2-D gridded values.

4. SHIFTO shifts the origin of a 2-D direct Fourier transform from the south-west corner, where the IMSL subroutine FFT3D sets it, to the center of the 2-D complex array representing the 2-D Fourier transform.

5. FFTINTER interpolates a set of 2-D values sampled on a grid with spacings Δx, Δy so that another set of 2-D values sampled on a new grid having spacings Δx_1 , Δy_1 results. The former grid spacings are multiples of the new spacings, i.e. $\Delta x = M.\Delta x_1$, $\Delta y = N.\Delta y_1$, where M, N are positive integers. The interpolation is done with the help of FFT and the whole procedure is analyzed in section 3.1.5 of this research.

6. SPECDEZ computes the transfer function of the airborne gradients T_{zz}; T_{xz}, T_{yz}; T_{xz}, T_{yz}, T_{zz} with respect to the gradient T_z at the earth's surface. These transfer functions obviously combine plane integration and downward continuation. Depending on the first-order gradient which has to be estimated and the corresponding gradient data (i.e. T_x is estimated from T_{zz}; T_{xz}; T_{xx}, T_{xy}; T_{xx}, T_{xy}, T_{xz}) this subroutine changes accordingly. In the case of plane integration estimation only, the downward continuation operator $e^{2\pi hq}$ becomes unity.

   The subroutine FFT3D (IMSL, 1981) evaluating the 1-D, 2-D, 3-D FFT is used very frequently in most of the previously described 25 programs to compute the 2-D direct and inverse FFT.

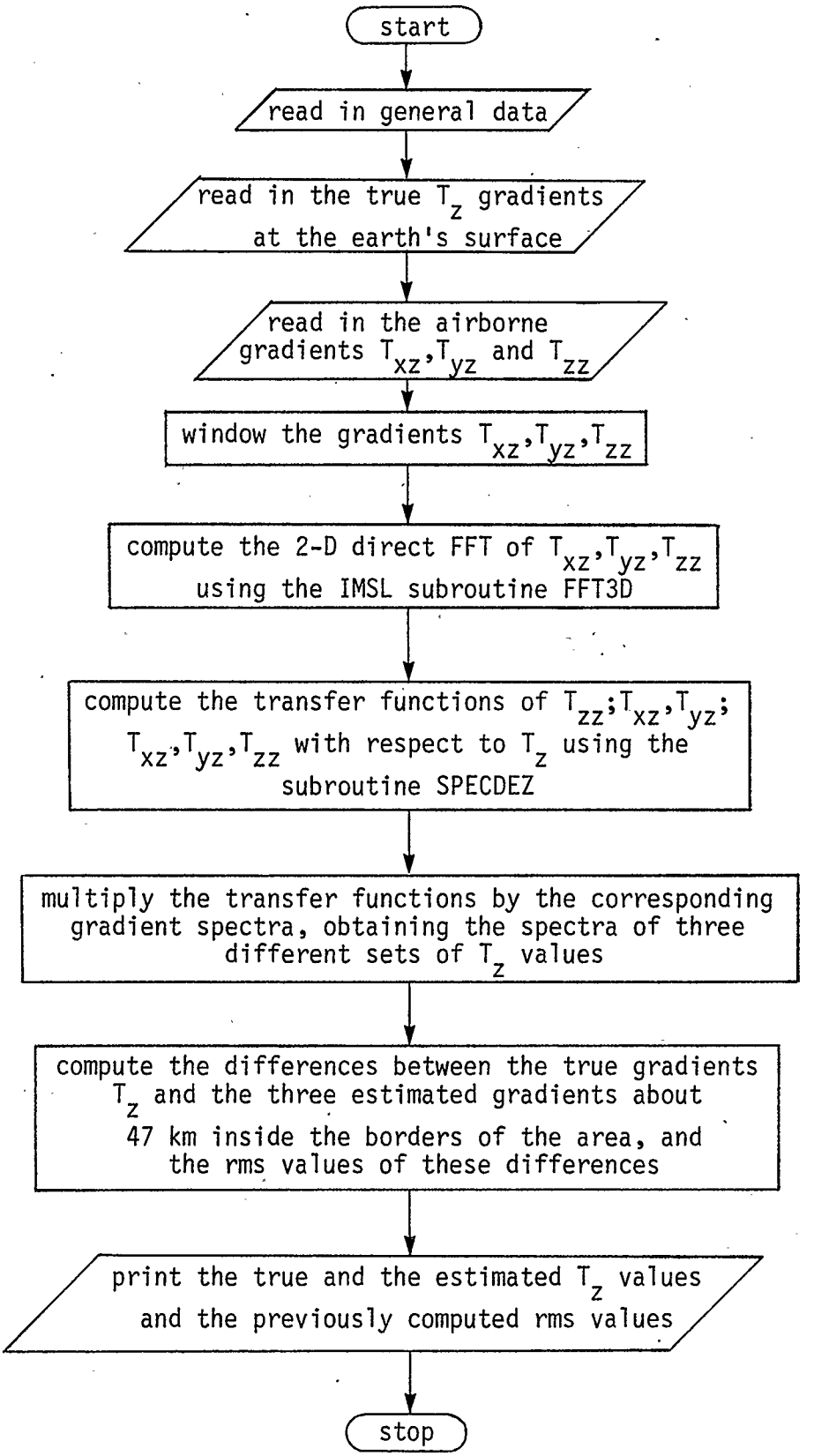

Fig. 6.1. Flow chart of the program DOWNWTZD

Chapter 7

TESTS AND RESULTS

In this chapter the results of estimating T_x, T_y, T_z from airborne second-order gradient data are discussed focussing on five points. First the practical proof, provided by computer implementation, that the method developed in chapter 4 yields satisfactory results for the estimation of the gradients T_x, T_y, T_z, in terms of accuracy and computer time requirements. This first point is discussed in all sections of this chapter. Second, the optimal choice of second-order gradients which provide the most precise determination of T_x, T_y, T_z. Third, the analysis of the effect of the gradiometer noise on the estimation of the first-order gradients. Fourth, the analysis of the effect of downward continuation on the accuracy of the estimation of T_x, T_y, T_z. Finally, the estimation of T_x, T_y, T_z at points other than those below the measurement points.

The results are presented in five sections. In the first one the edge effects due to the windowing are analyzed. In the second section the results from the determination of T_x, T_y, T_z directly below the measurement grid points by neglecting the gradiometer noise are discussed. In addition, the optimal choice of the second-order gradients providing the most accurate estimates of the first-order gradients is studied. The third section deals with the estimation of T_x, T_y, T_z at the same points as in the previous section taking the gradiometer noise into account. Also, in the same section the effect of higher gradiometer noise is analyzed. In the fourth section the

effect of downward continuation is studied by analyzing the results obtained from the plane integration of the second-order gradients. Finally, in the last section of this chapter the first-order gradients are estimated at points other than those directly below the measurement grid points. In all sections the estimated first-order gradients are compared to the true values of T_x, T_y, T_z. To avoid edge effects the comparison of the estimated and the true T_x, T_y, T_z is done in an inner area, about 45 km inside the borders of the total area. The computer times cited in the following refer to the Honeywell Multics DPS 68 computer of the University of Calgary.

All the following results are subject to the parameters of the simulation. Those parameters are the grid spacings of the gradient data grid, the flying altitude, the gradiometer noise level and the depths of the layers used for the simulation of the gradient data. Somewhat different conclusions have to be expected when all those parameters change. More specifically higher flying altitude guarantees lower accuracy in the estimation of T_x, T_y, T_z and stronger downward continuation effects. Larger grid spacings will result in a smoother gravity signal which in turn will definitely create significantly worse estimates of T_x, T_y, T_z at points other than those directly below the measurement points. Higher gradiometer noise means lower accuracy in the estimation of T_x, T_y, T_z, especially when the noise is not taken into account. Larger layer depths will necessarily imply larger grid spacings, in order to avoid downward continuation effects, and thus the same effects as for larger grid spacings will be apparent.

7.1 THE EFFECT OF WINDOWING

Spectral leakage problems arising from the application of the 2-D Fourier transform to all gradient data, are minimized by windowing the data sets. The two windows used are the Kaiser-Bessel and the cosine taper window. Both have been discussed in section 3.1.4. The windowing percentages for both directions are 10%. Due to the windowing, edge effects are created, i.e. the estimation gets poorer towards the edges of the area. To find out how far from the borders of the area the edge effects extend, the following test was conducted. The first-order gradients T_x, T_y, T_z were computed from the gradients T_{xz}, T_{yz}, T_{zz} respectively as described in section 4. Then the differences between the estimated and the true T_x, T_y, T_z and the RMS of those differences were computed. The minimum acceptable RMS level was set to 1.0 mgal and the distances from the borders of the area at which the RMS value becomes smaller than 1.0 mgal were determined. These distances were 46 km from the north and south borders and 48 km from the east and west borders of the area. The inner area is shown in Fig. 7.1 and all subsequent results refer to this area.

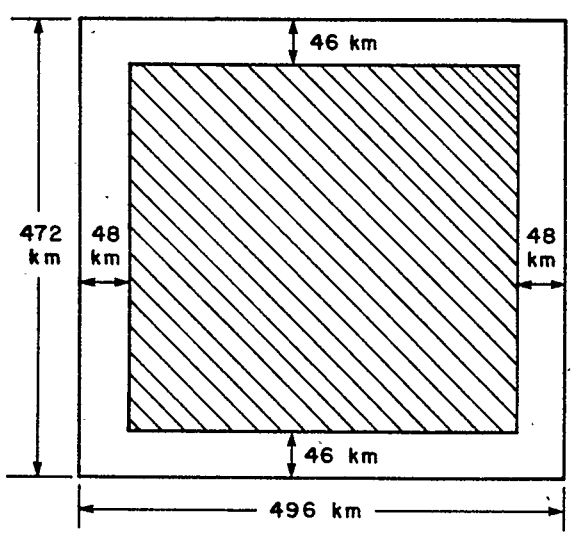

Fig. 7.1 Inner area used for comparison of estimated and true T_x, T_y, T_z

7.2 ESTIMATION OF T_x, T_y, T_z WITHOUT THE GRADIOMETER NOISE

The estimation of T_x, T_y, T_z in this section as well as in the next section is done only at points lying directly below the measurement grid points. No interpolation between points on the same or neighboring tracks takes place. In this way the usefulness of T_{zz} gradients for downward continuation can be demonstrated numerically. In addition, the possibility of using a gradiometer measuring only T_{zz} gradients can be investigated. The results obtained and the computer times required are listed in Table 7.1.

Table 7.1

Results and CPU Times for the Estimation of T_x, T_y, T_z, Neglecting the Noise

Measurements		
	RMS error of T_z(mgals)	CPU time required (seconds)
T_{zz}	0.70	545
T_{xz}, T_{yz}	0.46	560
T_{xz}, T_{yz}, T_{zz}	0.41	578
	RMS error of T_x(mgals)	
T_{zz}	0.79	584
T_{xz}	0.87	583
T_{xx}, T_{xy}	0.79	601
T_{xx}, T_{xy}, T_{xz}	0.63	617
$T_{xx}, T_{xy}, T_{xz}, T_{zz}$	0.62	632
	RMS error of T_y(mgals)	
T_{zz}	0.49	583
T_{yz}	0.69	584
T_{xy}, T_{yy}	0.76	601
T_{xy}, T_{yy}, T_{yz}	0.60	615
$T_{xy}, T_{yy}, T_{yz}, T_{zz}$	0.56	634

Table 7.1 allows some interesting conclusions. First the estimation of T_x, T_y, T_z using T_{zz} only is in general comparable in accuracy to all other second-order gradient combinations used. This means that a single vertical axis gravity gradiometer measuring T_{zz} only can be considered as an alternative to a three axis gradiometer providing all elements of the second-order gradient tensor for downward continuation. Second, T_x, T_y, T_z are estimated with essentially the same level of accuracy which is usually well below the 1 mgal level. Third, the horizontal gradients T_x, T_y are estimated with better accuracy from T_{zz} than from T_{xz}, T_{yz}, respectively. The explanation of this result is that the transfer functions of T_{zz} with respect to T_x, T_y (eqns. 4.67, 4.76) are less sensitive to the combined downward continuation gradiometer noise effects than the transfer functions of T_{xz}, T_{yz} with respect to T_x, T_y respectively (eqns. 4.51, 4.73). Fourth, there is always an improvement in accuracy when the vertical gradient T_{iz} of any first-order gradient T_i is added to the combination of its two horizontal second-order gradients T_{ix}, T_{iy}, i.e. it is better to choose the combination T_{xx}, T_{xy}, T_{xz} for T_x instead of the combination T_{xx}, T_{xy}. This is expected from equations (4.64), (4.65) which show an increase in the signal to noise ratio. Fifth, in general, the most precise estimate of the first-order gradients T_i is obtained from the combination of its second-order gradients T_{ji}, i.e. T_z is most precisely estimated from the combination of T_{xz}, T_{yz}, T_{zz}. Sixth, the estimation method developed is very efficient computationally. It takes about 10 CPU minutes to compute one first-order gradient at 41616 grid points from 167000 values of airbone gradient data including input and output.

The computational efficiency can be attributed to the efficiency of the FFT and to the fact that inversion of matrices larger than 1x1 are avoided.

Table 7.1 shows a surprisingly high accuracy achieved in the estimation of T_y from T_{zz} gradients. In addition T_y is more precisely estimated from T_{yz} than from T_{xy}, T_{yy}. This result is unexpected. However there is a simple explanation for it. In this specific test field the gradient T_y varies much more in the y direction than in the x direction. The signal to noise ratio for the gradient T_{yy} is high and it is very low for the gradient T_{xy}. Therefore, when the T_{xy} gradients are included in the determination of T_y the results are getting poorer. Thus the estimation of T_y from T_{xy}, T_{yy}, T_{yz} provides less accurate results than those obtained from the gradient T_{zz} only.

The block diagrams of the T_z errors estimated from T_{zz}; T_{xz}, T_{yz}; T_{xz}, T_{yz}, T_{zz} are shown in Figs. 7.2, 7.3 and 7.4 respectively. They illustrate clearly the edge effects and they show the improvement in accuracy obtained when using more than one gradient.

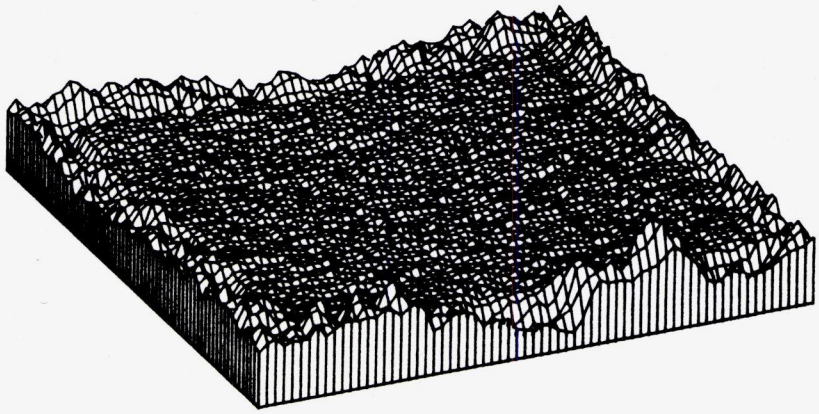

Fig. 7.2 Block diagram of T_z error determined from T_{zz}

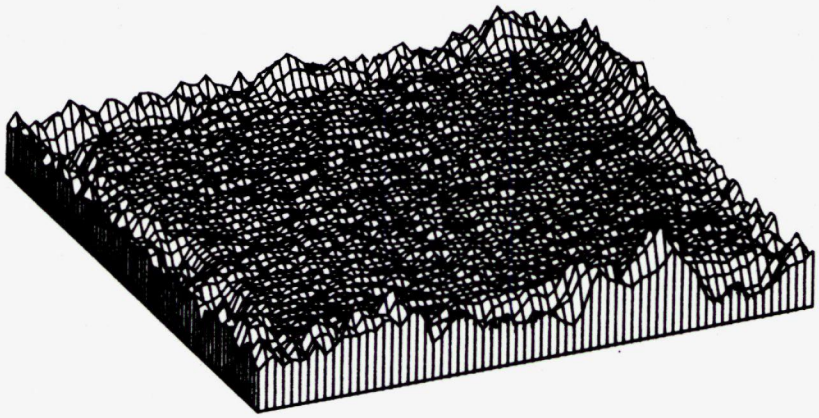

Fig. 7.3 Block diagram of T_z error computed from T_{xz}, T_{yz}

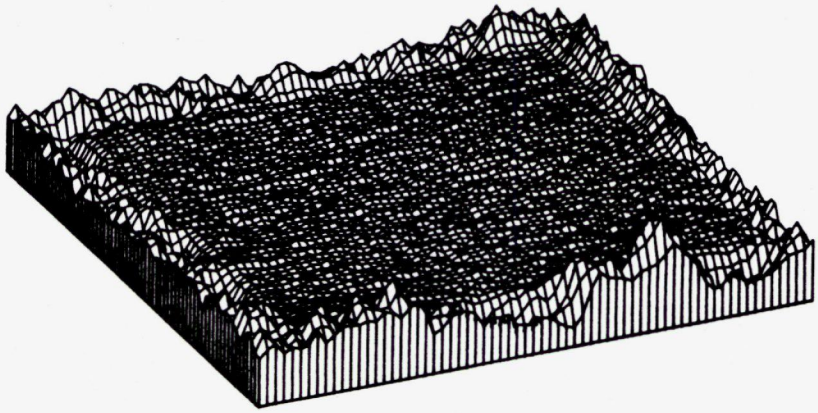

Fig. 7.4 Block Diagram of T_z error estimated from T_{xz}, T_{yz}, T_{zz}

7.3 EFFECT OF THE GRADIOMETER NOISE IN THE ESTIMATION OF T_x, T_y, T_z

This section has two objectives. First, to investigate how much improvement is obtained in accuracy when the gradiometer noise is included in the estimation model. Second to analyze the effect of higher noise level in the determination of the first-order gradients T_x, T_y, T_z.

For the first objective, the gradients T_x, T_y, T_z are computed and the gradiometer noise is taken into account. For this purpose it is necessary to have an estimate of the power spectral density of the anomalous potential $S_{T,T}(u,v)$ as shown in eqns. (4.29), (4.37), (4.38), etc.) The following model was used (Vassiliou and Schwarz, 1985).

$$S_{T,T}(q) = \frac{A}{q^{1.6}} \tag{7.1}$$

where the constant A was computed from gravity anomalies in the sample area. The PSD of the gradiometer noise $S_{n,n}(u,v)$ was computed from the simulated gradiometer noise data and the white noise PSD level is $80E^2/Hz$.

For the second objective of the present section, the gradiometer noise is very significantly changed by increasing the white noise PSD level to 300 E^2/Hz. The gradients T_x, T_y, T_z are computed first by neglecting the gradiometer noise and second by taking the noise into account. The results from both parts of the section are summarized in Table 7.2

Table 7.2

Results of Estimating of T_x, T_y, T_z Taking the Gradiometer Noise into Account

Measurements	Noise: 80 E^2/Hz without noise	Noise: 80 E^2/Hz with noise	Noise: 300 E^2/Hz without noise	Noise: 300E^2/Hz with noise
	RMS error of T_z(mgals)			
T_{zz}	0.70	0.63	0.83	0.67
T_{xz}, T_{yz}	0.46	0.44	0.48	0.44
T_{xz}, T_{yz}, T_{zz}	0.41	0.37	0.47	0.41
	RMS error of T_x(mgals)			
T_{zz}	0.79	0.76	0.81	0.77
T_{xz}	0.87	0.88	0.99	0.88
T_{xx}, T_{xy}	0.79	0.73	0.80	0.74
T_{xx}, T_{xy}, T_{xz}	0.63	0.66	0.67	0.65
$T_{xx}, T_{xy}, T_{xz}, T_{zz}$	0.62	0.64	0.66	0.64
	RMS error of T_y(mgals)			
T_{zz}	0.49	0.50	0.56	0.50
T_{yz}	0.69	0.70	0.85	0.71
T_{xy}, T_{yy}	0.76	0.74	0.84	0.83
T_{xy}, T_{yy}, T_{yz}	0.60	0.60	0.65	0.63
$T_{xy}, T_{yy}, T_{yz}, T_{zz}$	0.56	0.55	0.62	0.61

Table 7.2 shows that at the noise level of 80 E^2/Hz there is only a slight improvement in the accuracy of T_x, T_y, T_z by taking the noise into account instead of neglecting it. This slight improvement in accuracy is obtained at the expense of a 15% increase in the computation time.

Four major points can be inferred from Table 7.2 for the case of gradiometer noise level of 300 E^2/Hz. First, there is only a small deterioration in accuracy when each gradient T_i is computed from either its two horizontal second-order gradients T_{ix}, T_{iy} or its three second-order gradients T_{ix}, T_{iy}, T_{iz}. Second, there is also a small deterioration in accuracy when the first-order gradients T_x, T_y are computed from T_{zz} only. This shows that for downward continuation a vertical single axis gradiometer measuring T_{zz} only, can be considered as an alternative to a 3 axis gradiometer even for high noise levels. Third, when the gradiometer noise is not taken into account there is a pronounced deterioration in the estimation of T_x, T_y, T_z computed from their vertical second-order gradients T_{xz}, T_{yz}, T_{zz} respectively. This fact can be explained by the low signal to noise ratios in the PSD of the residuals of T_x, T_y, T_z from T_{xz}, T_{yz}, T_{zz}, respectively. Therefore for the estimation of any first-order gradient from its corresponding vertical second-order gradient the noise should be taken into account. Fourth, the same accuracy in estimating T_x, T_y, T_z is achieved for noise at the level of 80 E^2/Hz or 300 E^2/Hz when the gradiometer noise is included in the estimation process. This shows the stability of the estimation method.

7.4 THE EFFECT OF DOWNWARD CONTINUATION

Since the results of the estimation of T_x, T_y, T_z reported so far incorporate both plane integration and downward continuation, it is of interest to investigate how much the estimation of T_x, T_y, T_z is affected by downward continuation. This investigation can be easily

performed by computing T_x, T_y, T_z at flying altitude from the airborne second-order gradients and comparing them to the previous results. All formulas necessary for this estimation have been developed in chapter 4. The results of this estimation when the gradiometer self-noise is neglected are summarized in Table 7.3.

Table 7.3

Determination of T_x, T_y, T_z at Flying Altitude

Measurements	
	RMS error of T_z(mgals)
T_{zz}	0.61
T_{xz}, T_{yz}	0.36
T_{xz}, T_{yz}, T_{zz}	0.34
	RMS error of T_x(mgals)
T_{zz}	0.71
T_{xz}	0.81
T_{xx}, T_{xy}	0.73
T_{xx}, T_{xy}, T_{xz}	0.58
$T_{xx}, T_{xy}, T_{xz}, T_{zz}$	0.54
	RMS error of T_y(mgals)
T_{zz}	0.44
T_{yz}	0.60
T_{xy}, T_{yy}	0.73
T_{xy}, T_{yy}, T_{yz}	0.56
$T_{xy}, T_{yy}, T_{yz}, T_{zz}$	0.55

Comparing Table 7.3 to Tables 7.1 and 7.2, the conclusion is that downward continuation generate errors of less than 0.1 mgal and usually less than 0.06 mgal. This conclusion agrees well with the covariance analysis results obtained by Jordan (1982). Similar results are obtained when the gradiometer noise is taken into account.

The small effect of downward continuation can be explained from the ratio of flying altitude to grid spacing. In this research the ratio is about 1:4. This means that the values of the downward continuation operator $e^{2\pi hq}$ vary between 1.0 and 2.1. This is more clearly illustrated in Fig. 7.5.

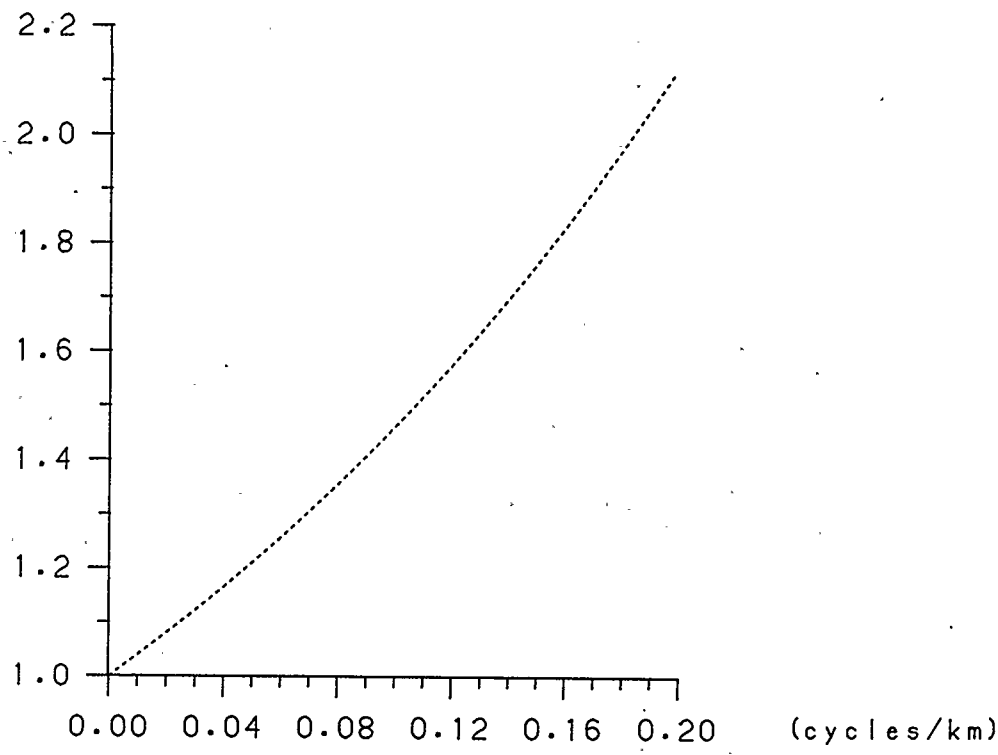

Fig. 7.5 Downward continuation operator for flying altitude of 0.6 km and grid spacing of 2.4 km.

Fig. 7.5 shows that for frequencies between 0.0 and 0.18 cycles/km, the downward continuation operator is below 2, so any errors introduced from the plane integration of the second-order gradients are amplified by a very small factor. With an increase in the flying altitude/grid spacing ratio, the downward continuation operator becomes larger and thus high frequency errors are greatly amplified. Fig. 7.6 illustrates the downward continuation operator for both flying altitude and grid spacing equal to 2.4 km, and the strong downward continuation effect becomes clear.

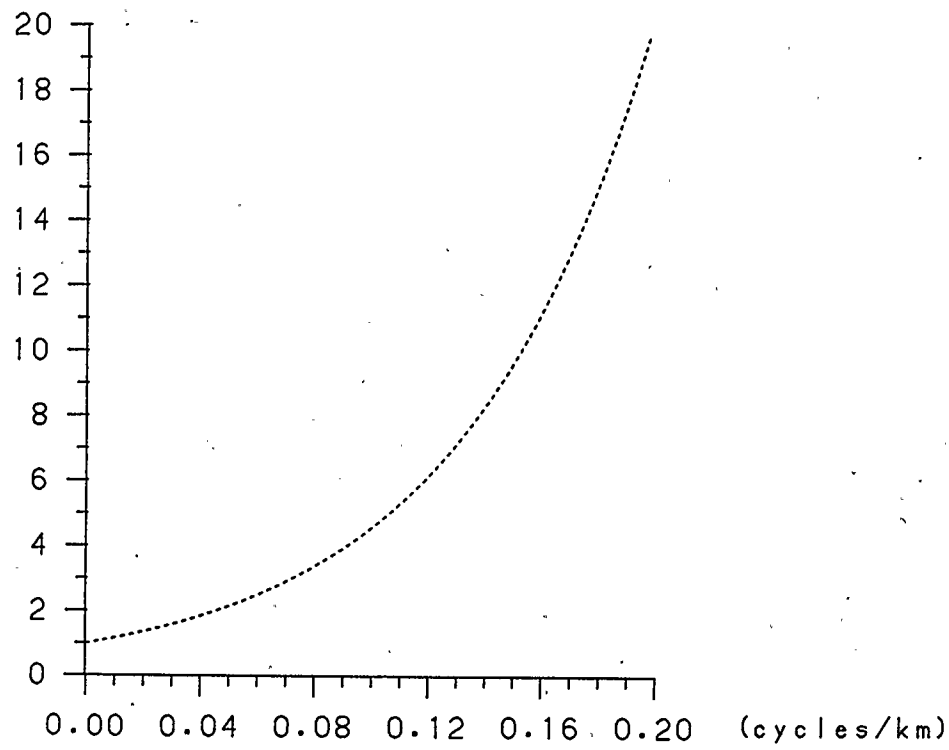

Fig. 7.6 Downward continuation operator for flying altitude and grid spacing equal to 2.4 km.

7.5 INTERPOLATION OF T_x, T_y, T_z BETWEEN PROFILE POINTS

To test the estimation method developed in chapter 4, the estimated first-order gradients T_x, T_y, T_z were interpolated between the grid points. For simplicity, the interpolation was done on a grid with spacings half the spacings of the measurement grid. In other words, the interpolation grid has north and east spacings equal to 1.16 km and 1.22 km, respectively. The interpolated values of the estimated T_x, T_y, T_z were compared to the true values of T_x, T_y, T_z at the surface of the earth. The interpolation of the estimated and the true gradients is performed using the FFT algorithm discussed in section 3.1.5. The root mean square values of the differences between the true and the estimated gradients T_x, T_y, T_z at the earth's surface are given in Table 7.4.

Table 7.4

Results from the Interpolation of T_x, T_y, T_z Between Profile Points

Measurements	
	RMS error of T_z(mgals)
T_{zz}	0.85
T_{xz}, T_{yz}	0.64
T_{xz}, T_{yz}, T_{zz}	0.62
	RMS error of T_x(mgals)
T_{zz}	0.93
T_{xz}	0.97
T_{xx}, T_{xy}	0.73
T_{xx}, T_{xy}, T_{xz}	0.71
	RMS error of T_y(mgals)
T_{zz}	0.92
T_{yz}	0.95
T_{xy}, T_{yy}	0.78
T_{xy}, T_{yy}, T_{yz}	0.67

Two major conclusions can be drawn from Table 7.4. First the accuracy of the interpolated gradients T_i from their vertical second-order gradients T_{iz} is about 0.2 mgal poorer than the accuracy of T_i interpolated from their horizontal second-order gradients T_{ix}, T_{iy}. This confirms results reported in earlier investigations for the gradient T_z, namely that the gradient T_{zz} is preferable for downward continuation while T_{xz}, T_{yz} are better for the interpolation of T_z (Schwarz, 1976; Schwarz, 1977). Second, the accuracy of the

interpolated horizontal gradients T_x, T_y from gradients T_{zz} is significantly poorer than the accuracy of T_x, T_y computed from T_{zz} at points directly below the measurement points. Therefore T_{zz} is not recommended for interpolation of T_x, T_y.

Chapter 8

CONCLUSIONS AND RECOMMENDATIONS

This research deals with the estimation of first-order gradients T_i of the anomalous gravity potential from airborne second-order gradients T_{ij}. Three major problems had to be solved by the estimation technique developed. First, it should be capable of combining all gradient data. Second, gradiometer noise should be included in the estimation. Third, computational efficiency was of high importance.

The theoretical development, discussed in chapters 3 and 4 leads to the following conclusions. First, for stationary and ergodic signals a multiple input-single output filter system is equivalent to Wiener filtering in the plane. Second 2-D Wiener filtering can be derived as 2-D Fourier transform of least squares collocation under the above assumptions. Thus, the multiple input-single output filtering equations take into account the gradiometer noise and the interrelations among the gradients of the anomalous potential. Assuming flat earth approximation these interrelations can be derived through the transfer functions of the gradients with respect to the anomalous potential. They combine plane integration and downward continuation as does least-squares collocation. Third, new interesting integral formulas relating each first-order gradient with its second-order gradients are derived using the transformation of the frequency domain plane integration formulas to the space domain. In addition a new integral formula is derived relating the anomalous potential to the deflections of the vertical and the gravity disturbance. Those formulas hold assuming smooth topography for the survey area.

Since no airborne gradiometer data are available at present the method was tested with simulated data as close as possible to the planned mission. The following conclusions can be drawn with respect to the results obtained. First, each first-order gradient is most precisely determined by combining its second-order gradients, i.e. T_z is most precisely estimated from the combination of T_{xz}, T_{yz}, T_{zz}. Second, the gradient T_{zz} provides accurate estimates of all first order gradients at points below the measurement points, however it provides significantly poorer interpolation results. Therefore a vertical single axis gravity gradiometer measuring the gradient T_{zz} only, may be considered as a less costly alternative to a three axis gradiometer if the decrease in accuracy is acceptable. Third, assuming gradiometer noise at the level of 80 E^2/Hz, there is no difference between solutions modelling the noise or neglecting it. When the noise is at the level of 300 E^2/Hz however, the accuracy of the estimation of T_x, T_y, T_z computed from T_{xz}, T_{yz}, T_{zz} respectively is significantly deteriorated when the noise is neglected while it remains almost the same as before when the noise is taken into account. For the same higher noise level of 300 E^2/Hz, the accuracy of each first-order gradient computed from all other investigated second-order gradient combinations is essentially the same by either neglecting or taking the gradiometer noise into account. Fourth, the vertical second-order gradient of each first-order gradient is most useful for downward continuation, while the horizontal second-order gradients are better for interpolation. The accuracy to be expected from the currently available Bell gradiometer and the proposed survey geometry is about 0.7 mgals. This accuracy was obtained by assuming

constant flying altitude. For actual surveys this accuracy can be achievable if the aircraft altitude is measured with an accuracy less than 1 m, thus introducing errors in T_x, T_y, T_z less than 0.3 mgals. Fifth, downward continuation from a flying altitude of 600 m and grid spacing of about 2.4 km amounts to less than 0.1 mgals of the total estimation error of about 0.7 mgals. However, since this error contribution depends strongly on the ratio of flying altitude to grid spacing, this result is specific to the simulated gradiometer mission. Much higher values can be expected for a larger ratio. Sixth, the method is computationally fast. It takes about 10 CPU minutes to compute one first-order gradient at 41616 grid points, from 167000 values of airborne second-order gradients including input and output. A fully optimized-vectorized version of these programs would take less than 30 CPU seconds on the Supercomputer CDC Cyber 205. Thus, computationally this method is superior to least-squares collocation.

Recommendations for the continuation of this research are made in four areas. First, airborne gravity gradiometry recovers wavelengths of up to 500 km. Therefore the estimated first-order gradients from airborne second-order gradient data do not contain long wavelength trends and the estimated gravity signal surface is tilted with respect to the actual gravity signal surface. Nevertheless the estimated gravity surface can be tied down to the actual gravity surface using a few astrogravimetric tie points in the following way. The differences between the measured and the estimated T_x, T_y, T_z from airborne gradients are computed at a few strategically placed tie points. Then, these differences can be used in a low frequency least-squares collocator to tie the estimated T_x, T_y, T_z to the actual

T_x, T_y, T_z at any point of the gradiometry survey area. In this research long wavelength trends of the gravity signal were provided by means of the Rapp 1978 spherical harmonic expansion truncated at degree 36. Second, all estimation methods already proposed for the estimation of T_x, T_y, T_z from airborne second-order gradients should be tested on a common data set. Such a test will reveal the strong and weak points of each method and in addition it will show which method is the most efficient computationally. Third, the effect of terrain and variable density on the airborne gravity gradients has not been investigated in this thesis. However the theoretical development for this investigation already exists (Parker, 1972; Dorman and Lewis, 1974). Since this effect can amount to several tenths or even a few hundreds of Eötvos, these formulas should be implemented. Finally, another area of future importance is the use of airborne gravity gradiometry in geophysical exploration. Advantages of airborne gravity gradiometry as compared to terrestrial gravity methods are the much finer resolution of the local anomalous gravity field and the much higher sensitivity to shallow structures (Schwarz and Vassiliou, 1986). Airborne gravity gradiometry as an inverse potential method does not provide a unique solution, however when combined with other geophysical methods (seismic, aeromagnetic methods, etc.) it may prove very useful.

BIBLIOGRAPHY AND REFERENCES

1. Bendat, J.S. and A.G. Piersol (1971). *Random Data: Analysis and Measurement Procedures*. John Wiley & Sons. New York.
2. Bendat, J.S. and A.G. Piersol (1980). *Engineering Applications of Correlation and Spectral Analysis*. John Wiley & Sons. New York.
3. Bloomfield, P. (1975). *Fourier Analysis of Time Series: An Introduction*. John Wiley & Sons. New York.
4. Bracewell, R. (1978). *The Fourier Transform and its Applications*. 2nd Edition, McGraw-Hill; New York.
5. Brigham, E.O. (1974). *The Fast Fourier Transform*. Prentice-Hall Inc. Englewood Cliffs, N.J.
6. Brozena, J.M. (1984). A preliminary Analysis of the NRL Airborne Gravimetry System. *Geophysics*, Vol. 49, No. 7, pp. 1060-1069.
7. Colombo, O.L. (1981). Numerical Methods for Harmonic Analysis on the Sphere. Ohio State University. Reports of the Department of Geodetic Science and Surveying. Report No. 310. Columbus, Ohio.
8. Cooley, J.W. and J. W. Tukey (1965). An Algorithm for the Machine Calculation of Complex Fourier Series. *Math. Computation*, Vol. 19, pp. 297-301.
9. Coons, R.L. Strange, W.E. and G.P. Woolard (1962). Evaluation Study of Airborne Gravimeter Operational Test. University of Wisconsin Geophysical and Polar Research Center. Report No. 62-2.
10. Crochiere, R.E. and L.R. Rabiner (1981). Interpolation and Decimation of Digital Signals - A Tutorial Review. *Proceedings*

of the IEEE, Vol. 9, No. 3, pp. 300-331.

11. Dorman, L.M. and T.R. Lewis (1974). The Use of Nonlinear Functional Expansions in Calculation of the Terrain Effect in Airborne and Marine Gravity and Gradiometry. *Geophysics*, Vol. 39, No. 1, pp. 33-38.

12. Eren, K. (1980). Spectral Analysis of GEOS-3 Altimeter Data and Frequency Domain Collocation. Ohio State University. Reports of the Department of Geodetic Science and Surveying. Report No. 297. Columbus, Ohio.

13. Forsberg, R. (1984a). A Study of Terrain Reductions, Density Anomalies and Geophysical Inversion Methods in Gravity Field Modelling. Ohio State University. Department of Geodetic Science and Surveying. Report No. 355. Columbus, Ohio.

14. Forsberg, R. (1984b). Local Covariance Functions and Density Distributions. Ohio State University. Department of Geodetic Science and Surveying. Report No. 356. Columbus, Ohio.

15. Forward, R.L. (1971). Geodesy with Orbiting Gravity Gradiometers. Hughes Research Laboratories. Research Report No. 442, Malibu, California.

16. Forward, R.L. and C.B. Ames (1977). Prototype Moving Base Rotating Gravity Gradiometer. Program Status Review, Hughes Research Lab. Malibu, California.

17. Gumert, W.R., and G.E. Cobb (1970). Helicopter Gravity Measuring System. Included in *Advances in Dynamic Gravimetry*, W.T. Kattner (Editor), pp. 79-83.

18. Hammer, S.I. (1982). Airborne Gravity is Here! *Oil and Gas Journal*, Vol. 80, pp. 113-122.

19. Hammer, S.I. (1983). Airborne Gravity is Here! *Geophysics*, Vol. 48, No. 2, pp. 213-223.

20. Harris, F.J. (1978). On the Use of Windows for Harmonic Analysis with the Discrete Fourier Transform. *Proceedings of the IEEE*, Vol. 66, No. 1, pp. 51-83.

21. Heiskanen, W.A. and H. Moritz (1967). *Physical Geodesy*. W.H. Freeman, San Fransisco.

22. Heller, W.G. and W.J. Senus (1983). Emergent Moving-Base Gravity Gradiometer Systems and their Ultimate Potential Impact on Terrestrial Gravimetric Data Bases. *Proceedings of the XVIII General Assembly of the International Union of Geodesy and Geophysics*, Hamburg, Germany.

23. Herring, T.A. (1978). Determination of the Deflections of the Vertical from Horizontal Gravity Gradients. M.Sc. Thesis. University of Queensland. Department of Surveying Engineering.

24. Hodus, M.F. (1985). The Vectorization of BIEM. Included in *Supercomputer Applications*, A.H. Emmen (Editor). Elsevier Science Publishers B.V. (North-Holland).

25. Hutcheson, W.J. and A.D. Grierson (1985). Gravity Gradiometer Post Mission Data Processing. *Proceedings of the Third International Symposium on Inertial Technology for Geodesy and Surveying*. Banff, Canada.

26. International Mathematical and Statistical Library (IMSL) reference manual (1981). Edition 8. Houston, Texas.

27. Jekeli, C. (1983). Achievable Accuracies for Gravity Vector Estimation from Airborne Gravity Gradiometry. *Proceedings of the XVII General Assembly of the International Union of Geodesy and*

Geophysics. Hamburg, Germany, pp. 577-594.

28. Jekeli, C. (1984a). Analysis of Airborne Gravity Gradiometer Survey Accuracy. *Manuscripta Geodaetica*, Vol. 9, No. 4, pp. 323-379.

29. Jekeli, C. (1984b). Data Processing Techniques for Airborne Gravity Gradiometry. *Proceedings of the International Summer School on Local Gravity Field Approximation*. Beijing, China, pp. 583-602.

30. Jekeli, C. (1985). Gravity Vector Estimation from a Large and Densely Spaced Heterogeneous Gradient Data Set Using Closed-Form Kernel Approximations. *Proceedings of the Third International Symposium on Inertial Technology for Surveying and Geodesy*. Banff, Canada.

31. Jordan, S.K. (1978). Moving-Base Gravity Gradiometer Surveys and Interpretation. *Geophysics*, Vol. 43, No. 1, pp. 94-101.

32. Jordan, S.K. (1982). Airborne Gravity Gradiometer Survey Accuracy. Geospace Systems Corporation. Report No. TR-34-1.

33. Krarup, T. (1969). A Contribution to the Mathematical Foundation of Physical Geodesy. Danish Geodetic Institute. Meddelelse No. 44.

34. LaCoste, L., Ford, J., Bowles, R., and K. Archer. (1977). Gravity Measurements in an Airplane using State-of-the-Art Inertial Navigation. Paper presented at the 47th Annual International SEG Meeting.

35. Meissl, P. (1970). Probabilistic Error Analysis of Airborne Gravimetry. Ohio State University. Reports of the Department of Geodetic Science and Surveying. Report No. 138. Columbus, Ohio.

36. Metzger, E.H. and A. Jircitano (1977). Application Analysis of Gravity Gradiometers for Mapping of Earth Gravity Anomalies and Derivation of the Density Distribution of the Earth Crust. *Proceedings of the First International Symposium on Inertial Technology for Surveying and Geodesy*. Ottawa, Canada, pp. 334-342.

37. Metzger, E.H. and A. Jircitano (1981). Application of Bell Rotating Accelerometer Gravity Gradiometers and Gravity Meters to Airborne or Land Vehicle Gravity Surveys. *Proceedings of the Second International Symposium on Inertial Technology for Surveying and Geodesy*. Banff, Canada, pp. 521-535.

38. Moritz, H. (1967). Kinematical Geodesy. Ohio State University. Reports of the Department of Geodetic Science and Surveying. Report No. 92. Columbus, Ohio.

39. Moritz, H. (1971). Kinematical Geodesy II. Ohio State University. Reports of the Department of Geodetic Science and Surveying. Report No. 165. Columbus, Ohio.

40. Moritz, H. (1975). Combination of Aerial Gravimetry and Gradiometry. Ohio State University. Reports of the Department of Geodetic Science and Surveying. Report No. 223. Columbus, Ohio.

41. Moritz, H. (1980). *Advanced Physical Geodesy*. Herbert Wichmann Verlag, Karlsruhe. Abacus Press, Tunbridge Wells, Kent.

42. Nashed, M.A. (1976). Aspects of Generalized Inverses in Analysis and Regularization. In *Generalized Inverses and Applications* M.Z. Nashed (Editor). New York.

43. Nettleton, L.L., LaCoste, L. and J.C. Harrison (1960). Tests on an Airborne Gravity Meter. *Geophysics*, Vol. 25, pp. 181-202.

44. Paik, H.J. (1976). Superconducting Tunable-Diaphragm Transducer for Sensitive Acceleration Measurements. *Journal of Applied Physics*, Vol. 47, No. 3, pp. 1168-1178.

45. Paik, H.J. (1979). Unified Theory of Gravitational Radiation Detectors for Pulses and Monochromatic Signals. *Proceedings of the Second Marcel Grossmann Meeting on the Recent Developments of General Relativity*. Trieste, Italy.

46. Paik, H.J. (1981). Superconducting Tensor Gravity Gradiometer. *Proceedings of the Second Inertial Symposium on Inertial Technology for Surveying and Geodesy*. Banff, Canada, pp. 555-568.

47. Paik, H.J. (1985). Review of Superconducting Accelerometer and Gravity Gradiometer Research at the University of Maryland. Paper presented at the Thirteenth Moving Base Gravity Gradiometer Conference. Colorado Springs, U.S.A.

48. Paik, H.J. Mapoles E.R. and K.Y. Wong (1978). Superconducting Gravity Gradiometers. *Proceedings of the Conference on Future Trends in Superconductive Electronics*. Charlottesville, U.S.A.

49. Papoulis, A. (1968). *Systems and Transforms with Applications in Optics*. McGraw-Hill. New York.

50. Parker, R.L. (1972). The Rapid Calculation of Potential Anomalies. *Geophys. J.R. Astr. Soc*, Vol. 31, pp. 447-455.

51. Rapp, R.H. (1978). A Global 1°x1° Anomaly Field Combining Satellite GEOS-3 Altimeter and Terrestrial Anomaly Data. Ohio State University. Reports of the Department of Geodetic Science and Surveying. Report No. 278. Columbus, Ohio.

52. Rummel, R. (1975). Downward Continuation of Gravity Information from Satellite to Satellite Tracking or Satellite Gradiometry in Local Areas. Ohio State University. Reports of the Department of Geodetic Science and Surveying. Report No. 221. Columbus, Ohio.

53. Schafer, R.W. and L.R. Rabiner (1973). A Digital Signal Processing Approach to Interpolation. *Proceedings of the IEEE*, Vol. 61. No. 6, pp. 692-702.

54. Schwarz, K.P. (1976). Geodetic Accuracies Obtainable from Measurements of First and Second Order Gravitational Gradients. Ohio State University. Reports of the Department of Geodetic Science. Report No. 242. Columbus, Ohio.

55. Schwarz, K.P. (1977). Simulation Study of Airborne Gradiometry. Ohio State University. Reports of the Department of Geodetic Science and Surveying. Report No. 253. Columbus, Ohio.

56. Schwarz, K.P. (1979). Geodetic Improperly Posed Problems and Their Regularization. *Bolletino di Geodesia E Scienze Affini*, No. 3, pp. 389-416.

57. Schwarz, K.P. and A.A. Vassiliou (1986). Requirements for the Use of Airborne Gravity Gradiometry in Geophysical Exploration. Paper presented at the Fourteenth Moving Base Gravity Gradiometer Conference. Colorado Springs, U.S.A.

58. Szabo, B. and D. Anthony (1971). Results of AFCRL'S Experimental Aerial Gravity Measurements. *Bulletin Geodesique*, Vol. 45, pp. 179-202.

59. Thompson, L.G.D. (1959). Airborne Gravity Meter Test. *Journal of Geophysical Research*, Vol. 64, pp. 488-497.

60. Trageser, M.B. (1970). A Gradiometer System for Gravity Anomaly Surveying. The Charles Stark Draper Laboratory. Report R-588. Cambridge, Massachusetts.

61. Trageser, M.B. (1975). Feasibility Model Gravity Gradiometer Test Results. The Charles Stark Draper Laboratory. Report P-179. Cambridge, Massachusetts.

62. Tscherning, C.C. (1977). A Note on the Choice of Norm when Using Collocation for the Computation of Approximations to the Anomalous Potential. *Bulletin Geodesique* Vol. 51, pp. 137-147.

63. Tscherning, C.C. (1984). Local Approximation of the Gravity Potential by Least Squares Collocation. *Proceedings of the International Summer School on Local Gravity Field Approximation*. Beijing, China, pp. 277-361.

64. Vassiliou, A.A. (1985a). The Use of Spectral Methods for the Spatial Modelling of Gravity Data. *Manuscripta Geodaetica*. Vol. 10, No. 4, pp. 235-244.

65. Vassiliou, A.A. (1985b). Comparison of Methods for the Processing of Gravity Gradiometer Data. *Proceedings of the Third International Symposium on Inertial Technology for Surveying and Geodesy*. Banff, Canada.

66. Vassiliou, A.A. and K.P. Schwarz (1985). Study of the High Frequency Spectrum of the Anomalous Gravity Potential. Paper presented at the Thirteenth Moving Base Gravity Gradiometer Conference. Colorado Springs, U.S.A.

67. White, J.V. (1980). Error Models for Gravity Gradiometers in Airborne Surveys. Report No. AFGL-TR-80-0220, Government Access No. ADA097745. Prepared by the Analytic Sciences Corporation

(TASC) for the Air Force Geophysics Laboratory. Bedford, Massachusetts.

68. White, J.V. and J.D. Goldstein (1984). Gravity Gradiometer Survey Data Processing. Report No. AFGL-TR-84-0198. Prepared by the Analytic Sciences Corporation (TASC). Reading, Massachusetts.